# By-pass pigging

## Experiments and simulations

H.P. IJsseldijk

Delft University of Technology

TU Delft

# By-pass pigging

## Experiments and simulations

by

H.P. IJsseldijk

to obtain the degree of Master of Science
at the Delft University of Technology,
to be defended publicly on Wednesday August 24, 2016 at 10:00 AM.

| | | |
|---|---|---|
| Student number: | 1517856 | |
| Project duration: | September 2015 – August 2016 | |
| Thesis committee: | Prof. dr. ir. R.A.W.M. Henkes, | TU Delft, supervisor |
| | Dr. ir. B.W. Van Oudheusden, | TU Delft |
| | Dr. ir. M.J. Tummers, | TU Delft |
| | Dr. ir. F.F.J. Schrijer, | TU Delft |
| | Ir. M.H.W. Hendrix, | TU Delft |

An electronic version of this thesis is available at `http://repository.tudelft.nl/`.

TU Delft

**Abstract**

Pipelines are used in many industries as a means of transporting fluids, for example in the oil and gas industry. Pigs are devices that move through such pipelines, for instance to clean the pipeline or to perform internal inspections. They are driven by a pressure difference over the pigs. Since this is a risky operation, there is a strong motivation to control the motion of these pigs. One possibility is to use so-called by-pass pigs. These pigs have a hole through their body such that fluids can by-pass the device. This lowers the pig velocity. If the by-pass area can be varied during a pigging operation, it is possible to control the pig velocity. This concept is relatively new and not yet completely understood. Research is currently carried out at the TU Delft in collaboration with Shell to get a better understanding of the behaviour of conventional pigs of by-pass pigs. This MSc thesis is part of that project and focuses on performing experiments for pigging operations in a laboratory environment. The relevance is two-fold. From one hand, more insight will be obtained in the encountered phenomena. From the other hand, the results can be used to validate the numerical pigging model which is currently in development.

The experiments were carried out in a flowloop at the department of Process & Energy at the TU Delft. The flowloop has a length of 65 $m$ and a diameter of about 52 $mm$. Air is used as working fluid and the flowloop has an atmospheric outlet pressure. During the pigging experiments, the bulk velocity and pressure in the flowloop were recorded. Three cameras were used for visual observation from which the velocity was deduced. The modular pig design made it possible to quickly change between different pig configurations. It turned out that small variations in this configuration can have large influence on the pig motion. A predominant characteristic of the pig motion is the so-called stick-slip motion. This motion is characterized by a quick acceleration and deceleration of the pig as a consequence of a varying friction. A module was added to the numerical pigging model to include the effect of variations in the friction, which forces the simulation to give a stick-slip behaviour. Besides this, also an analytical approach was taken to obtain first insights into this behaviour. The experimental results show that the maximum pig velocity can become significantly larger than the average pig velocity. The ratio of the maximum velocity over the average velocity increases at lower bulk velocities. The stick-slip models can give a reasonable good estimation of the maximum pig velocity. Besides this, they predict a similar trend in the pressure fluctuations. To compare the influence of the bulk velocity and the by-pass area, an extensive parameter study was carried out. Results of 132 pigging runs with two different types of sealing were included. The by-pass area was varied from 0 % to 4 % and the bulk velocity was varied in the range of 1.5 $m/s$ to 7 $m/s$ . The focus was on the effects of these changes on the average pig velocity, the average friction and the standard deviation of the pressure. It turned out that the friction of the pigs used in the experiments was not depending on the velocity. The standard deviation of the pressure, which is a measure of the intensity of the stick-slip behaviour, was different for both types of sealing. However, for a certain configuration no dependence on the pig velocity was found. The average pig velocity itself is largely dependent on the by-pass area. The results were compared with the numerical pigging model, a commercial package and a steady-state analytical model. It turned out that the average velocity can accurately be determined with all these models, even if the pig motion shows a strong stick-slip behaviour.

**Preface**

Before starting this MSc project, I had never heard of pigging at all. And when I tell people that it has to do with the internal cleaning of pipelines, no one really gets excited. However, when thinking of the phenomena encountered during pigging operations one starts seeing that it is actually quite fascinating. During the course of the project, these phenomena were better and better understood. It was exciting to see the experimental and numerical work coming together in the last phase of the project.

This could all only be achieved with the help of others. First and most of all I have to thank Maurice Hendrix. He carries out the overarching PhD project where this MSc project is part of. I could always contact him, which is even more remarkable if you know that he does not have a smart phone. Without him, this report was not at the level it is now. Next to Maurice, I have to thank my two supervisors Bas van Oudheusden and Ruud Henkes, who made sure I kept on the right track and provided me with useful feedback on my writing. For constructing the experimental set-up, a big thanks has to go to the technical staff of the department of process & energy, especially to Jasper Ruigrok. The same holds for the other people in the department of process & energy and the people within Shell I worked with. And a big thanks goes to my fellow students. They made sure there was always enough coffee, and helped improving my football skills during the breaks. Last but not least, as expected, a special thanks to my parents. Their help was not of technical nature, but their moral support was evenly important.

*H.P. IJsseldijk*
*Delft, August 2016*

# Contents

# List of Figures

# List of Tables

# Nomenclature

| Symbol | Definition | Unit |
|---|---|---|
| $A_0$ | Cross-sectional area of the pipe | $m^2$ |
| $A_h$ | Cross-sectional area of the by-pass hole | $m^2$ |
| $c$ | Speed of sound | $m/s$ |
| $D$ | Diameter of the pipe | $m$ |
| $D_h$ | Diameter of the by-pass hole | $m$ |
| $E_{kin}$ | Kinetic energy of the pig | $J$ |
| $E_{pot}$ | Potential energy in the system | $J$ |
| $F_{drive}$ | Driving force exerted on the pig | $N$ |
| $F_{friction}$ | Friction experienced on the pig | $N$ |
| $F_s$ | Static friction experienced by the pig | $N$ |
| $F_d$ | Dynamic friction experienced on the pig | $N$ |
| $k_{eq}$ | Equivalent spring stiffness | $N/m$ |
| $L_{tot}$ | Total pipeline length | $m$ |
| $L_L$ | Length of pipeline upstream of the pig | $m$ |
| $L_R$ | Length of pipeline downstream of the pig | $m$ |
| $M_{pig}$ | Pig mass | $kg$ |
| $\dot{m}$ | Mass flux per second | $kg/s$ |
| $p$ | Pressure | $Pa$ |
| $p_{out}$ | Outlet pressure | $Pa$ |
| $v_{pig}$ | Pig velocity | $m/s$ |
| $v_0$ | Bulk velocity of the fluids | $m/s$ |
| $v_{eq}$ | Steady-state velocity | $m/s$ |
| $x_{p,eq}$ | Pressure equilibrium position | $m$ |
| $x_{f,eq}$ | Friction equilibrium position | $m$ |
| $\Delta m$ | Total mass flux | $kg$ |
| $\Delta x$ | Length of slippage | $m$ |
| $\Delta t$ | Duration of sticking part | $s$ |
| $\delta$ | Wall roughness | $m$ |
| $\mu$ | Kinematic viscosity | $m^2/s$ |
| $\nu$ | Dynamic viscosity | $kg/(ms)$ |
| $\rho$ | Density | $kg/m^3$ |
| $\zeta$ | Pressure drop coefficient | – |
| Re | Reynolds number | – |

# 1 Introduction

This chapter will explain what pigging actually is and how pigging operations are performed. Also some commonly encountered problems are addressed. The main objective of this research is to get a better understanding of pigging operations. It is therefore necessary to give a quick overview of what has already been done, which will form a basis for the approaches followed in this research project.

## 1.1. Background

Pipelines are used in many industries as a means of transporting fluids. A device which travels through a pipeline, driven by the fluid flow, is referred to as a pipeline inspection gauge, or shortly a pig [1]. Some reasons to insert pigs are [2]:

- Internal cleaning of the pipeline
- Separation of two products
- Distribution of corrosion inhibitor
- Inspection of the pipeline

There is a wide variety of pigs to perform these tasks. Three common pig types are (1) the mandrel pig, (2) the solid cast pig and (3) the foam pig ,which are shown in figures 1.1a to 1.1c respectively [3]. A mandrel pig consists of a metal core with elements mounted on this core. It depends on the purpose of the pigging operation which elements are mounted. Typical elements are scrapers for cleaning, guiding discs to ensure a proper alignment with the pipe and sealing elements to seal the pipe, as can be seen in figure 1.1a and 1.2a. These elements are normally made from polyurethane. A solid cast pig differs from a mandrel pig in the sense that it is made out of one material, often also polyurethane. A foam pig is made of softer material and has a larger volume. The pigging purpose and the costs determine which of the types is most appropriate to perform pigging operation.

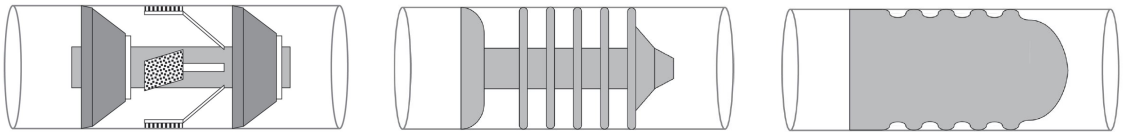

(a) Mandrel pig (b) Solid cast pig (c) Foam pig

Figure 1.1: Several pig types [1]

Pigs are inserted into a pipe with a so-called pig launcher and are taken out with the help of a pig receiver [2]. These stations split up the pipeline and redirect the flow as soon as the pig is in position. Once in the pipe, the pig is driven by a pressure difference over the device. Some problems encountered during pigging operations are:

- The pig moves too fast and is thereby unable to perform the desired task or it can even damage the pipe internally. Reducing the flow rates avoids these problems but this also implies a reduced operation performance.
- Large liquid build up in front of a pig in two-phase flow, called a pig-generated slug. This can cause problems at the end of the pipeline where phases are separated by using so-called slug catchers.
- Pig getting stuck when the driving force cannot overcome the friction force.

To avoid the first two problems, it is desirable that the velocity of the pig does not exceed a certain speed limit. To ensure this, a certain speed control should be built in. One method is to make use of so-called by-pass pigs [4, 5]. These pigs have a hole through the body such that flow can by-pass the pig, as can be seen in figure 1.2b. This lowers the pressure difference over the pig, resulting in a reduced velocity. Besides this, in two-phase pipe flow the higher velocity of the gas with respect to the fluid will smear out the slug in front of the pig. Furthermore, the jet ejected at the nose of the pig can have a positive effect on the efficiency of the pigging operation. For example when it is used to dislodge debris from the pipe wall or to distribute corrosion inhibitor along the pipe wall.

Using a by-pass pig lowers the chance of encountering the first two problems mentioned above, but it increases the risk of the pig getting stuck in the pipe since the pressure drop over the pig will be lower. To avoid such a risk, an instrument could be built-in that controls the by-pass area. These pigs are called speed controlled by-pass pigs [6]. Reducing the by-pass area results in a higher pressure difference and therefore a higher velocity [7].

[1] Obtained from Quarini et al. [3]

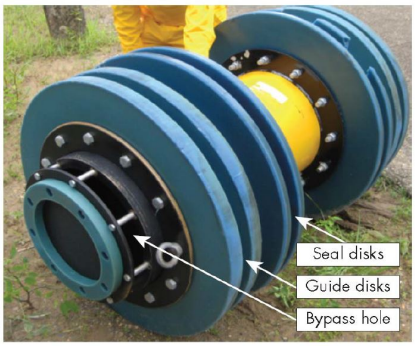


(a) Difference between pigs without and with by-pass hole

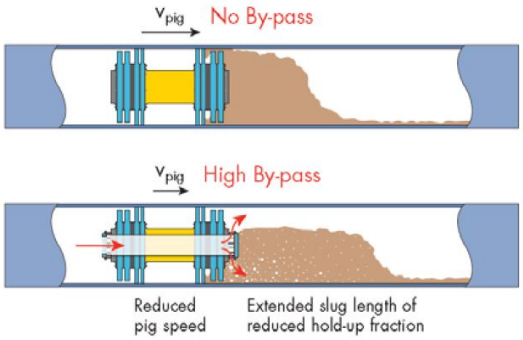


(b) By-pass pig

Figure 1.2: By-pass pigs [2]

Three types of pigs were mentioned: (1) conventional pigs without a by-pass hole, (2) by-pass pigs with a fixed by-pass hole and (3) speed controlled by-pass pigs with an adjustable by-pass hole. When using a conventional pig, the pig acts as a moving boundary that separates the fluid domains upstream and downstream of the pig. When using by-pass pigs, the domains are directly coupled since fluid can by-pass the pig through the hole. However, the effects of the pig are not completely understood and an accurate pigging model to predict the behaviour is not yet developed.

The behaviour of the pig depends on the design of the pig and on the flow conditions. Currently, a research project is carried out at the TU Delft with the aim to develop a by-pass pigging model which can be used in industry. Part of that research is to carry out experimental work on by-pass pigging operations. This task is incorporated in this Master Thesis project. The relevance of the results are two-fold: (1) Gaining more insight into the encountered phenomena and (2) validating the pigging model which is currently under development. This leads to the research questions stated below.

## 1.2. Research questions

Main question:

- How do the motion of a by-pass pig and the characteristics of the surrounding flow depend on the design of the by-pass pig in single-phase flow?

Subquestions:

- What is the relation between the driving force and friction force acting on a pig and how is the driving force acting on a by-pass pig related to the pressure drop over the pig?
- How does the friction of a by-pass pig depend on the following design characteristics: (1) The dimensions of the pig-pipe contact elements of the pig, (2) the material of the contact elements of the pig and (3) the ratio of the outer pig diameter and inner pipe diameter, called the oversize.
- What is the pressure drop over a by-pass pig in single-phase pipe flow as a function of the by-pass area ratio and of the bulk velocity for both stationary and moving by-pass pigs?
- What is the velocity of a by-pass pig in single-phase pipe flow as function of the area ratio, the flow velocity and friction force of a by-pass pig?
- Is the pigging model that is currently being developed able to predict the velocity of a by-pass pig and the characteristics of the pig-generated slug as a function of the area ratio , the liquid velocity, the bulk velocity and the friction of the by-pass pig?

[2] Obtained from Entaban et al. [4]

## 1.3. Outline

To answer these questions it is first necessary to give an overview of what has already done. In the next chapter some analytical approaches are described to give insight in the encountered phenomena. Two situations are described: (1) the steady state motion of by-pass pigs and (2) the quick acceleration and deceleration of a conventional pig, as was observed during the experiments. In the subsequent chapter, a description of the numerical pigging model is given. All models will be compared with the experimental results. The experimental set-up is described in section 3. Properties of the flowloop, the measurement devices and the pigs as used during the pigging experiments are provided. The results of this research are given in chapter 4. That chapter starts with an overview of the experimental results. These are compared with the models in the second part of that chapter. A discussion of the results is given in chapter 5, followed by the conclusions and the recommendations.

## 1.4. Literature review

The advantages of by-pass pigs with respect to conventional pigs have already led to the use of by-pass pigs in the industry. Although experimental work on (by-pass) pigging is rarely found in the literature, some experiences that the operators had during the pigging operations have been published. Entaban et al. [4] use a by-pass pig with a fixed by-pass hole equal to 12% of the pipe area in a two-phase pipeline. The pig-generated slug was reduced by almost a factor two with respect to using a conventional pig. The average velocity during the runs was reduced by more than a factor two. The major advantage such a reduction is that the fluid flow rate could be kept at the same level. When a conventional pig was used, the fluid flow rates had to be reduced, resulting in a lower economical profit. Wu et al. [5] did similar pigging operation but used a by-pass area of 15%. The reason for choosing this area ratio is that the velocity of the pig is sufficiently reduced while the risk of getting stuck is considered small enough. The results they got were similar to the results published by Entaban et al. Results from the use of a more advanced by-pass pig in single-phase flow were given by Money et al. [6]. They used a pig which has a by-pass hole that can be varied from 0% to 50% by rotating certain blades. The required opening area was determined by using a rather simple control method that applied the input from a velocity sensor. With this mechanism they were able to keep the velocity steady throughout the whole pigging operation. These studies show that by-pass pigs can give major advantages while keeping the risks low. Further research on the behaviour of by-pass is required to get a better understanding of the characteristics of the by-pass pig. Based on this knowledge the design can be optimized such that a good control over the pig can be obtained.

*Pigging models*

The oil and gas industry strives for a pigging model to predict the behaviour of pigs moving through pipes. The motion of a pig in a horizontal pipe is normally described by applying Newton's Second Law [8], which states that the mass of the pig multiplied with the acceleration is equal to the net force acting on the pig. The net force is then split up in a friction force and a driving force. This driving force is exerted by the fluid(s) on the pig whereas the opposing friction force is due to the friction between the pig and the pipe wall.

Friction phenomena form a research field on their own. For the pig-wall interface, two main types of friction can be distinguished: (1) dry friction and (2) lubricated friction [9]. Dry friction occurs when two solids are sliding over one another. In lubricated friction, a thin liquid layer is formed in between the two solids that is said to lubricate the relative motion. Such a lubrication layer normally reduces the friction considerably. Which of the two types of frictions is encountered and the corresponding friction force depends on many factors such as the fluid properties, the pig and pipe dimensions, the relative velocities and the materials used [9]. In the pigging industry, most contact elements are made of polyurethane. The friction is normally expressed as the product of a normal force and a friction coefficient. In pigging models, this approach is often adopted with the assumption that the friction coefficient is constant. However, Tan et al. [10] used experiments to show that this assumption is in many cases not valid. The contact elements of mandrel and solid-cast pigs have a disc shape, as can be seen in figure 1.2a. Instead of being compressed, these sealing discs are normally bended. Zhu et al. [11] constructed a finite element model that showed a much higher friction force in comparison with the linear assumption.

The driving force acting on the pig is exerted by the fluid(s). The force is normally computed as the product of the frontal area and the pressure difference over the pig, $F_{driving} = \Delta p\, A_{pig}$. A good understanding of the flow phenomena is therefore essential. The pigging models can be split into models for single-phase

pipe flow and models for two-phase pipe flow. Single-phase pipe flow is rather well understood whereas two-phase flow phenomena are much less accurately predicted. Furthermore, a distinction must be made between models for conventional pigs and models for by-pass pigs. The underlying principles to predict the behaviour of these pigging operations are fundamentally different. Note that the present research is focused on single-phase pigging operations.

The governing equations to describe single-phase flow are based on the conservation laws for mass, momentum and energy. The general formulations can be considerably simplified depending on the situation under consideration. In many situations the flow behaviour can be described by the Navier-Stokes equations. The most important parameter in these equations is the ratio of the inertial forces divided by the viscous forces, which is the so-called the Reynolds number. In the pipeline industry one is often only interested in cross-sectional averaged quantities. It is therefore common to use relative simple one-dimensional formulations to describe the behaviour of the flow. To find the pressure on both sides of the pig, the balance equations must be incorporated in the pigging model. Some models use the whole pipeline as the domain of computation for the fluid.

Nguyen has developed several numerical models in corporation with other researchers where they made use of the method of characteristics [12–16]. Nieckele et al. [8] and Tolmasquim et al. [17] used a finite difference scheme to model the behaviour of a pig. Since both methods use the whole pipe as the fluid domain, the velocity or pressure at the inlet and outlet must be described as boundary conditions. This makes it possible to simulate a pigging operation based on the inlet and outlet conditions measured during a real pigging operation.

There are also models that only use part of the pipe to model the fluid behaviour. The model constructed by Saeidbakhsh et al. [18] even assumes a constant driving force. They tried, however, to include the effects of pipe curvatures. A curvature in the pipe results in a different normal force to compensate for the centrifugal force. This in return results in a higher friction force. The model of Saeidbakhsh et al. [18] was later adjusted by Lesani et al. [19] by including a small part of the fluid domain and assuming incompressible flow. Further improvements were made by Mirshami et al. First, they included incompressibility effects [20] and later they adjusted the friction force computation to include long pigs [21].

Some of the pigging models mentioned above are for by-pass pigs only. To include the effect of the by-passing flow, they all incorporate a similar pressure drop model as taken from the work by others [22]. The general pressure drop formula is normally given as a coefficient multiplied by the dynamic pressure relative to the by-pass pig [23]. The difficulty lies in the determination of the pressure loss coefficient. This coefficient strongly depends on the geometry of the by-pass hole. In the pigging models, the coefficient is split in terms depending on the contraction, the expansion and a possible valve inside the by-pass hole. The contraction and expansion coefficients are depending on the by-pass hole. An overview of pressure drops over an extensive range of configurations is given in the book by Idelchik [23]. By-pass pigs with a straight hole and without internal valves are comparable with orifices. By-pass pigs are different in the sense that the pipe walls are moving with respect to the pig. However, Singh & Henkes [7] have performed numerical simulations to show that the discrepancy is negligible for higher Reynolds numbers. The expression suggested by Idelchik can therefore give a good prediction of the pressure drop over a by-pass pig.

The by-pass area determines the pressure drop over the pig and therefore also the velocity of the pig. If the by-pass area can be varied along the pigging operation, it is possible to control the velocity of the pig. Lesani et al. [24] and Nguyen et al. [15] both included an imaginary control in their numerical model to test these opportunities. In both work it was concluded that a control device would be effective in retaining the velocity of the pig within a certain allowable range.

# 2

# Models

This chapter will explain several aspects of pigs moving through pipelines. The motion of pigs will be described depending on several input parameters, including the pig characteristics (mass, by-pass hole), the pipe geometry (length, cross-sectional area, roughness) and the flow conditions (flow velocity, density, pressure, equation of state). First, an analytical approach is taken. Many assumptions on the input parameters are required to simplify the problem such that the model is analytically solvable. It is doubtful whether all these assumption can be justified. However, they give a quick first insight into the expected phenomena. Second, a numerical approach is made. This approach allows the parameters to be prescribed much more according to reality, resulting in a more detailed simulations of the pig motion. However, the computations are rather time consuming and they need to be analysed with care. The methods of both the analytical and numerical approach are given below. The results will later be compared with the outcomes of the experimental work.

## 2.1. Analytical models

To obtain first insights in the phenomena to be encountered, the pig motion is described analytically. First, a generic model of a pig is given to introduce some basic aspects playing a roll in the motion of the pig. In the more detailed models these basic aspects will be worked out depending on the situation and the assumptions. The first more detailed model describes the motion of a by-pass pig. From this model, a steady-state equilibrium can be found which would be reached in perfectly smooth pipelines. From the experimental observation, it turned out that the pig often moves in a so-called stick-slip motion. A new model was constructed to describe this type of motion. It gives a first insight in when to encounter stick-slip motion and the corresponding frequency and amplitude.

### 2.1.1. General pig model

In the most basic form, the pig is considered as a cylindrical shaped device, which is unconformable and has a constant mass. Whether or not it has a by-pass hole is yet to be specified. This situation is shown in figure 2.1. The motion of such a pig can be described by Newton's second law of motion:

$$M_{pig}\frac{dv_{pig}}{dt} = F_{drive} - F_{friction} \tag{2.1}$$

where: $M_{pig}$ = Mass of the pig
$v_{pig}$ = Velocity of the pig
$F_{drive}$ = Driving force
$F_{friction}$ = Friction force

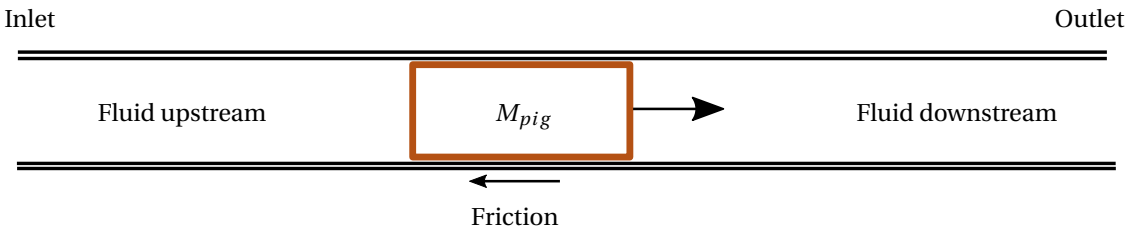


Figure 2.1: Simple pig model

The left hand side is of the equation self explaining. The right hand side consists of a driving force and a friction force. The driving force is generated by the fluid. The main driving contribution is due to the pressure difference between the upstream and downstream sides. This is counteracted by the pressure acting at the downstream side. The pressure drop over the pig gives the net pressure and is therefore the dominant factor in determining the driving force. In case of a by-pass pig, an extra force may be acting due to shear between the pig and the fluid. Together they make up the total driving force.

The opposing force consist of the friction between the pig and the wall. This is a rather difficult term to model as since it depends on many parameters. Several of these parameters were already described in the introduction. There also two types of friction were mentioned: dry friction and lubricated friction. A friction model that includes all factors that play a role may therefore become rather complicated. In the remainder of this report, we will limit ourselves to a simpler approach which covers the static friction and the dynamic friction. For low pig velocities, the friction is assumed to be equal to a constant static friction whereas for high velocities the friction is assumed to be equal to a lower dynamic friction. This is in line with the transition between dry friction and lubricated friction. A more detailed modeling of the friction is outside the scope of this research.

### 2.1.2. By-pass pig model

A by-pass pig has strong analogies with an orifice. The difference is the ability of a by-pass pig to move, whereas an orifice is stationary with respect to the pipe wall. Within a frame of reference moving with the pig, the walls move relative to the pig. Numerical work [7] has shown that the pressure drop coefficient for a by-pass pig (with moving walls) and the pressure drop coefficient over an orifice (with stationary walls) can both be approximated by a formula suggested by Idelchik [23]. CFD computations have shown that the results deviate by less than 2% as soon as the Reynolds number defined in the orifice ($\mathrm{Re} = \frac{\rho v_h D_h}{\mu}$) becomes larger than 10 000 [7]. Also in the lower Reynolds regions the numerical simulations show good agreement. We will therefore use the pressure drop coefficient for an orifice to find the pressure drop over a moving by-pass pig.

A schematic representation of a moving by-pass pig is shown in figure 2.2. The by-pass pig is depicted in blue and travels with a velocity $V_p$ to the right. The flow is also coming from the right but with a larger cross-sectional averaged velocity $V_0$ and therefore by-passes the pig. The cross-sectional averaged velocity of the fluid in the by-pass hole is denoted as $V_h$. When approaching the rear of the pig, the flow must contract. Some separation may occur at the intersection corners of the wall and the pig. Once in the by-pass hole, the flow will contract even further. This phenomena is called a vena contracta. The largest velocities will be observed in the middle of this vena contraction. From there the flow will expand and reattach in the by-pass hole. This expansion gives rise to separation losses. Further downstream in the by-pass hole, the flow will develop to a constant velocity profile. At the exit of the pig, a second flow expansion will take place. This separation in front of the pig is the main contributor of the pressure losses. Further downstream in the pipe the flow will reattach and a new velocity profile can develop.

In the following section the conservation laws for the fluid are given. Next, several formulas are given to predict the pressure at certain locations along the domain. The section thereafter gives a prediction of the force acting on the pig, based on the pressure distribution. In the last section a short description of a model built in Matlab is given to estimate the velocity or the pressure drop of a by-pass pig in a steady-state situation.

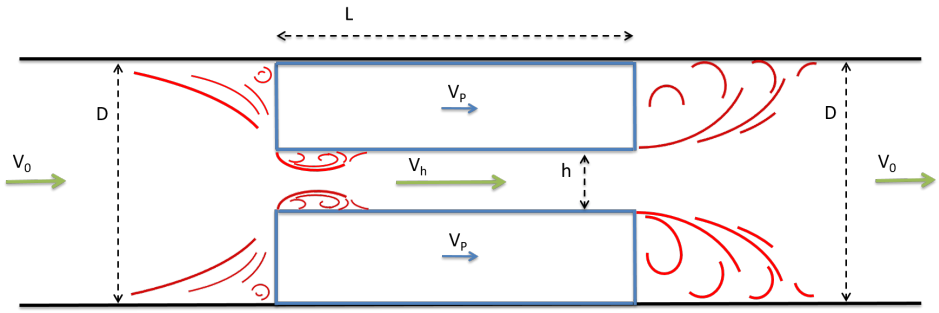


Figure 2.2: Flow around a by-pass pig

#### 2.1.2.1. Governing equations

Before proceeding, it is good to state the conservation laws. For pipe flow, these can be defined in a 1-dimensional form, as will be shown below. The situation is considered to be in a steady-state, which removes all time derivatives. Depending on the assumptions, more simplifications can be made. The governing equations will later be used in a model for the forces on a by-pass pig in a steady-state situation.

*Conservation of mass*

Conservation of mass is as follows:

$$\frac{d}{dt}\int_{\Omega} \rho \, d\Omega = \int_{\Gamma} \rho(\mathbf{v}\cdot\mathbf{n})\, d\Gamma \tag{2.2}$$

where: $\rho$ = Density
$\mathbf{v}$ = Velocity
$\mathbf{n}$ = Vector normal to the boundary
$\Omega$ = Domain
$\Gamma$ = Boundary of domain

The time derivative drops out since we consider a steady-state situation. The term on the right represents the inflow and outflow of mass. For flow in a single pipe, there is just one inlet and one outlet. The velocities are given perpendicularly to these boundary areas. When the pressure is assumed to be constant over the cross-sectional area, also the density variation can be neglected. Furthermore, the velocities can be given as cross-sectional averaged velocities. The integrals can therefore be omitted.

$$\rho_{in} v_{in} A_{in} = \rho_{out} v_{out} A_{out} \tag{2.3}$$

where: $\rho_{in,out}$ = Cross-sectional averaged density at the inlet/outlet
$v_{in,out}$ = Cross-sectional averaged velocity at the inlet/outlet
$A_{in,out}$ = Cross-sectional area at the inlet/outlet

Further simplifications can be made based on the situation. If the density does not change over the pipe segment, the density can be canceled out. The same holds for the cross-sectional area, leaving the statement that the cross-sectional averaged velocity in the inlet and outlet should be the same.

*Conservation of energy*

Many expressions for the conservation of energy can be found in the literature depending on the considered system. A general expression for open flow systems is as follows:

$$\frac{d}{dt}\left\{\int_\Omega \rho e \, d\Omega\right\} = \int_\Gamma \rho e \, (\mathbf{v}\cdot\mathbf{n}) d\Gamma + \dot{Q} - \dot{W} \tag{2.4}$$

where: $\dot{Q}$ = Heat power added to the system
$\dot{W}$ = Power delivered by the system
$e$ = Energy of system per unit mass = $(e_{internal} + e_{kinetic} + e_{potential} + e_{other})$

The power exerted by the fluid can be split into several components. A common way is to divide it into power exerted by viscous forces ($W_v$), power exerted by the fluid flowing across the boundary ($W_p$) and power exerted by other devices, for example shafts ($W_e$). The power exerted by the fluid flowing across the boundary is equal to the integral of the pressure multiplied with the velocity normal to the boundary. Since a steady state is considered, the time derivative drops out. Furthermore, it is assumed that there is no heat transfer across the boundaries and that no power is exerted by other devices. Those terms drop therefore out as well. The energy per unit mass is split into internal energy ($\hat{u}$), kinetic energy ($1/2v^2$) and potential energy ($gz$). Since pipe flow is considered, there is just one inflow and one outflow. Again, the pressure and density are considered constant over the area. For the velocity a cross-sectional averaged value is used to get rid of the integrals. This averaging method can cause an error in the kinetic energy term since the average of a product is in general not equal to the product of averages. In the expression below, a kinetic energy coefficient is introduced to compensate for this:

$$v_{in}A_{in}\left(\rho_{in}\hat{u}_{in} + 1/2\alpha_{in}\rho_{in}v_{in}^2 + \rho_{in}gz_{in} + p_{in}\right) - v_{out}A_{out}\left(\rho_{out}\hat{u}_{out} + 1/2\alpha_{out}\rho_{out}v_{out}^2 + \rho_{out}gz_{out} + p_{out}\right) = \dot{W}_v \tag{2.5}$$

where: $\hat{u}_{in,out}$ = Internal energy at the inlet/outlet
$\alpha_{in,out}$ = Kinetic energy coefficient to compensate for uniformity in velocity profile
$g$ = Gravity constant
$z_{in,out}$ = Height at inlet/outlet
$p_{in,out}$ = Cross-sectional average pressure at the inlet/outlet
$\dot{W}_v$ = Work done by viscous forces

When comparing the equation above with the conservation of mass, one can see that the two terms in front of the brackets are equal to the volumetric flow rate. The ratio between the volume flow rates in the inlet and outlet is equal to the density ratio. Diving the viscous power $\dot{W}_v$ by the volume flux through the inlet yields a pressure loss. Rearranging gives the following expression:

$$\Delta p_{tot} = \left(\hat{u}_{in} + p_{in} + 1/2\alpha_{in}\rho_{in}v_{in}^2 + \rho_{in}gz_{in}\right) - \frac{\rho_{in}}{\rho_{out}}\left(\hat{u}_{out} + p_{out} + 1/2\alpha_{out}\rho_{out}v_{out}^2 + \rho_{out}gz_{out}\right) \tag{2.6}$$

where: $\Delta p_{tot}$ = Total pressure drop over a pipe segment

Further simplifications can be made depending on the situation under consideration. In many situations it can be assumed that the internal energy does not change. If the velocity profiles at the two locations is the same, both kinetic energy coefficients are equal and can be set to 1 when an appropriate choice for the cross-sectional averaged velocity is made. A major simplification is obtained when the density is considered constant. Substituting all assumptions yields the following relation:

$$\Delta p_{tot} = \underbrace{p_{in} - p_{out}}_{\text{static pressure}} + \underbrace{1/2\rho(v_{in}^2 - v_{out}^2)}_{\text{dynamic pressure}} + \underbrace{\rho g(z_{in} - z_{out})}_{\text{hydrodynamic pressure}} \tag{2.7}$$

*Conservation of momentum*

Also the conservation law for momentum can be stated in several ways. A common way is the following:

$$\frac{d}{dt}\int_{\Omega} \rho \mathbf{v} d\Omega = \int_{\Gamma} \rho \mathbf{v}(\mathbf{v}\cdot\mathbf{n}) d\Gamma + \sum \mathbf{F} \tag{2.8}$$

where: $\sum \mathbf{F}$ = Sum of forces acting on the fluid

The left hand side drops out again since we consider a steady state system. The first term on the right side represents the inflow and outflow of momentum. For pipe flow, this can be split into one part representing the inflow and one part representing the outflow. The sum of the forces can consist of several components and are often split into internal and boundary forces. Here, the only internal force considered is gravity. The boundary forces are due to pressure and shear stresses. In the situation of a by-pass pig, there average flow is aligned with the pipe direction, denoted with $s$. The momentum equation needs to be considered in that direction only. The same holds for the gravity force and for the forces on the boundaries. The integrals of the inflow and outflow of momentum can be omitted when using cross-sectional averaged quantities. One should again keep in mind that the average of a product is not equal to the product of averages. Coefficients are introduced to correct for this. When drawing a control volume around a by-pass pig as done in figure 2.3, the boundaries are either normal to the cross-sectional averaged velocity or parallel to these velocities. The force term is therefore split into two parts. The forces at the sides parallel to the flow are due to shear ($\tau$), whereas the forces at the sides normal to the flow are due to the pressure ($p$). This yields the following expression:

$$\rho_{in}\alpha_{in}v_{in}^2 A_{in} - \rho_{out}\alpha_{out}v_{out}^2 A_{out} = -\int_{\Gamma_{\parallel}} \tau d\Gamma_{\parallel} - \int_{\Gamma_{\perp}} p d\Gamma_{\perp} - \int_{\Omega} \rho g d\Omega \tag{2.9}$$

where: $\tau$ = Shear stress

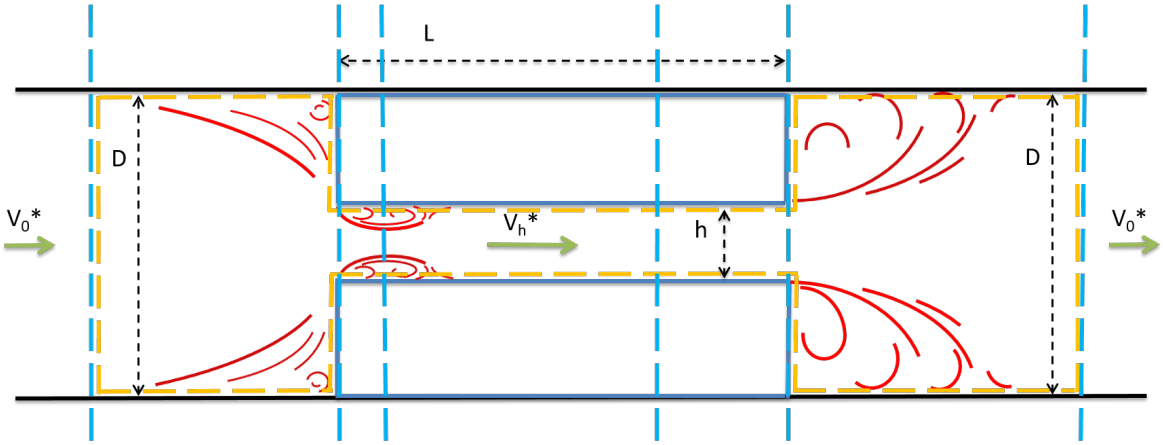


Figure 2.3: Control volume around the by-pass pig

### 2.1.2.2. Pressure distribution

Consider the same schematic view as in figure 2.2, but now in a frame of reference moving with respect to the pig. In figure 2.3 this situation is shown. Blue lines are shown at the following six locations:

- Before the contraction, where $p = p_0$
- At the rear of the pig, where $p = p_r$
- In the vena contracta, where $p = p_v$
- In the by-pass hole, where $p = p_h$
- At the front of the pig, where $p = p_f$
- After the expansion, where $p = p_1$

Several expressions can be found in the literature to predict the pressure drop between two locations. The pressure drop is normally expressed in terms of a pressure drop coefficient, which is defined as follows:

$$\varsigma_{tot} = \frac{p_{in} - p_{out}}{1/2\rho V^2} + \frac{1/2\rho_{in} v_{in}^2 - 1/2\rho_{out} v_{out}^2}{1/2\rho V^2} + \frac{\rho g(z_{in} - z_{out})}{1/2\rho V^2} \tag{2.10}$$

where: $\varsigma_{tot}$ = Pressure drop coefficient

This is just the total pressure drop normalized by a certain dynamic pressure. Which dynamic pressure is used depends on the situation, but it is most intuitive to take the dynamic pressure at the point where separation occurs. The total pressure drop was split in a term due to the static pressure drop, a term due to the dynamic pressure drop and a term due to the hydrodynamic pressure drop, as was also done in equation 2.7. For a by-pass pig moving through a horizontally aligned pipe system, the gravity can be ignored. If the density is considered constant ($\rho_{in} = \rho_{out} = \rho$), the following expression is obtained:

$$\varsigma_{tot} = \underbrace{\frac{p_{in} - p_{out}}{1/2\rho V^2}}_{\varsigma_{static}} + \underbrace{\frac{v_{in}^2 - v_{out}^2}{V^2}}_{\varsigma_{dynamic}} \tag{2.11}$$

where: $\varsigma_{static}$ = Static pressure drop coefficient
$\varsigma_{dynamic}$ = Dynamic pressure drop coefficient

In the following sections expressions are given for the pressure drop coefficient over the following segments:

- The contraction:
  Starting ahead of the contraction ($v_{in} = v_0$) and ending in the by-pass hole ($v_{out} = v_h$)
- The expansion:
  Starting in the by-pass hole ($v_{in} = v_h$) and ending behind the expansion ($v_{out} = v_1$)
- The orifice as a whole:
  Starting ahead of the contraction ($v_{in} = v_0$) and ending behind the expansion ($v_o ut = v_1$)

The expressions are obtained from the book by Idelchik [23]. This book is often used as reference since it gives an overview of expressions to be used in a variety of configurations. The expressions are valid for situations where the density over the segment is constant. In his book, Idelchik uses different dynamic pressures $1/2\rho V^2$ for the normalization. The expression in the next sections are rewritten such that they are all normalized with the dynamic pressure in the pipe upstream or downstream of the by-pass pig, i.e. with $1/2\rho V^2 = 1/2\rho_0 v_0^2 = 1/2\rho_1 v_1^2$ .

*Inlet*

The flow domain starts before the contraction and ends inside the by-pass hole, downstream of the vena contracta. The inflow velocity is equal to $v_0$, the outflow velocity is equal to $v_h$. The pressure is made dimensionless with the dynamic pressure in the orifice:

$$\varsigma_{in,tot} = \underbrace{\frac{p_0 - p_h}{1/2\rho_h v_h^2}}_{\varsigma_{in,st}} + \underbrace{\frac{A_h^2}{A_0^2} - 1}_{\varsigma_{in,dyn}} \tag{2.12}$$

The expression for the pressure drop coefficient suggested by Idelchik is given in equation 2.17 in equation 2.13. This coefficient is split into a dynamic and static pressure drop coefficient below.

$$\varsigma_{in,tot} = \underbrace{\left(0.5\left(1 - \frac{A_h}{A_0}\right)^{0.75}\right)}_{\varsigma_{in,st}} + \underbrace{\left(\frac{A_h^2}{A_0^2} - 1\right)}_{\varsigma_{in,dyn}} \tag{2.13}$$

*Outlet*

The outlet section starts in the by-pass hole and ends behind reattachment region. The inflow velocity is equal to $v_h$, the outflow velocity is equal to $v_1$. The pressure is made dimensionless with the dynamic pressure in the orifice:

$$\varsigma_{out,tot} = \underbrace{\frac{p_h - p_1}{1/2\rho_h v_h^2}}_{\varsigma_{out,st}} + \underbrace{1 - \frac{A_h^2}{A_1^2}}_{\varsigma_{out,dyn}} \tag{2.14}$$

For the pressure drop coefficient in this region, Idelchik suggests the expression given in equation 2.15. This can again be split into a coefficient for the static pressure drop and the dynamic pressure drop, as shown below.

$$\varsigma_{out,tot} = \underbrace{2\left(1 - \frac{A_0}{A_h}\right)}_{\varsigma_{out,st}} + \underbrace{\left(1 - \frac{A_h^2}{A_1^2}\right)}_{\varsigma_{out,dyn}} \tag{2.15}$$

*Orifice*

To consider the orifice as a whole, the inlet should be chosen just before the contraction and the inlet right behind the reattachment region. A consequence of this choice is that the cross-sectional averaged velocities

at the inlet and outlet are the same ($v_{in} = v_{out} = v_0 = v_1$), and so are the dynamic pressures. The total pressure drop is therefore the same as the static pressure drop:

$$\varsigma_{or,tot} = \frac{p_0 - p_1}{1/2\rho_h v_h^2} \tag{2.16}$$

The expression for the pressure drop coefficient over an orifice as suggested by Idelchik is:

$$\varsigma_{or,tot} = \left\{ \underbrace{0.5\left(1 - \frac{A_h}{A_0}\right)^{0.75}}_{\text{inlet}} + \underbrace{\tau\left(1 - \frac{A_h}{A_0}\right)^{1.375}}_{\text{velocity profile}} + \underbrace{\left(1 - \frac{A_h}{A_0}\right)^2}_{\text{outlet}} + \underbrace{\lambda\frac{l}{D_h}}_{\text{friction}} \right\} \tag{2.17}$$

The first and third term represent the inlet and outlet pressure drop coefficients, respectively. They are equal to the coefficients given before where the situations were considered separately. Due to some extra phenomena, two extra terms are included. The second term on the right hand side accounts for an undeveloped velocity profile encountered in shorter orifices. Since here only relative long orifices are considered, the term drops out. The fourth term on the right hand side accounts for the shear in the orifices. This shear stress depends on the length of the orifice, the diameter of the orifice and a friction coefficient. Depending on the configuration, this term might be neglected with respect to the other terms and drops out as well.

In figure 2.4 the pressure drop coefficient associated with an inlet, an outlet and a whole orifice are plotted versus the area ratio. The blue line for the orifice is computed without taking the shear stress in the orifice into account. The black and red lines do take shear into account. For the friction coefficient, which is required to compute the shear, a formula suggested by Churchill is used (see appendix A.1.1). This formula is depending on the Reynolds number inside the orifice and on a wall roughness. Some typical roughness values for several materials are shown in table 2.1. The black line in figure 2.4 shows the pressure drop coefficient for a smooth wall, whereas the other two lines use the roughness corresponding to PVC and steel. One can see that the friction alters the pressure drop only slightly. The influence of the roughness is modest. For a smooth material like PVC, the difference between the smooth and rough pipe can hardly be seen. Only for very rough materials the friction drop coefficient increases significantly.

All cases show a strong increase as soon as the area ratio approaches zero. This is in line with the expectations. The main contribution of the pressure drop is the outlet section. It covers approximately 2/3 of the total pressure drop.

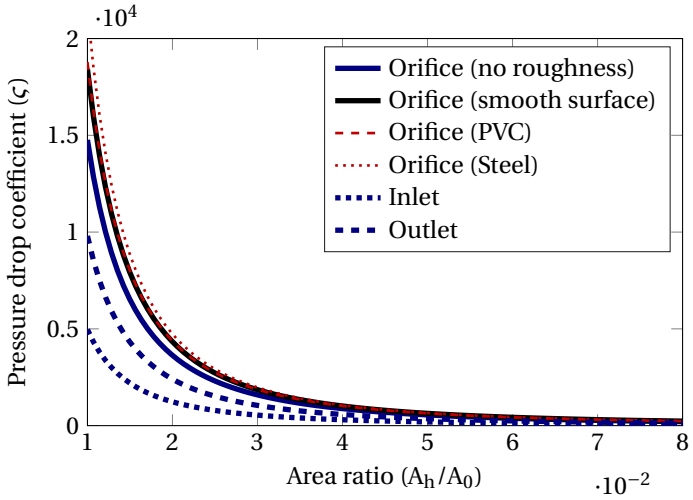


Figure 2.4: Pressure drop coefficient for an orifice

Table 2.1: Parameters of the stick-slip model

| **Material** | **Roughness ($\varepsilon$)** [1] |
|---|---|
| Aluminium, copper | $1.5 \cdot 10^{-3} mm$ |
| PVC, plastic pipes | $4 \cdot 10^{-3} mm$ |
| Steel | $60 \cdot 10^{-3} mm$ |

[1] http://www.engineeringtoolbox.com/surface-roughness-ventilation-ducts-d_209.html

### 2.1.2.3. By-pass pig model

In this section, a simple model for the motion of a by-pass pig is constructed, which can be used to estimate the velocity of the pig. The model assumes a quasi steady-state. This implies that the forces acting on the pig are balanced and the velocity of the pig is adjusted accordingly. This assumptionis valid if the inertial force of the pig is small in comparison with the other forces. It is therefore essential to figure out what the other forces are that act on the pig. Combining them gives a first insight into the velocity of a by-pass pig depending on (1) the friction, (2) the fluid velocity, (3) the density and (4) the area ratio.

*Forces on the pig*

The driving force acting on the pig is induced by the fluid, whereas the opposite force is due to the friction between the pig and pipe wall. When considering the simple by-pass pig shown in figure 2.3, one can further split the driving force into a contribution of the pressure and a contribution of the shear stress. The pressure force is computed by multiplying the pressure difference between the rear and back of the pig by the normal area of the pig ($A_{pig}$). The shear force is induced by the fluid by-passing the pig through the hole and thereby 'dragging' the pig forward. The friction force is a rather difficult force to model. First of all it depends on the design of the pig and of the pipe, i.e. the dimensions and the materials used. Furthermore, it may depend on the velocity. If wear occurs, the friction will also vary over time. Here it is assumed that the friction is known and that it has a constant value. The sum of the forces therefore becomes:

$$\sum F = \underbrace{(p_r - p_f)\, A_{pig} + F_{shear}}_{F_{driving}} - \underbrace{F_{friction}}_{F_{friction}} \tag{2.18}$$

The pressure difference can be obtained from the pressure drop coefficients given in the previous section. Expressions were given for the pressure drop coefficient over the contraction segment, over the outlet segment and over an orifice as a whole. The relevant pressures here are the ones at the rear and front of the pig. It turns out that these can be computed based only on the expression for the pressure drop coefficient over the whole orifice. To see this, consider again the sketch of the by-pass pig system as shown in figure 2.2. Now, apply the conservation of momentum law over the control volume that is indicated in orange:

$$\rho_{in}\alpha_{in}v_{in}^2 A_{in} - \rho_{out}\alpha_{out}v_{out}^2 A_{out} = -\int_{\Gamma_\parallel} \tau\, d\Gamma_\parallel - \int_{\Gamma_\perp} p\, d\Gamma_\perp \tag{2.19}$$

It is assumed that the left and right boundaries are far enough from respectively the contraction and expansion and that the system is in a steady-state such that the velocity distributions are equal. Since the areas are equal, also the average velocities must be the same. The left hand side of the formula above therefore drops out. Next, the pressure term is written out. Since only the boundaries perpendicular to the flow are of interest, the integral is split into four terms: (1) the inlet, (2) the outlet, (3) the rear of the pig and (4) the front of the pig. Also the shear term is written out, it is split in a term accounting for the shear in the by-pass hole and a term for the shear outside the by-pass hole. The momentum balance will therefore look as follows:

$$\int_{\Gamma_{pipe}} \tau\, d\Gamma_\parallel + \int_{\Gamma_{hole}} \tau\, d\Gamma_\parallel + p_0 A_0 + p_r A_{pig} - (p_1 A_1 + p_f A_{pig}) = 0 \tag{2.20}$$

Comparing the above equation with the driving force acting on the pig (eq. 2.18), one can see the same terms appearing. The integral over the shear stress in the by-pass hole is equal to the shear force ($F_{shear}$). The shear stress in the segment outside the by-pass hole can be neglected since the velocity gradients at the wall are small. When rewriting the equation, the following expression for the driving force is obtained:

$$F_{driving} = (p_r - p_f)A_{pig} + F_{shear} \tag{2.21}$$

$$= (p_1 - p_0)A_0 \tag{2.22}$$

The next step is to find an expression for the term on the right hand side as a function of known parameters. This term is equal to the pressure drop over a segment starting before the expansion and ending behind the reattachment region. In the previous section an expression for this was given as function of the density, incoming velocity and pressure drop coefficient (eq. 2.16). There, also the pressure drop coefficient suggested by Idelchik was listed (eq. 2.17). Once should take care that those expressions hold for a stationary orifice. For

a moving by-pass pig, the relative velocity of the flow in the pipe with respect to the velocity of the pig must be used. This is simply the velocity of the fluid minus the velocity of the pig. Note that in this analysis the time derivatives were neglected, implying that the expressions are only valid when the system is in a steady-state. Substituting all expression back into equation 2.18 gives the following relation for the sum of force acting on a simple by-pass pig:

$$\sum F = F_{drive} - F_{friction} \tag{2.23}$$

$$= \varsigma_{or,tot} \tfrac{1}{2} \rho_0 (v_0 - v_{pig})^2 A_0 - F_{friction} \tag{2.24}$$

$$= \left(0.5\left(1 - \frac{A_h}{A_0}\right)^{0.75} + \left(1 - \frac{A_h}{A_0}\right)^2 + \lambda \frac{l}{D_h}\right)\left(\frac{A_0}{A_h}\right)^2 \tfrac{1}{2} \rho_0 (v_0 - v_{pig})^2 A_0 - F_{friction} \tag{2.25}$$

$$\tag{2.26}$$

### 2.1.2.4. Equation of motion

The motion of a simple by-pass pig as shown in figure 2.2 is modelled with Newton's second law of motion. In the previous section, the forces acting on such a simple by-pass pig when moving in a steady-state were given. The equation of motion for a by-pass pig moving in a quasi steady-state is therefore as follows:

$$M_{pig} \frac{dv_{pig}}{dt} = \left(0.5\left(1 - \frac{A_h}{A_0}\right)^{0.75} + \left(1 - \frac{A_h}{A_0}\right)^2 + \lambda \frac{l}{D_h}\right)\left(\frac{A_0}{A_h}\right)^2 \tfrac{1}{2} \rho_0 (v_0 - v_{pig})^2 A_0 - F_{friction} \tag{2.27}$$

It can be seen that the velocity of the pig is a function of the following variables:

- Mass of the pig ($M_{pig}$)
- Density of the fluid ($\rho_0$)
- Ratio of by-pass area over pipe area ($A_h / A_0$)
- Fluid velocity ($v_0$)
- Friction force ($F_{friction}$)

### 2.1.2.5. Results

The equation given to describe the quasi steady-state of a by-pass pig can be used to get a first insight into the behaviour. First, the situation where the pig has a constant velocity is discussed. The inertia terms drop out in this case. Second, situations where a pig undergoes small velocity changes is analysed. Besides an estimation of the motion, this analysis will also give the limits up to where the quasi-steady state model is valid.

*Steady-state velocity*

The simplest way to describe the motion of a by-pass pig is obtained when the velocity of the pig is assumed to be constant. The pig is then in a steady-state. The left hand side of equation 2.27 drops out and the situation is described by the terms on the right hand side. In that case, there are only four parameters describing the motion: (1) the ratio of the by-pass area over the pipe area, (2) the relative velocity of the pig with respect to the fluid, (3) the density and (4) the friction force. With three of these known, the fourth can be computed. In the part below, a range of frictions and area ratios is taken and the density is assumed to be constant. By using equation 2.27 the relative velocity to balance all forces can then be computed. Combining this relative velocity with the fluid velocity relative to the pipe gives a prediction of the velocity of a by-pass pig when traveling in a steady-state.

In figure 2.5 the relative velocity is shown for a range of area ratios and a range of friction ratios. The density is taken as 1.2 $[kg/m^3]$, which is typical for air at room temperature and atmospheric pressure. All points on the coloured surface are situations for cases in which the forces on the pig cancel each other out. The friction force is exactly balanced by the driving force, which is a function of the area ratio and of the relative velocity. Since the net force is zero, the acceleration is zero and the velocity is therefore constant, i.e. a steady-state situation.

Figure 2.5 shows the relative velocity when the friction force is equal to the driving force. However, if the flow in the pipe is low, the driving force might not be high enough to overcome the friction force. The surface

plot is therefore also a boundary indicating the minimum fluid velocity required to set a pig into motion. If, for a certain friction and area ratio, the fluid velocity in the pipe is below the surface, the pig will not start moving. However, if the fluid velocity is higher than the required relative velocity, the driving force is large enough to overcome the friction and the pig will start to move. The lower the area ratio and the lower the friction, the lower the fluid velocity required to set a pig into motion. The steady-state velocity is equal to the difference between the required relative velocity and the actual velocity of the fluid in the pipe. To illustrate this, assume that the fluid velocity in the pipe is 5 $[m/s]$. This is indicated in figure 2.5 with the red bars on the axis. Situations corresponding to the region in which the required velocity is higher than the fluid velocity will not cause the pig to start moving. On the other hand, in the region where the required relative velocity is low, the driving force is large enough to overcome the friction force. The steady-state velocity is equal to 5 $[m/s]$ minus the required velocity. Using this simple formula, it is possible to compute the steady-state velocity for the same range of area ratios and frictions, belonging to a fluid velocity in the pipe of 5 $[m/s]$. The result is shown in figure 2.6. Note that the axes are reversed for clarity. The by-pass pig will not start moving if the friction and area ratio are high. Lowering these parameters will at some point result in a situation where the driving force can overcome the friction force. The surface indicates what the corresponding steady-state velocity will be.

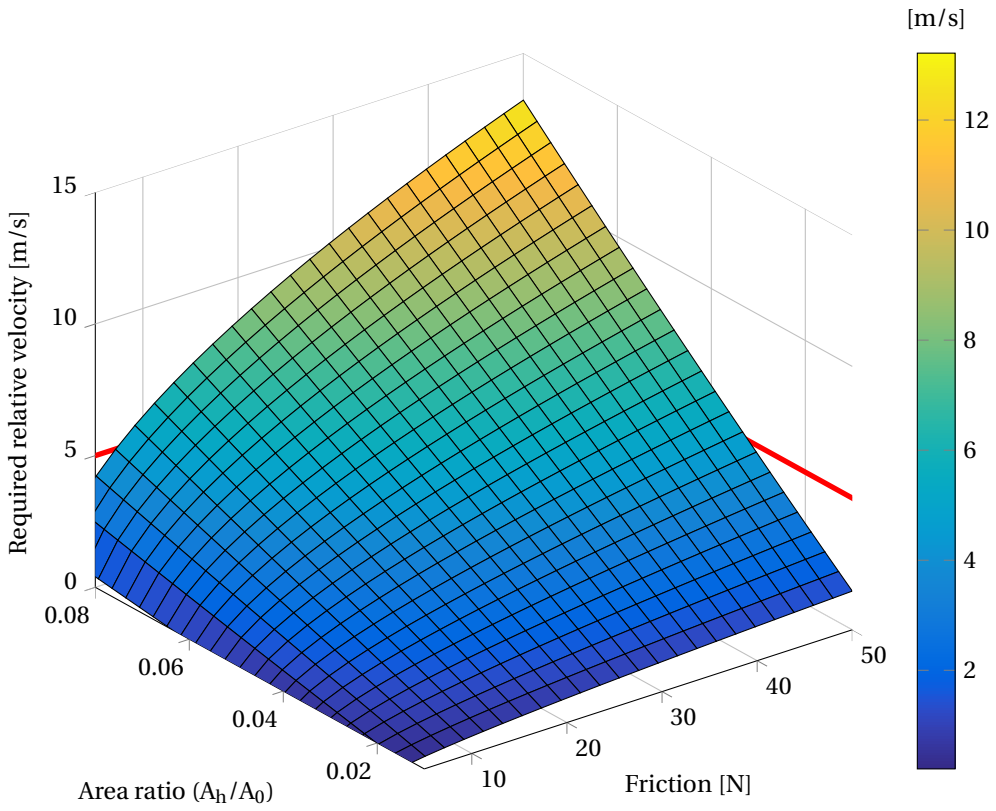


Figure 2.5: Required velocity to balance the friction force

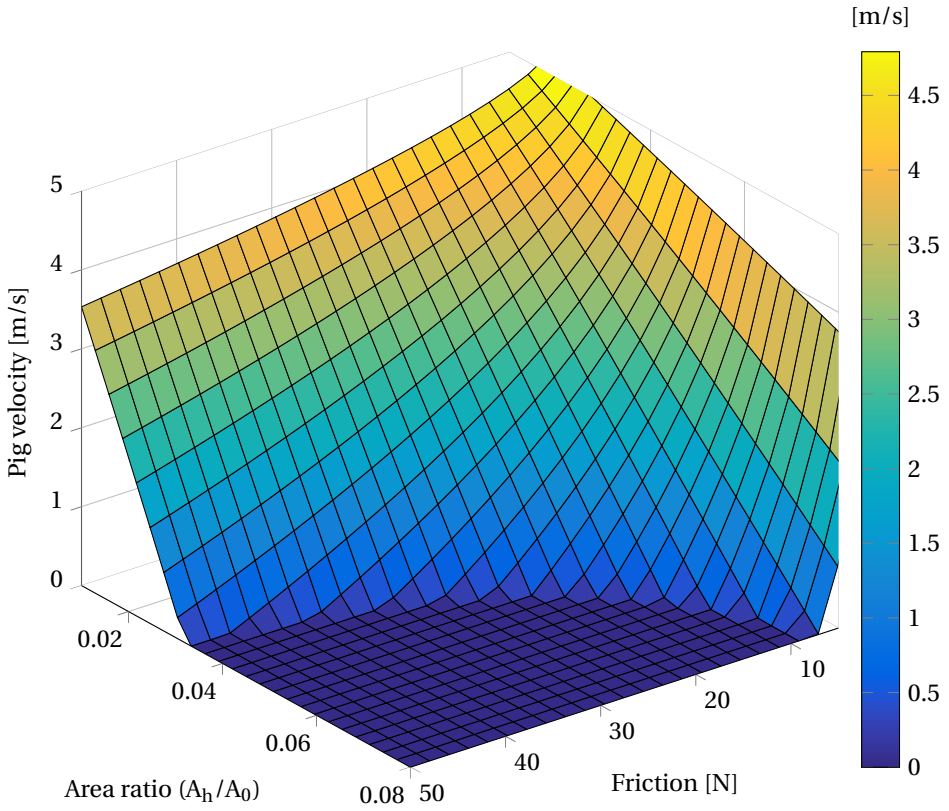


Figure 2.6: Steady-state velocity of a by-pass pig

### 2.1.3. Stick-slip model

In the pigging experiments it was observed that a steady-state motion with the pig moving at a constant velocity does hardly ever occur. Instead, the pig moves with strong oscillations. At some instances the pig is sticking, whereas at other instances the pig quickly slips through the pipe. This behaviour is therefore called a stick-slip motion. This phenomena is reflected in the pressure measurements, where a build-up of pressure was measured when the pig was sticking, whereas a quick drop of the pressure was observed as soon as the pig slipped forward. A possible reason for this is the variation in the inner pipe diameter. This causes changes in the friction which can cause the pig to stick. The motion shows a rather regular variation in this stick-slip phenomenon. Both the length of the slippage and the frequency of the slippage seem to vary only within a certain range. The variation in the inner pipe diameter seems to be a trigger of the stick-slip motion only, whereas the general characteristics of the system as a whole behaves according to a certain pattern. Another phenomenon that could cause a stick-slip motion is the friction variation as function of the velocity. For many contact materials, the friction between two surfaces depends on the relative velocity at the contact area. In general, a larger friction is observed when the two surfaces are not moving with respect to each other than when there is a certain velocity difference between the surfaces. This difference is often modeled as a static friction and a dynamic friction, respectively.

To get a better understanding of this stick-slip phenomenon, a simplified model was constructed. This model splits the motion into two parts: a stick part when the pig has no velocity and a slip part when the pig quickly moves forward. The conservation laws upon which this model is based were derived for conventional pigs only. However, this model can also give some insight in the stick-slip behaviour of by-pass pigs. With the stick-slip model an estimation of the length and frequency of the stick-slip cycles as well as the maximum attained velocity can be made. The parameters determining this are (1) the cross-sectional area of the pipe, (2) the operating pressure, (3) the mass flow rate, (4) the mass of the pig, (5) the friction of the pig and (6) the relation between the fluid properties, expressed in an equation of state. The underlying equations as well as the results are discussed in the following sections.

#### 2.1.3.1. Problem definition

The situation considered here is shown in figure 2.7. A pig is inserted into a pipeline which has two ends: an inlet and outlet. A list of the parameters involved is given in table 2.2. Basically, every parameter can be varied in the model. However, in the actual experimental set-up some of these parameters can not be changed. The values of those 'unchangeable variables' were already given in table 2.2. Furthermore, various assumptions are needed to simplify the actual situation. These assumptions are stated first. In later sections, these assumptions are used to rewrite the conservation laws on which the stick-slip model is based.

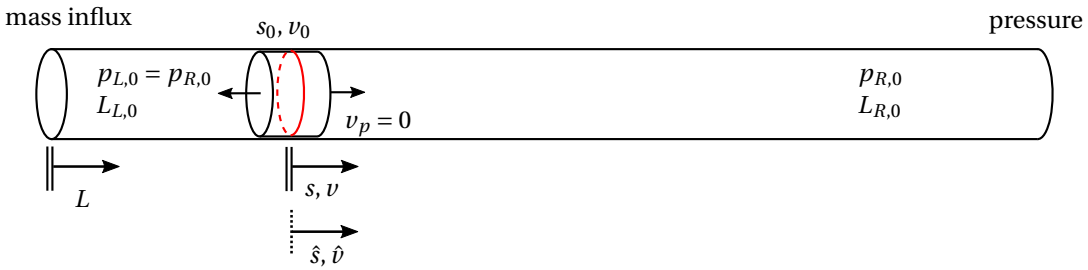


Figure 2.7: Pig inside a pipeline, initial state

Table 2.2: Parameters of the stick-slip model

| Parameter | Symbol | Value * | Unit |
|---|---|---|---|
| Pipe diameter | $D$ | 0.052 | $m$ |
| Cross-sectional area | $A$ | $2.123 \cdot 10^{-3}$ | $m^3$ |
| Total pipe length | $L_{tot}$ | 66.72 | $m$ |
| Pig mass | $M_{pig}$ | - | $kg$ |
| Static friction | $F_s$ | - | $N$ |
| Dynamic friction | $F_d$ | - | $N$ |
| Mass in-flow | $\dot{m}_{in}$ | - | $kg/s$ |
| Mass out-flow | $\dot{m}_{out}$ | - | $kg/s$ |
| Outlet pressure | $p_{out}$ | 100 000 | $Pa$ |
| Initial velocity | $v_{p,0}$ | 0 | $m/s$ |
| Initial position | $s_{p,0}$ | - | $m$ |

* A value is shown only when it is not or hardly varying during the experiments

*Assumptions*

The dimensions of the pipeline are significantly simplified. The pipe is assumed to be perfectly horizontal, the cross-sectional area is constant and the length is fixed. Furthermore, the friction acting on the pig is idealized in the following way: when the pig has zero velocity, the friction equals the static friction whereas the friction is equal to the dynamic friction when the pig is moving. At the inlet and outlet, boundary conditions are required. Here, a constant mass in-flux is assumed at the inlet. For the outlet, two approaches can be taken. The most general one is to assume a certain mass out-flux. More realistic is to assume a certain pressure outlet. It will be shown that the latter is actually a specific case of using the fixed mass out-flux. To see this, the most important assumption should be formulated first.

This assumption states that the properties of the fluid properties left and right of the pig are uniform. This is similar to assuming that the system undergoes a quasi-equilibrium process. Whether this assumption represents real pigging situations is questionable. A sudden acceleration of the pig will result in shock waves travelling through the domain, resulting in varying density and pressure over the pipeline. However, if these variation are small, the assumptions might work well and reduce the complexity of the model significantly. A consequence of assuming uniform fluid properties is that the conservation laws for the upstream and downstream section of the pig can now be applied rather easily. At the outlet, either a mass out-flux or a pressure is prescribed. If a pressure is prescribed, the complete downstream segment should be at that same outlet pressure.

A next assumption is the relation between the density and pressure. This relation is described using the ideal gas law, where the temperature and universal gas constant are considered constant. As soon as the density and pressure at one location are known at the same instant of time, they can be used to determine $RT$.

$$\frac{p}{\rho} = RT = \frac{p*}{\rho*} \tag{2.28}$$

*Notations*

In explaining the model, some notations appear which should be clarified first. The initial position of the pig with respect to the inlet is $L_{L,0}$. The position of the pig with respect to that initial position is called $x$. Summing up the two position gives the length of the upstream side called $L_L$. The length of the downstream side is called $L_R$ and is equal to the total length minus the length of the left pocket. For every pressure distribution, there is a position of the pig in which the average pressure on both side would be equal. This position is denoted as $x_{p,eq}$. The position of the pig with respect to that equilibrium position is denoted as $\hat{x}$. Next to this, there is a position at which the driving force on the pig is equal to the friction force. This friction equilibrium position is denoted at $x_{f,eq}$. The two equilibrium position depend on the inflow of mass and are moving at a certain velocity downstream through the pipe, called $v_{eq}$.

### 2.1.3.2. Governing equations

In this section, the governing equations describing the stick-slip motion of a pig are given under the assumption that the properties on both side of the pig are uniform. Furthermore, some general formulas for the system are given. The governing equations are further simplified and split into a stick and slip part.

*Conservation of mass*

At both sides of the pig, the mass conservation laws should hold. The mass inflow and outflow should be taken into account. For the upstream side, this mass flow is known, whereas for the downstream it is not. The conservation of mass is stated below for both the upstream and downstream side. Note that the mass inflow as well as the mass outflow are taken positive.

$$\rho_L(L_{L,0}+s)A = \rho_{L,0}L_{L,0}A + \Delta m_{in} \tag{2.29}$$

$$\rho_L = \rho_{L,0}\frac{L_{L,0}}{L_{L,0}+s} + \frac{\Delta m_{in}}{A(L_{L,0}+s)} \tag{2.30}$$

$$\rho_R(L_{R,0}-s)A = \rho_{R,0}L_{R,0}A - \Delta m_{out} \tag{2.31}$$

$$\rho_R = \rho_{R,0}\frac{L_{R,0}}{L_{R,0}-s} - \frac{\Delta m_{out}}{A(L_{R,0}-s)} \tag{2.32}$$

The pressure at both sides of the pig can be obtained from the equation of state. Using the ideal gas law (eq. 2.28) and substituting the initial pressure and density yields the following expression for the pressure as function of the displacement and the total mass flux:

$$p_L = p_{L,0}\frac{L_{L,0}}{L_{L,0}+s} + \frac{p_{L,0}}{\rho_{L,0}}\frac{\Delta m_{in}}{A(L_{L,0}+s)} \tag{2.33}$$

$$p_R = p_{R,0}\frac{L_{R,0}}{L_{R,0}-s} - \frac{p_{R,0}}{\rho_{R,0}}\frac{\Delta m_{out}}{A(L_{R,0}-s)} \tag{2.34}$$

In section 2.1.3.1 it was mentioned that two outlet conditions can be used. One is that the pressure at the downstream part of the pig is equal to the outlet pressure. For this to hold, one can derive an expression for the mass flux through the outlet ($\Delta m_{out}$) as function of the displacement of the pig, based on equation 2.34. This expression states that the total mass out-flux should be equal to the displacement of the pig times the area and density of the fluid on the downstream part ($\Delta m_{out} = \rho_{R,0}As$). Taking the time derivative of this expression yields the condition that the mass out-flow per second is equal to the velocity of the pig times the area and density. This is expected to hold, since the velocity of the pig and the mass out-flux are exactly balanced, which keeps the conditions at the downstream segment constant.

For the remainder of this report, it is assumed that the pressure at the downstream part of the pipeline is equal to the outlet pressure $p_{out}$.

*Driving force*

Using the formulas for the pressure upstream and downstream over the pig, one can construct an expression for the driving force by simply multiplying the pressure difference with the cross-sectional area. Doing so yields the following formula:

$$F_{drive} = \left( \left[ \underbrace{p_{L,0}\frac{L_{L,0}}{L_{L,0}+s}}_{\text{A}} + \underbrace{\frac{p_{L,0}}{\rho_{L,0}}\frac{\Delta m_{in}}{A(L_{L,0}+s)}}_{\text{B}} \right] - p_{out} \right) A \tag{2.35}$$

where: term A = Change in pressure upstream of the pig due to a change in position of the pig
term B = Change in pressure upstream of the pig due to inflow of mass
term C = Outlet pressure

*Average pressure*

The average pressure in the pipe is computed using a length weighted average, which results in equation 2.36.

$$\bar{p} = p_L\frac{L_L}{L_{tot}} + p_{out}\frac{L_R}{L_{tot}} \tag{2.36}$$

*Equilibrium positions*

The position of the pig in which case the pressure at both side are equal can be computed by equating the pressure at the upstream and downstream part of the pig. The result is given in equation 2.37. If the upstream pressure is instead equated with the downstream pressure plus the dynamic friction divided by the area, the friction equilibrium is obtained. The expression is shown in equation 2.38. The equilibrium position move through the pipeline due to the mass in-flux. This velocity is can be computed with equation 2.39.

$$x_{p,eq} = \frac{p_L L_R - p_{out} L_L}{p_{out} - p_L} \tag{2.37}$$

$$x_{f,eq} = \tfrac{1}{2}\frac{\left(p_L + p_{out}\right)A}{F} + \tfrac{1}{2}\left(L_R - L_L\right) + \tfrac{1}{2}\sqrt{\left(L_L - L_R - \frac{\left(p_L + p_{out}\right)A}{F_{friction}}\right)^2 + 4\left(L_R L_L + p_{out} L_L - p_L L_R\right)} \tag{2.38}$$

$$v_{eq} = \frac{\dot{m}_{in}}{\rho_L A} \tag{2.39}$$

If the pig moves along this position, the driving and pressure force on the pig are exactly canceled out. This implies that the pig moves in a steady-state. In section 2.1.2 a method for finding the steady-state velocity for a by-pass pig was discussed. That velocity turned out to be a function of the by-pass ratio, the fluid velocity, the density and the friction. Here, a steady-state velocity was computed for a conventional pig. This expression is merely a function of the mass in-flux for cross-sectional area and the density.

*Equation of motion*

The motion of a pig in situations where the assumption mentioned in section 2.1.3.1 are valid can be described by a s single equation of motion. This equation can be constructed in several ways. Two methods which give good insight into the behaviour of the system are discussed below.

*Newton's second law of motion:*

The most obvious method is to apply Newton's second law of motion, similar as was done in section 2.27 for quasi steady-state situations for by-pass pigs. The opposing force is due to friction. The driving force is due to a pressure difference over the pig, as was given in equation 2.35. Substituting this into Newton's second law of motion yields the following equation of motion:

$$M_{pig}\frac{dv_{pig}}{dt} = \left(p_{L,0}\underbrace{\frac{L_{L,0}}{L_{L,0}+x} + \frac{p_{L,0}}{\rho_{L,0}}\frac{\Delta m_{in}}{A(L_{L,0}+x)}}_{p_L} - p_{out}\right)A - F_{friction} \tag{2.40}$$

The right hand side of the above equation contains the driving force and friction force. Before, a pig position was computed in which these two forces exactly cancel out. The pig was said to be in a steady state. From equation 2.40 one can indeed see that this is true, since the acceleration of the pig should in that case be zero.

*Energy approach:*

The energyapproach is another method to construct the equation of motion for the pig. One method is to use the kinetic and potential energy in the system. The kinetic energy of the pig is:

$$E_k = \tfrac{1}{2}M_{pig}v_p^2 \tag{2.41}$$

The potential energy in the system can be computed when one considers the work exerted on the pig when it moves from its position $s$ to the equilibrium position while neglecting the friction. This can be computed by taking the work exerted over a distance $ds$ and integrating this over the total distance, as shown below.

$$E_{pot} = \Delta W = \int_x^{x_{p,eq}} \left(p_{L,0}\frac{L_{L,0}}{L_{L,0}+x'} + \frac{p_{L,0}}{\rho_{L,0}}\frac{\Delta m_{in}}{A(L_{L,0}+x')} - p_{out}\right)A dx' \tag{2.42}$$

$$= \left(p_{L,0}AL_{L,0} + \frac{p_{L,0}\dot{m}_{in}\Delta t}{\rho_{L,0}}\right)\ln\left(\frac{x_0 + x_{p,eq}}{x_0 + x}\right) - p_{out}A\left(x_{p,eq} - x\right) \tag{2.43}$$

The total energy is equal to the sum of the kinetic and potential energy. A change in the total energy is caused by dissipative forces, which in this case is the friction force. When one takes the time derivative of the work done by the friction force and the time derivative of the total kinetic energy, the following relation is obtained:

$$\begin{aligned}\frac{dW}{dt} &= \frac{dE_{tot}}{dt}\\ F_{friction}\left(\frac{dx}{dt}\right) &= \frac{d}{dt}\left(\tfrac{1}{2}M_{pig}\left(\frac{dx}{dt}\right)^2\right) + \frac{d}{dt}\left(\left(p_{L,0}AL_{L,0} + \frac{p_{L,0}\dot{m}_{in}\Delta t}{\rho_{L,0}}\right)\ln\left(\frac{x_0 + x_{p,eq}}{x_0 + x}\right) - p_{out}A\left(x_{p,eq} - x\right)\right)\\ &= M_{pig}\frac{d^2x}{dt^2}\left(\frac{dx}{dt}\right) - \left(p_{L,0}L_{L,0}A + \frac{p_{L,0}\Delta m_{in}}{\rho_{L,0}}\right)\frac{1}{L_{L,0}+x}\frac{dx}{dt} + \left(p_{out}A\right)\frac{dx}{dt}\end{aligned}$$

Dividing by $\frac{ds}{dt}$ and rewriting the equations yields the same equation of motion as stated in equation 2.40.

### 2.1.3.3. Simplified equation of motion

Equation 2.40 described the motion of a pig under the assumption as stated in section 2.1.3.1. One should keep also in mind that the friction force in this equation is depending on the velocity of the pig. Unfortunately, there is no analytical solution to this equation. Some extra simplifications are therefore made such that an analytical solution can be constructed. This might seem dispensable since the system could also be solved numerically. However, the further simplifications made here do not result in strongly deviating results. In addition, the analytical solution helps understanding the observed phenomena and results in a quick insight in the main characteristics of the motion as a function of the parameters that describe the pig motion (table 2.2).

Instead of solving the system at an arbitrary instant of time, the motion is split into a sticking and slipping part, as mentioned before. In the initial condition, the pressure at the upstream part of the pig is set to a value such that the driving force is lower than the static friction force. The pig location can be chosen arbitrarily and the velocity of the pig is set to zero. The pig therefore starts in the stick part of the motion, which is also a good representation of an actual pigging operation.

**Sticking part**

As long as the pressure difference over the pig is not high enough to overcome the friction, the pig has zero velocity and is said to be sticking. Due to the mass inflow at the inlet, the upstream pressure will rise. At the downstream part nothing is changing. This situation is maintained until the pressure difference is equal to the static friction divided by the cross-sectional area. The time this takes depends on the value of the mass in-flux and can be computed with formula 2.35. The mass in-flux ($\Delta m_{in}$) is equal to the elapsed time multiplied with the mass in-flux per second. This results in the following formula to compute the time required to overcome the static friction force:

$$\Delta t_i = \frac{\rho_{L,0}AL_{L,0}}{p_{out}\dot{m}}\left(p_{R,0} + \frac{F_{friction}}{A} - p_{L,0}\right) \tag{2.44}$$

**Slipping part**

The pig will start slipping as soon as the driving force equals the static friction force. The situation at the end of the sticking part will be used as input for the initial conditions of the slipping part. The equation of motion of the pig is described by equation 2.40, where now the dynamic friction should be used.

Since the equation of motion is not analytically solvable, it is rewritten in the form of a mass-spring system with an external force acting on the system, as stated in equation 2.45. A sketch of this is shown figure 2.8. This mass-spring system moves along with the dynamic friction equilibrium position. The displacement of the pig with respect to the initial position can therefore be computed by adding up the position relative to the equilibrium position and the position of the equilibrium position itself; $x = x_{p,eq} + \hat{x}$. The terms in the mass-spring system are assumed to be constant during one cycle only and are therefore denoted with subscript $i$. The methods of computing those terms as well as the initial conditions are discussed below.

$$M_{pig}\frac{d^2\hat{s}}{dt^2} + k_{eq,i}\hat{s} = F_{friction} \tag{2.45}$$

where: $\hat{s}$ = Displacement with respect to the equilibrium position
$k_{eq,i}$ = Equivalent spring stiffness

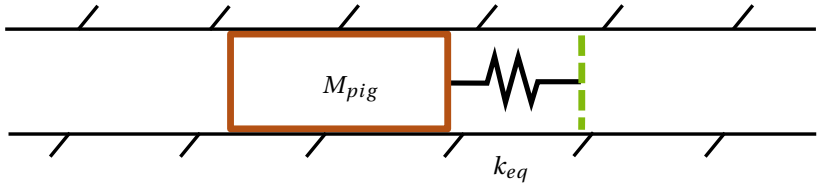


Figure 2.8: Mass-spring system moving with the equilibrium position

*Friction*

The right hand side of equation 2.45 represent the external force and consists of the friction only. A first difficulty is the fact that the friction force switches sign as soon as the motion is reversed. During the sticking part, this friction is assumed to be equal to the static friction whereas for the slipping part a constant dynamic friction is used.

Equation 2.45 is similar to a mass-spring system. Since it was just argued that the friction force can be taken constant, the system is actual equal to a mass-spring system in vertical position with gravity acting in the opposite direction as the displacement. The gravity force acts analogue to the friction force. In a static situation, this constant force leads to a offset equal to $\frac{-F_d}{k_{eq}}$. The solution to equation 2.45 is significantly simplified if it is expressed with respect to that fictive equilibrium position. The substitution causes the constant friction force to cancel out, which makes the right hand side of equation 2.45 equal to zero.

*Initial conditions*

A consequence of splitting the motion of the pig in a sticking and slipping part is that each cycle can be considered as a new initial value problem. If the velocity is zero, the friction force is equal to the static friction force. As soon as the pig starts moving, the friction drops to the dynamic friction force. This approach implies that the static friction is only responsible for the initial condition. It results in an initial position of the pig with respect to the equilibrium position. To determine the initial velocity, one should take into account that the equilibrium position is moving. This implies that although the pig has zero velocity with respect to the pipe, it has a negative velocity with respect to the frame of reference.

*Equivalent spring stiffness*

The extensive pressure force in the original equation is replaced by the simple term $k_{eq}\hat{s}$. This new force is equal to a constant times a displacement, similar as a spring force. The value of the equivalent spring stiffness should be chosen such that the original pressure force is represented as accurate as possible. A straightforward way is to compute the Taylor expansion of the force around the equilibrium position. The zeroth order term drops out and the first order term is used to find an equivalent spring stiffness.

$$k_{eq,i} = p_{out}A\frac{p_{out}}{(p_{out} + \frac{F_{friction}}{A})L_L} \tag{2.46}$$

Instead of using a Taylor expansion, also other approaches could be taken to compute an equivalent spring stiffness. The simplest method is to divide the pressure force by the distance with respect to the pressure equilibrium. A more complex method uses the energy approach. It turned out that all methods to model the pigging runs give comparable values. It was therefore decided to use the equivalent spring stiffness given in equation 2.46. Note that the equivalent spring stiffness is a function of the displacement. Since every slipping part is considered as a new new problem, a new equivalent stiffness should be computed accordingly.

**Solution**

The solution to equation 2.45 is given in equation 2.47. Taking the derivative of the displacement yields the velocity, which is given in equation 2.48.

$$\hat{x}(t) = C_i \sin(\omega_i (t - t_i) + \theta_i) \tag{2.47}$$

$$v(t) = C_i \omega_i \cos(\omega_i (t - t_i) + \theta_i) \tag{2.48}$$

where: $t_i$ = Starting time of the sticking part

$C_i = \sqrt{x_{f,eq,i}^2 + \left(\frac{v_{eq}}{\omega_i}\right)^2}$

$x_{f,eq,i} = L_L \left( \frac{p_{out} + \frac{F_s}{A}}{p_{out} + \frac{F_d}{A}} - 1 \right)$

$\omega_i = \sqrt{\frac{k_{eq,i}}{M_{pig}}}$

$\theta_i = \arctan2(s_{feq,i}, \frac{v_{eq}}{\omega_i})$

= phase shift

Figure 2.9 and 2.10 show the velocity and displacement of the pig with respect to the equilibrium, respectively. The figures on the left correspond to a bulk velocity of 2.5 $m/s$ whereas the figures on the left correspond to a bulk velocity of 5 $m/s$. After a quick acceleration, the velocity drops again and becomes negative with respect to the equilibrium position. The end of the slip part is ended when the relative velocity of the pig is again equal to minus the velocity of the equilibrium position. The pig velocity is set at zero and a new sticking part will start. A plot of the corresponding pressure as function of time during the first cycle is shown in figure 2.11. From the figures and the equation 2.48 it becomes clear that the pig will always return to a stick motion. Note that the displacement is computed with respect to the equilibrium position. The position of the pig with respect to the initial position is found after adding the equilibrium position. The cycle is visualized in figure 2.15

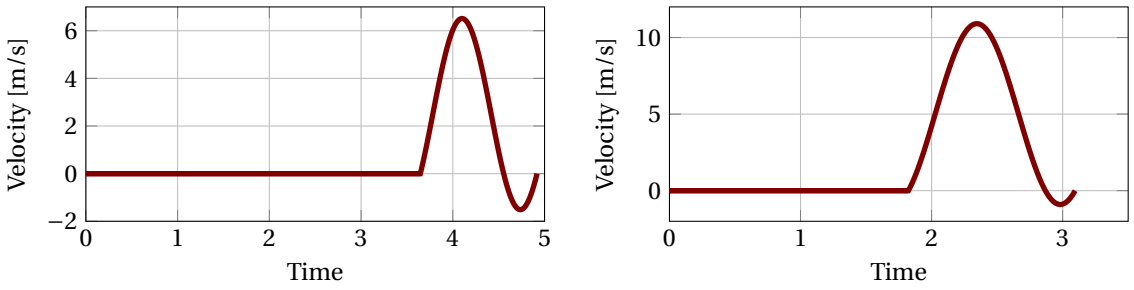


(a) Bulk velocity of 2.5 $m/s$

(b) Bulk velocity of 5 $m/s$

Figure 2.9: Velocity w.r.t. equilibrium position

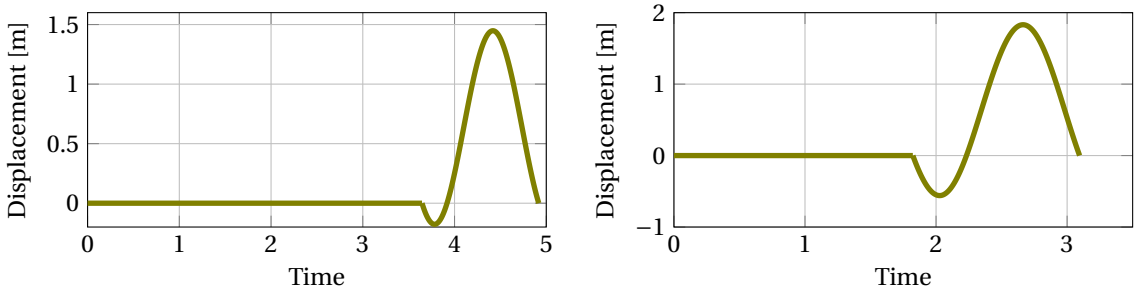


(a) Bulk velocity of 2.5 $m/s$

(b) Bulk velocity of 5 $m/s$

Figure 2.10: Pig displacement w.r.t. equilibrium position

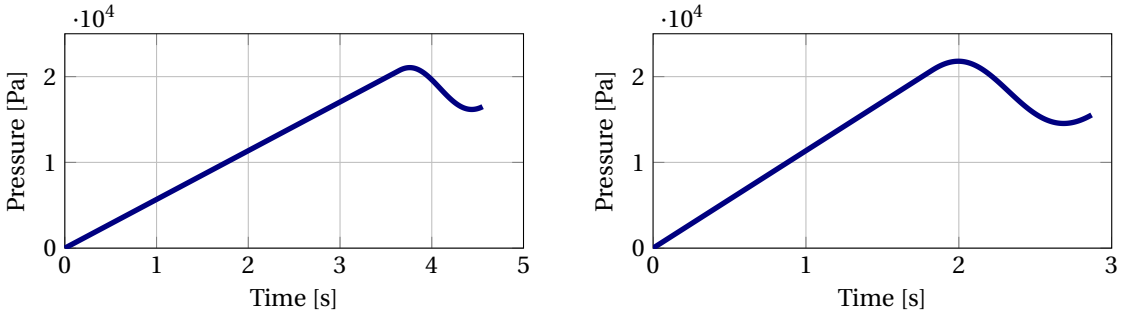


(a) Bulk velocity of 2.5 $m/s$

(b) Bulk velocity of 5 $m/s$

Figure 2.11: Pressure difference over the pig

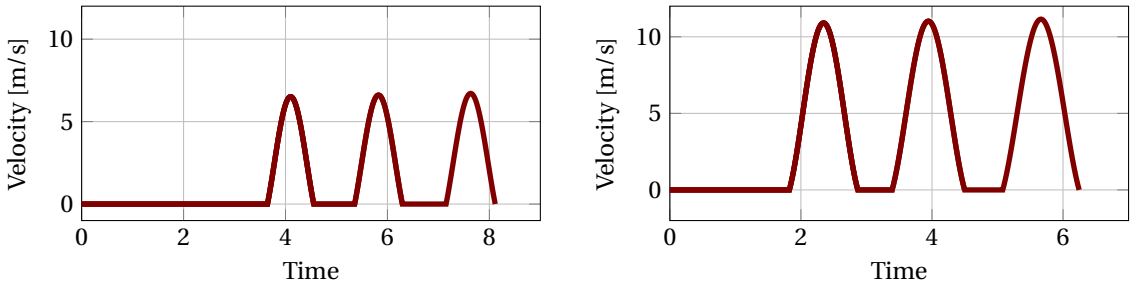


(a) Bulk velocity of 2.5 $m/s$

(b) Bulk velocity of 5 $m/s$

Figure 2.12: Pig velocity during first 3 cycles

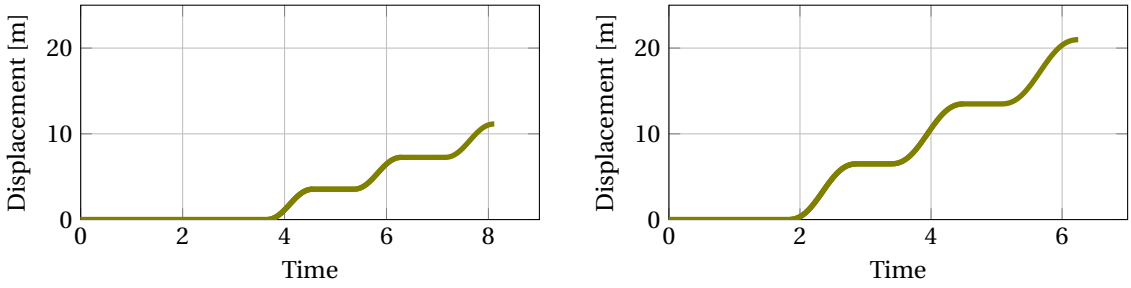


(a) Bulk velocity of 2.5 $m/s$

(b) Bulk velocity of 5 $m/s$

Figure 2.13: Driving pressure during first 3 cycles

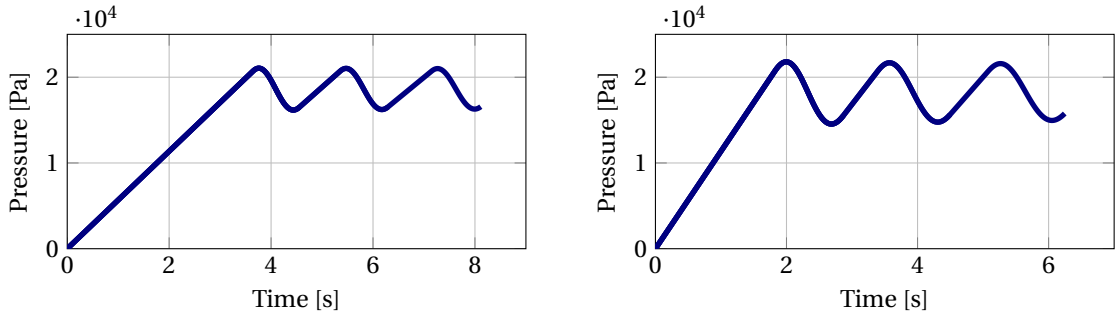


(a) Bulk velocity of 2.5 $m/s$

(b) Bulk velocity of 5 $m/s$

Figure 2.14: Pig displacement during first 3 cycles

### 2.1.3.4. Results

When adding the individual sticking and slipping parts, a complete (semi) analytical solution is obtained for a complete pigging run. This process is visualized for three cycles in figures 2.12 to 2.14. The results of the individual slip solutions give information on the characteristics of the stick-slip motion, as will be described below.

*Maximum velocity*

The maximum velocities observed during stick-slip motion are considerably higher than the steady-state velocity. The method to compute a steady-state velocity was discussed in section 2.1.3.4. The solution of the stick-slip model as stated in equation 2.48 can be used to get a quick estimation of the maximum velocity during a stick-slip cycle. Adding the maximum velocity with respect to the equilibrium velocity to that equilibrium velocity yields the following estimation:

$$v_{max} = v_{eq} + \sqrt{\frac{k_{eq,i} x_{f,eq}}{M_{pig}} + v_{eq}^2} \tag{2.49}$$

$$= v_{eq} + \sqrt{\frac{p_{out} A L_L}{M_{pig}} \frac{p_{out}}{p_{out} + \frac{F_s}{A}} \left( \frac{p_{out} + \frac{F_s}{A}}{p_{out} + \frac{F_d}{A}} - 1 \right)^2 + v_{eq}^2} \tag{2.50}$$

It is interesting to evaluate the influence of each the terms. First we look at the equilibrium velocity. The higher the equilibrium velocity, the higher the maximum velocity. When the other terms are all negligible with respect to the equilibrium velocity, the pig will reach a maximum velocity that is equal to twice the equilibrium velocity. This is due to the fact that the initial velocity of the pig is assumed to be zero with respect to the pipe.

The maximum velocity becomes even larger when the other terms are not negligible. These terms dictate the initial displacement. From the first factor under the square root sign in equation 2.50 one can conclude

that the maximum velocity will increase with an increasing value of the outlet pressure, cross-sectional area or length of the upstream pocket. The maximum velocity reduces when the mass of the pig is increased. This latter conclusion might seem counter-intuitive since a larger overshoot is expected when the mass is increased. However, the influence of the mass of the pig is incorporated in the frequency of the motion. A higher pig mass results in a lower frequency which lowers the maximum velocity. The last contribution to discuss is the friction. From expression 2.50 it becomes clear that a larger difference between the static and the dynamic friction results in a higher maximum velocity. If there is no difference, the initial deflection is zero and the maximum velocity is determined by the equilibrium velocity only. Furthermore, the larger the static friction is with respect to the outlet pressure, the larger the maximum velocity will be.

*Slipping distance*

The slipping distance can be estimated by looking at the displacement of a pig during the slipping part. The oscillating motion with respect to the equilibrium starts with a negative displacement and ends with a positive displacement. These displacements are associated with a certain angle that describes the oscillation. From the initial condition, one can compute the initial angle $\theta_i$, as was shown below equation 2.48. The second angle is equal to $2\pi - \theta_i$. The difference between the initial displacement and the final displacement with respect to the equilibrium position can be computed based on these angles and the amplitude. For the total displacement, one has to add the displacement of the equilibrium itself. This displacement is equal to the velocity times the time difference. The formula for the total slipping distance is as follows:

$$\Delta x = 2C_i \sin(\theta_i) + 2(\pi - \theta_i)\sqrt{\frac{M_{pig}}{k_{eq}}} \tag{2.51}$$

*Stick-slip frequency*

During a stick-slip motion, two frequencies are distinguished. The first frequency is the frequency of the slipping part. The expression for this frequency is shown below the solutions of the slipping oscillating, equation 2.47 and 2.48. Next to this, there is a frequency of the combined stick-slip motion. After a slipping part, the pressure behind the pig is lowered. It takes some time for the pressure to build up again before a new cycle is started. The frequency can therefore be computed from the displacement of the pig during a cycle and the equilibrium velocity. This is expressed with the following formula:

$$Frequency = \frac{v_{eq}}{\Delta x} \tag{2.52}$$

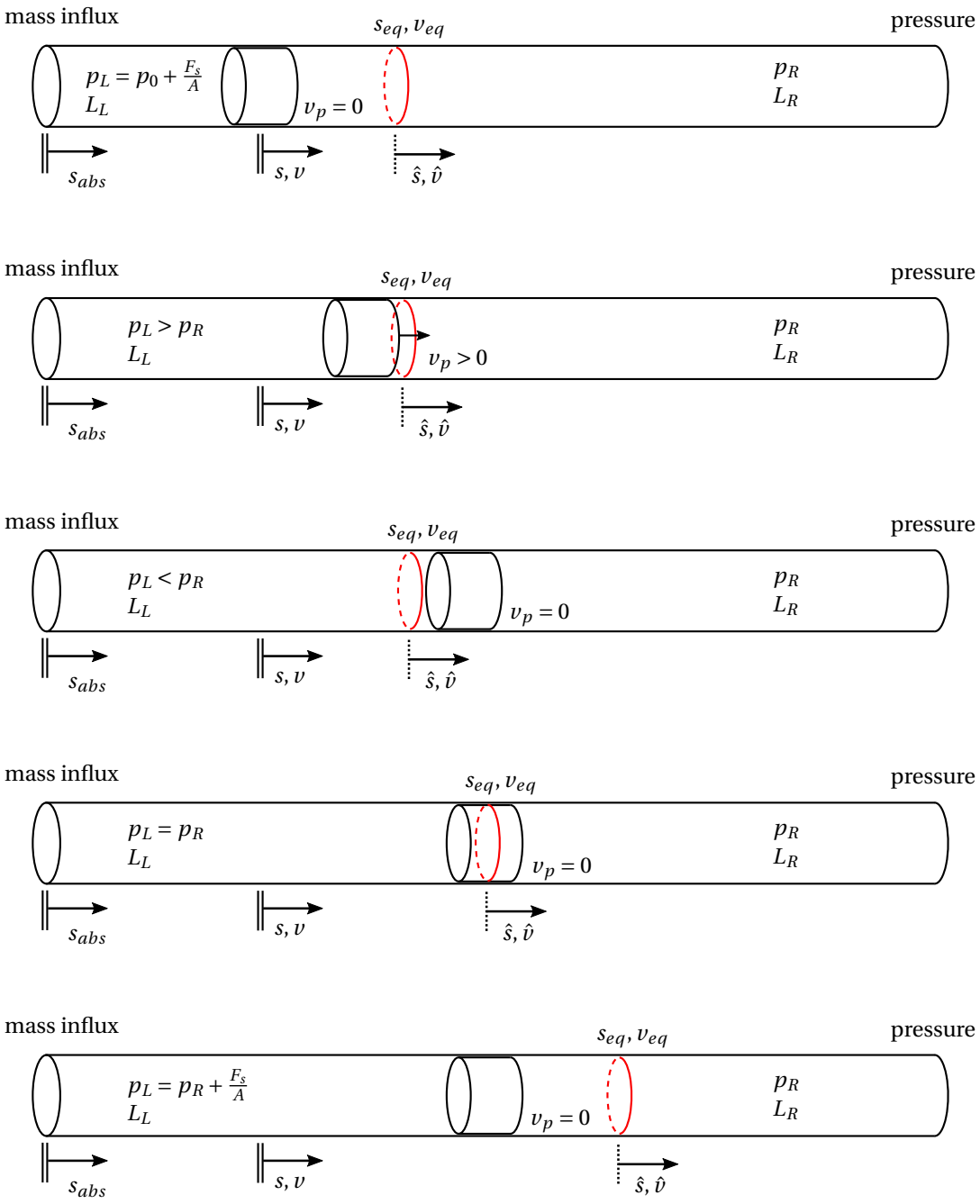


Figure 2.15: Stick-slip cycle

## 2.2. Numerical model

In the previous section a simple analytical model was constructed to get insight in the main characteristics of a pigging operation under the assumptions stated there. The rather rigorous simplifications were required to be able to solve the pigging model analytically. Instead of trying to find an analytical model, one can discretize the pipeline and use a numerical model. This requires less simplifications and can therefore result in a better simulation of an actual pigging operation.

The numerical pigging model discussed here was constructed by ir. M.H.W. Hendrix as part of his PhD research. Credits should also be given to B. Sanderse. The model has several solving options. Only the functions and methods used within this project will be discussed.

An overview of the continuous governing equations is given. These are subsequently be written in a discrete form. Those discrete governing equations are associated with a staggered grid, as will be explained. The boundary conditions are addressed, together with the method of incorporating the pig. Next, the approach of solving them is shortly discussed. Lastly, some preliminary results are provided.

### 2.2.1. Continuous governing equations

The pigging model is based on the one-dimensional Euler equations, which are extended to incorporate shear at the wall. Those Euler equations can be stated in various forms. Here, three different forms are discussed, as those are all used in the simulations.

*Extended Euler equations*

The Euler equations in one-dimensional form consist of a mass conservation law and a momentum conservation law. The normal Euler equations describe inviscid fluid flow. Pipe flow can in generally not be described accurately with the inviscid assumption. Wall shear in pipelines is generated by a velocity gradient perpendicular to the wall. Since one-dimensional equations are considered here, all information in the radial direction is lost. To account for this loss, a source term is added. The resulting extended Euler equations are given in equation 2.53 and 2.54, respectively. Next to this, an extra relation is required to solve for the three unknowns. This extra relation is provided by the equation of state, which is given in equation 2.56. It is common to write down the Euler equations in matrix form by gathering the time derivative terms and the spatial derivative terms, as shown in equation 2.57. This separation is useful when constructing a numerical model that marches in time.

$$\frac{\partial}{\partial t}(\rho) + \frac{\partial}{\partial x}(\rho u) = 0 \tag{2.53}$$

$$\frac{\partial}{\partial t}(\rho u) + \frac{\partial}{\partial x}(\rho u^2 + p) = \mathrm{s}_{friction} \tag{2.54}$$

$$\mathrm{s}_{friction} = \tfrac{1}{2}\rho u^2 \zeta_{friction} \frac{P_w}{A} \tag{2.55}$$

$$p + \hat{p} = \rho c^2 \tag{2.56}$$

$$\frac{\partial \mathbf{u}}{\partial t} + \mathbf{f}(\mathbf{u}, t) = \mathbf{0} \tag{2.57}$$

where:

| | | |
|---|---|---|
| $u$ | = | Velocity in the direction of $s$ |
| $\rho, \hat{\rho}$ | = | Density, reference density |
| $p, \hat{p}$ | = | Pressure, reference pressure ($\hat{\rho} c^2$) |
| $\mathrm{s}_{friction}$ | = | Source term accounting for friction |
| $\zeta_{friction}$ | = | Friction coefficient |
| $P_w$ | = | Circumference of the pipe |
| $A$ | = | Cross-sectional area |
| $c$ | = | Speed of sound |
| $x$ | = | Axis aligned with the pipe |

where:

$$\mathbf{u}(x,t) = \begin{bmatrix} \rho \\ \rho u \end{bmatrix}$$

$$\mathbf{f}(\mathbf{u},t) = \begin{bmatrix} \frac{\partial(\rho u)}{\partial x} \\ \frac{\partial(p+\rho u^2)}{\partial x} + \frac{1}{2}\rho u^2 \zeta_{friction} \end{bmatrix}$$

The friction force coefficient ($\zeta_{friction}$) can be computed in several ways. A common way is to use the relations suggested by Churchill. This approximation can be applied for both laminar and turbulent flow and is given in appendix A.1.1.

When combing the Euler equations and the equation of state, a quasi-linear system of equations can be constructed. Such equations consist of a time derivative of the variable **u** and a spatial derivative of the variable **u** multiplied with a so-called flux Jacobian. It depends on the used variable **u** how that flux Jacobian looks like. The most intuitive form uses $[\rho\, \rho u]^{\mathrm{T}}$, yielding the form shown in equation 2.58. This variable is called the conservative variable and the equations are called the conservative form. Another often used variable is $\mathbf{w} = [p\, u]^{\mathrm{T}}$, yielding equation 2.60. The variable is referred to as the primitive variable whereas the expression is denoted as the primitive form. A likewise transformation of variables is performed using a transformation matrix. Such a transformation matrix is a Jacobian matrix that consist of the derivative of the old variable with respect to the new variable. The transformation matrix **P** to go from the conservative to the primitive form is given in equation 2.2.1. For the reversed transformation, the derivative of the primitive variable with respect to the conservative variable is needed. This is simply the inverse of **P**. The new Jacobian flux matrix is constructed in a similar manner. The step-by-step transformation from equation 2.58 to 2.60 is given in appendix A.2.

$$\frac{\partial \mathbf{u}}{\partial t} + \mathbf{A}\frac{\partial \mathbf{u}}{\partial x} = -\mathbf{s}_u \tag{2.58}$$

$$\frac{\partial \mathbf{u}}{\partial t} + \mathbf{P}\mathbf{A}\mathbf{P}^{-1}\frac{\partial \mathbf{u}}{\partial x} = -\mathbf{s}_u \tag{2.59}$$

where:
$$\mathbf{A}(x,t) = \frac{\mathbf{f}(\mathbf{u},t)}{\partial \mathbf{u}} = \begin{bmatrix} 0 & 1 \\ c^2 - u^2 & 2u \end{bmatrix}$$
$$\mathbf{s}_u(x,t) = \begin{bmatrix} 0 \\ \mathrm{s}_{friction} \end{bmatrix}$$
$$\mathbf{P}^{-1} = \frac{\partial \mathbf{w}}{\partial \mathbf{u}} = \begin{bmatrix} 1/c^2 & 0 \\ u/c^2 & \rho \end{bmatrix}$$

$$\frac{\partial \mathbf{w}}{\partial t} + \mathbf{B}\frac{\partial \mathbf{w}}{\partial x} = -\mathbf{s}_w \tag{2.60}$$

$$\frac{\partial \mathbf{w}}{\partial t} + \mathbf{P}^{-1}\mathbf{B}\mathbf{P}\frac{\partial \mathbf{w}}{\partial x} = -\mathbf{P}^{-1}\mathbf{s}_u \tag{2.61}$$

where:
$$\mathbf{B}(x,t) = \mathbf{P}^{-1}\mathbf{A}(x,t) = \begin{bmatrix} u & \rho c^2 \\ 1/\rho & u \end{bmatrix}$$
$$\mathbf{s}_w(x,t) = \begin{bmatrix} 0 \\ \rho \mathrm{s}_{friction} \end{bmatrix}$$
$$\mathbf{P} = \frac{\partial \mathbf{u}}{\partial \mathbf{w}} = \begin{bmatrix} 1/c^2 & 0 \\ u/c^2 & \rho \end{bmatrix}$$

*Decoupled Euler equations*

Instead of choosing a new variable and finding the associated Jacobian flux matrix, one could also set a restriction on the Jacobian flux matrix and find the corresponding variable. A special situation is the one where the matrix is a diagonal matrix, which makes the two equations decoupled. The transformation matrix related to this can be found based on the eigenvalues and eigenvectors of the Jacobian flux matrix. The eigenvalues are the terms on the diagonal of the new Jacobian flux matrix, whereas the eigenvectors are used in the tranformation matrix. The whole procedure is given in appendix A.1. In equation 2.62 only the final form is provided with underneath the new variable and diagonal matrix. Next to this, the decoupled matrices are written out in full.

$$\frac{\partial \mathbf{q}}{\partial t} + \Lambda\frac{\partial \mathbf{q}}{\partial x} = -\mathbf{c}_q \tag{2.62}$$

$$\frac{\partial}{\partial t}(dp + \rho c\, du) + (u+c)\frac{\partial}{\partial x}(dp + \rho c\, du) = -\frac{1}{2\rho}\mathrm{s}_{friction} \tag{2.63}$$

$$\frac{\partial}{\partial t}(dp - \rho c\, du) + (u-c)\frac{\partial}{\partial x}(dp - \rho c\, du) = -\frac{1}{2\rho}\mathrm{s}_{friction} \tag{2.64}$$

where:
$$d\mathbf{q} = \begin{bmatrix} \frac{du}{2} + \frac{dp}{2\rho c} \\ \frac{du}{2} - \frac{dp}{2\rho c} \end{bmatrix}$$
$$\Lambda = \begin{bmatrix} u+c & 0 \\ 0 & u-c \end{bmatrix}$$
$$\mathbf{c}_q = \begin{bmatrix} \frac{1}{2\rho}\mathrm{s}_{friction} \\ \frac{1}{2\rho}\mathrm{s}_{friction} \end{bmatrix}$$

Now lets us consider the decoupled equations 2.63 and 2.64. The first equation states that the variable $dp + \rho c du$ does not change along the line $u + c$, whereas the second equation states that the variable $dp - \rho c du$ does not change along the line $u - c$. Variables which remain constant along a certain line are often referred to as invariants and corresponding lines as their characteristics. The velocity at which the information travels is equal to $u + c$ and $u - c$, respectively.

The diagonal matrix together with the transformation matrices can be used to decompose the quasi-linear equations stated before (eq. 2.58, 2.60). The results are shown in equation 2.66 and 2.65 respectively. Below, the transformation matrices are listed.

$$\frac{\partial \mathbf{u}}{\partial t} + \mathbf{T}\Lambda\mathbf{T}^{-1}\frac{\partial \mathbf{u}}{\partial x} = -\mathbf{c}_u \qquad (2.65)$$

where:
$$\mathbf{T} = \frac{\partial \mathbf{u}}{\partial \mathbf{q}} = \begin{bmatrix} \rho/c & -\rho/c \\ \rho(1+u/c) & \rho(1-u/c) \end{bmatrix}$$
$$\mathbf{T}^{-1} = \frac{\partial \mathbf{q}}{\partial \mathbf{u}} = \frac{1}{2}\begin{bmatrix} (c-u)/\rho & 1/\rho \\ -(u+c)/\rho & 1/\rho \end{bmatrix}$$

$$\frac{\partial \mathbf{w}}{\partial t} + \mathbf{S}\Lambda\mathbf{S}^{-1}\frac{\partial \mathbf{w}}{\partial x} = -\mathbf{c}_w \qquad (2.66)$$

where:
$$\mathbf{S} = \frac{\partial \mathbf{w}}{\partial \mathbf{q}} = \begin{bmatrix} \rho c & -\rho c \\ 1 & 1 \end{bmatrix}$$
$$\mathbf{S}^{-1} = \frac{\partial \mathbf{q}}{\partial \mathbf{w}} = \frac{1}{2}\begin{bmatrix} 1/(\rho c) & 1 \\ -1/(\rho c) & 1 \end{bmatrix}$$

The transformation matrices **S** and **T** that decouple the flux Jacobian matrices as stated above will be used in the numerical model to deal with the boundaries. To do so, the spatial terms are split into a term containing all information from the wave travelling to the left and a term containing all information from the wave travelling to the right. The full derivation is shown in appendix A.2.1. Below, only the final forms are shown in equation 2.67 and 2.68 for the conservative and primitive form, respectively. One could rewrite one equation into another rather easily by applying a transformation of the variables as was shown before.

$$\frac{\partial \mathbf{w}}{\partial t} + \mathbf{S}^+\mathscr{L}^+ + \mathbf{S}^-\mathscr{L}^- = -\mathbf{s}_w \qquad (2.67)$$

where:
$$\mathbf{S}^+ = \frac{1}{2}\begin{bmatrix} 1 \\ 1/(\rho c) \end{bmatrix}$$
$$\mathbf{S}^- = \frac{1}{2}\begin{bmatrix} 1 \\ -1/(\rho c) \end{bmatrix}$$
$$\mathscr{L}^+ = (u+c)\left(\frac{\partial p}{\partial x} + \rho c\frac{\partial u}{\partial x}\right)$$
$$\mathscr{L}^- = (u-c)\left(\frac{\partial p}{\partial x} - \rho c\frac{\partial u}{\partial x}\right)$$

$$\frac{\partial \mathbf{u}}{\partial t} + \mathbf{P}\mathbf{S}^+\mathscr{L}^+ + \mathbf{P}\mathbf{S}^-\mathscr{L}^- = -\mathbf{s}_u \qquad (2.68)$$

where:
$$\mathbf{P}\mathbf{S}^+ = \frac{1}{2}\begin{bmatrix} 1/c^2 \\ u/c^2 + 1/c \end{bmatrix}$$
$$\mathbf{P}\mathbf{S}^- = \frac{1}{2}\begin{bmatrix} 1/c^2 \\ u/c^2 - 1/c \end{bmatrix}$$

The matrices $\mathbf{S}^-$ and $\mathbf{S}^+$ contain the eigenvectors. The information coming from the left is captured in vector $\mathscr{L}^+$ whereas information coming from the right is captured in vector $\mathscr{L}^-$. Writing this out yields the following expressions:

$$\begin{bmatrix} \frac{\partial \rho}{\partial t} \\ \frac{\partial \rho u}{\partial t} \end{bmatrix} + \frac{1}{2}(u+c)\begin{bmatrix} 1/c^2\left(\frac{\partial p}{\partial x} + \rho c\frac{\partial u}{\partial x}\right) \\ \left(u/c^2 + 1/c\right)\left(\frac{\partial p}{\partial x} + \rho c\frac{\partial u}{\partial x}\right) \end{bmatrix} + \frac{1}{2}(u-c)\begin{bmatrix} \left(1/c^2\right)\left(\frac{\partial p}{\partial x} - \rho c\frac{\partial u}{\partial x}\right) \\ \left(u/c^2 - 1/c\right)\left(\frac{\partial p}{\partial x} - \rho c\frac{\partial u}{\partial x}\right) \end{bmatrix} = \begin{bmatrix} 0 \\ s_u \end{bmatrix} \qquad (2.69)$$

$$\begin{bmatrix} \frac{\partial p}{\partial t} \\ \frac{\partial u}{\partial t} \end{bmatrix} + \frac{1}{2}(u+c)\begin{bmatrix} \left(\frac{\partial p}{\partial x} + \rho c\frac{\partial u}{\partial x}\right) \\ \frac{1}{\rho c}\left(\frac{\partial p}{\partial x} + \rho c\frac{\partial u}{\partial x}\right) \end{bmatrix} + \frac{1}{2}(u-c)\begin{bmatrix} \left(\frac{\partial p}{\partial x} - \rho c\frac{\partial u}{\partial x}\right) \\ \frac{-1}{\rho c}\left(\frac{\partial p}{\partial x} - \rho c\frac{\partial u}{\partial x}\right) \end{bmatrix} = \begin{bmatrix} 0 \\ s_w \end{bmatrix} \qquad (2.70)$$

#### 2.2.1.1. Boundary conditions and initial conditions for euler equations

The Euler equations discussed in the previous sections are valid for the interior of the fluid domain, which in this case is a simple horizontal pipeline. The initial conditions together with the boundary conditions are required to uniquely solve the Euler equations. Essential in the formulation of the initial and boundary conditions is that they lead to a well-posed problem. Besides, they should represent a realistic pigging situation.

*Inlet conditions*

One can think of many different initial situations to start a computation. When looking at a pigging operations, a comparable initial condition would be obtained when the pig is inserted in a fully developed flow. To apply this, the fully developed pipe flow situation should be modelled first. The result of this can be used for the initial state of a pigging operation.

*Boundary conditions*

Also at the boundary, many different configurations are possible. For pipe flow a typical boundary condition for the inlet is a certain mass inflow. However, in experimental set-up a certain fluid velocity is set. For the outlet, one will typically find a certain pressure. A prescribed velocity at the inlet and atmospheric pressure at the outlet are therefore used when simulating pigging operations in the flowloop. To test the numerical pigging model, also other situations were considered.

### 2.2.1.2. Pig motion

The pig is considered as a cylindrical shaped object with fixed dimensions and mass. The motion is described by Newton's second law, which is stated in equation 2.1 in section 2.1.1. The friction force experienced by a pig is due to the contact surface between the pig and the pipe wall. It is a rather difficult phenomenon. There are many aspects playing a role, as was discussed in the introduction. Here, the friction force is strongly simplified. The assumption is that the pig experiences a relatively high static friction force when the velocity is close to zero, whereas a lower dynamic friction force is experienced at higher velocities. The method of implementing this into the numerical code is discussed in section 2.2.2.4. The driving force is caused by fluid. For a conventional pig, this force can be computed from the cross-sectional averaged pressure at the upstream and downstream part of the pig multiplied with the area. For by-pass pigs the approach is different. In section 2.1.2.3 it was shown that under the assumptions stated there, the driving force can be obtained from the pressure drop starting before the contraction and ending after the reattachment region. This pressure difference is computed as the pressure drop coefficient times the dynamic pressure in the by-pass. For the pressure drop coefficient, the formula suggested by Idelchik [23] as given in equation 2.17 is used. This results in the same equation of motion of the pig as was provided in section 2.1.2.4.

### 2.2.2. Discrete governing equations

The governing equations were derived in the previous section. These can be solved analytically only for very simple configurations. In general, the equations must be discretized and solved numerically. One can chose to discretize any form of the Euler equations. Here, the conservative form is considered. This sections explains the most important features of the numerical methods applied.

#### 2.2.2.1. Grid

First, a staggered grid as shown in figure 2.16 needs to be constructed. The domain is divided into $N$ elements with volume $\Omega^i$ and in $N+1$ elements with volume $\Omega^{i\pm\frac{1}{2}}$. The boundaries of the elements $\Omega^i$ in the interior are chosen to be halfway the elements of $\Omega^j$, and vice versa. At the boundary this is somewhat different, which also explains why the number of elements is not the same. The boundaries will be discussed in more detail in section 2.2.2.3. The quantities associated with $\Omega^i$ elements are the density $\rho^i$ and the mass flux represented by $\phi^{i\pm\frac{1}{2}}$. The quantities associated with $\Omega^{i\pm\frac{1}{2}}$ elements are the momentum along a line $q^{i\pm\frac{1}{2}}$, the momentum flux $\psi^i$ and the pressure $p_i$. The idea behind solving the system numerically is that these quantities are no longer continuously varying. Instead, they are only varying from volume to volume or from boundary to boundary. This is why it is referred to as discretisation. The total solution consist of a finite number of values associated to the volumes, which can be represented by vectors.

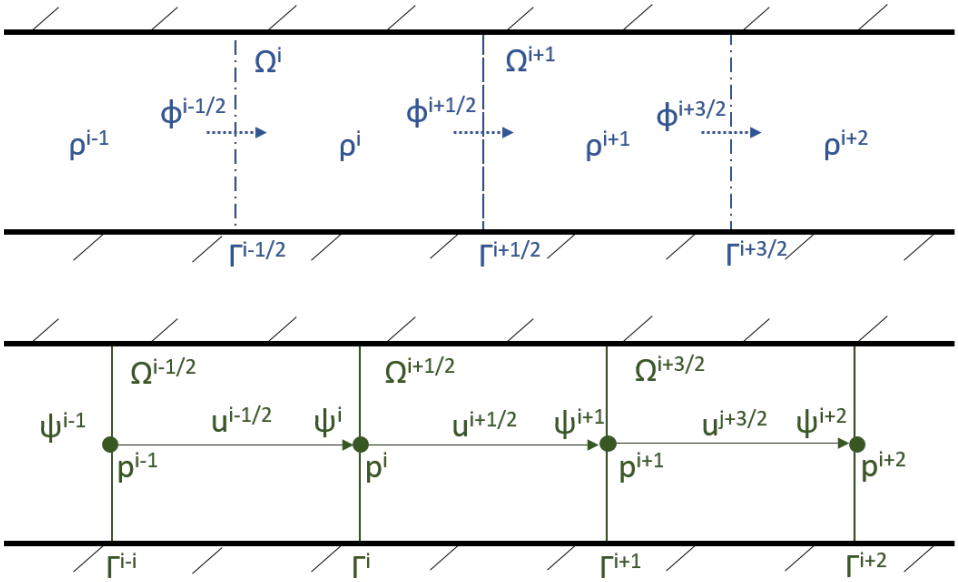


Figure 2.16: Staggered grid

#### 2.2.2.2. Discrete Euler equations

The extended Euler equations (eq. 2.53, 2.54) which are assumed to describe the system should still be satisfied. However, they must first be formulated in discrete form. Conservation of mass requires that the change in mass within element $\Omega^i$ plus the mass flux over its boundaries $\Gamma^{i-\frac{1}{2}}$ and $\Gamma^{i+\frac{1}{2}}$ should be equal to zero. This is stated in equation 2.71. The momentum equation is approached similarly. It says that the change in momentum within element $\Omega^{i+\frac{1}{2}}$ plus the momentum flux over its boundaries $\Gamma^i$ and $\Gamma^{i+1}$ should be equal to the pressure difference $p^{i+1} - p^i$ over the element. This is stated in equation 2.72. The mass and momentum equation contain three unknowns $(\rho, u, p)$. To close the system, a third relation is needed. This equation of state is similar to the one for the continuous case and is given in equation 2.73.

$$\frac{\partial}{\partial t}\left(\rho^i \Omega^i\right) + \phi^{i-\frac{1}{2}} - \phi^{i+\frac{1}{2}} = 0 \tag{2.71}$$

$$\frac{\partial}{\partial t}(u^{i+\frac{1}{2}} \rho^{i+\frac{1}{2}} \Omega^{i+\frac{1}{2}}) + \psi^i - \psi^{i+1} - p^i + p^{i+1} = \mathrm{s}_{friction} L^i \tag{2.72}$$

$$p^i + \hat{p}^i = \rho^i c^2 \tag{2.73}$$

where: $\Omega^i$ = Volume of element i

$\Gamma^i$ = Surface area of boundary between element $\Omega^{i-\frac{1}{2}}$ and $\Omega^{i+\frac{1}{2}}$

$L^i$ = Length of element i

$\phi_i$ = Total mass flux over boundary $\Gamma^i$

$\psi_i$ = Total momentum flux over boundary $\Gamma^i$

The total mass in an element is equal to the density integrated over the element whereas the total momentum in an element is equal to the density times the velocity integrated over the element. One can see that these integrals are rewritten as a constant times the size of the element. When working with the integrals, the above formulations are still exact. A first approximation comes in when one assumes the density $\rho^i$ and velocity $u^{i\pm\frac{1}{2}}$ to be constant in an element and use these to approximate the fluxes. In the numerical pigging code, the fluxes are approximated using a central interpolation scheme. This scheme is second order in space and is stated as follows:

$$\phi^{i+\frac{1}{2}} = \tfrac{1}{2}\left(\rho^i + \rho^{i+1}\right) u^{i+\frac{1}{2}} \Gamma^{i+\frac{1}{2}} \tag{2.74}$$

$$\psi^i = \rho^i \tfrac{1}{2}\left(u^{i-\frac{1}{2}} + u^{i+\frac{1}{2}}\right) \tag{2.75}$$

The right-hand-side of equation 2.72 represent the total wall shear in a volume element. This term is approximated by the friction force per unit length (eq. 2.55) multiplied with the length of the element. One should chose a density $\rho$ and velocity $u$ which are representative for the element under consideration. This involves interpolations from one grid to the other. The approximation of the friction is stated in equation 2.76 below. The friction coefficient is again computed with the Churchill relation (eq. A.5). This computation requires information about the quantities associated with the elements. A similar interpolation method as described above is used to approximate those variables.

$$\mathrm{s}_{friction}^{i+\frac{1}{2}} = \tfrac{1}{2} \cdot \tfrac{1}{2}(\rho^i + \rho^{i+1})(u^{i+\frac{1}{2}})^2 \zeta_{friction}^{i+\frac{1}{2}} P^{i+\frac{1}{2}} L^{i+\frac{1}{2}} \tag{2.76}$$

where: $P^{i+\frac{1}{2}}$ = Circumference of element $\Omega^{i+\frac{1}{2}}$

$L^{i+\frac{1}{2}}$ = Length of element $\Omega^{i+\frac{1}{2}}$

*System of first order differential equations*

In equation 2.57 in section 2.2.1 the continuous extended Euler equations were written into a form in which the time derivative term is split from the other terms. The same can be done for its discrete counterpart. In continuous form, the vector $\mathbf{u} = [\rho \quad \rho u]^{\mathrm{T}}$ is a continuous function depending on $x$ and $t$. In the discrete form, the vector $\mathbf{u}$ contains all the variables $\rho$ and $\rho u$ integrated over the volume of an element. In elements $\Omega^i$ the mass equation is satisfied, whereas in elements $\Omega^{i+\frac{1}{2}}$ the momentum equation is satisfied. This should hold for every element that builds up the domain. The total system of differential equations can be stated in a compact form when the solutions in each element are combined in one vector. This form is given in equation 2.77. The first term consist of the time derivatives, whereas the second term consist of the fluxes and sources. The vectors are given, where two interior elements are written out. The boundary elements are discussed in the next section. Note that only the location where the flux should be evaluated is indicated. The values might not be defined on that specific location, such that an interpolation from the center of an element to a boundary is required. This is done with a second order central interpolation scheme, as

was mentioned before. For this, an interpolation matrix can be constructed that performs the interpolation for all elements at once.

$$\frac{\partial \mathbf{u}}{\partial t} + \mathbf{f}(\mathbf{u}, t) = \mathbf{0} \tag{2.77}$$

where:

$$\mathbf{u}(t) = \begin{bmatrix} \vdots \\ \rho\Omega\big|^{i} \\ \vdots \\ \rho u\Omega\big|^{i+\frac{1}{2}} \\ \vdots \end{bmatrix} \tag{2.78}$$

$$\mathbf{f}(\mathbf{u}, t) = \begin{bmatrix} \vdots \\ \rho u\Gamma\big|^{i+\frac{1}{2}} - \rho u\Gamma\big|^{i-\frac{1}{2}} \\ \vdots \\ p + \rho u^2\Gamma\big|^{i+1} - p + \rho u^2\Gamma\big|^{i} + \frac{1}{2}\rho u^2 \zeta_{friction} PL\big|^{i+\frac{1}{2}} \\ \vdots \end{bmatrix} \tag{2.79}$$

### 2.2.2.3. Boundary conditions for the inlet and outlet

For the solution to become uniquely determined, boundary conditions should be applied and linked to the interior. In our model there are four boundaries. One at the pipe inlet, one at the pipe outlet, one at the left side of the pig and one at the right side of the pig. The pipe boundaries have a fixed position and part of the variables is prescribed there. In this section the method of finding the other variables at the boundaries will be explained. Once these are known, they can be linked to the interior by incorporating them into the flux term. In the next section, the method of incorporating the boundaries of the pig are explained. A difference with the pipe boundaries is that the pig boundaries can be moving. The method of dealing with these boundaries is similar to the method applied for the boundaries, as will become clear later.

*Pipe inlet and outlet*

As mentioned in section 2.2.1.1, a the condition at the inlet is a prescribed velocity, whereas at the outlet a certain pressure is often imposed. When looking at the quasi-linear continuous euler equations listed in section 2.2.1, one sees that one of the two variables in the vector is specified whereas the other is unknown. That other variable should follow from the conservation laws, which should be satisfied both in the interior as well as at the boundary. A problem that arises is that the governing equations as stated in the interior cannot be formulated likewise at the boundary. The interior was divided into elements in which the conservation of mass and momentum should be satisfied. At a boundary, there is no element, making it impossible to solve for the unknown variable in a similar way. A schematic view of the boundary is shown in figure 2.17.

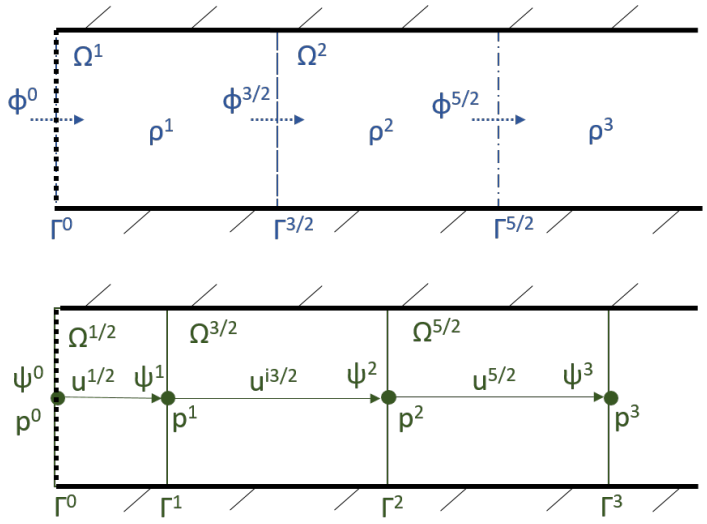


Figure 2.17: Staggered grid at inlet boundary

The approach used here to solve this problem is based on the travelling waves. In section 2.2.1 the Euler equations were decoupled using the eigenvectors of the flux Jacobian matrix. It was shown that so-called invariants could be constructed which do not change along the characteristics. The direction of the characteristics is defined by the eigenvalues of the flux Jacobian matrix. It is important to know that in subsonic flow, one characteristics is directed to the left whereas the other is directed to the right. For a point in the interior, both characteristics can be constructed numerically from the quantities defined at the surrounding elements. The information from both characteristics determines the solution. This relation between the characteristics and the solution is used in a smart way to link the boundary conditions to the interior: At the boundary only information from either the right side (left boundary) or left side (right boundary) is known. Therefore, only one characteristic can be constructed and the solution can not be found as in the interior. However, part of the solution is already described by means of the boundary conditions. The unknown characteristic can therefore be constructed by matching the boundary condition with the known characteristic coming from the interior and the unknown characteristic from the exterior. By doing so, the boundary is linked to the interior.

*Solving for the unknown boundary quantity*

The formulas to be used are the decoupled Euler equation given in equation 2.67 and 2.68. The first term in these equations includes all time derivatives. $\mathscr{L}^+$ in the second term includes the information that travels along the characteristic that moves with velocity $u+c$, whereas $\mathscr{L}^-$ in the third term includes the information that travels along the characteristic that moves with velocity $u-c$. The matrices $\mathbf{S}^-$ and $\mathbf{S}^+$ contain the eigenvectors. At the boundary, only the term associated with the characteristic coming from the interior can be constructed. By using the above mentioned matching approach, a characteristic coming from the exterior can be constructed and used to find the unknown part of the solution at the boundary.

Take for example the right boundary, where a constant pressure is prescribed. It is convenient to use expression 2.68 since this equation already includes the time-derivative of the pressure. The right boundary receives information from the interior, which is associated with $\mathscr{L}^+$. That term can therefore be computed using the solution in elements left of the boundary. $\mathscr{L}^-$ can be solved by making use of the known time derivative of the pressure, which is zero in this example situation. The calculation to be performed is stated in equation 2.80. Substituting $\mathscr{L}^-$ into the other equation gives an expression for the unknown variable at the boundary, as shown in equation 2.81. A similar procedure can be applied when other boundary conditions are prescribed. In subsonic situation as here, one of the variables should be applied at each boundary, the other follows from the above described approach.

$$\mathscr{L}^- = -\frac{\mathbf{S}^+(1)}{\mathbf{S}^-(1)}\mathscr{L}^+ \tag{2.80}$$

$$\frac{\partial u}{\partial t} = -\mathbf{S}^+(2)\mathscr{L}^+ - \mathbf{S}^-(2)\mathscr{L}^- + s_w \tag{2.81}$$

Once the conditions at the boundaries are known, they should be linked to the interior. This is done by incorporating them into the flux term. Equation 2.77 shows the Euler equation where the time derivative terms and the flux terms are separated. On the boundaries, the time-derivative of $\mathbf{u}$ is known. Moving this to the other side gives an expression for the flux terms for the element next to the boundary.

### 2.2.2.4. Pig motion

Also the pig is a boundary in the fluid domain. Its motion is described by Newton's second law, as explained in section 2.2.1.2 and stated in equation 2.1. This equation is monolithically incorporated into the code, implying that the equation of motion of the pig and the governing equations for the fluid domain are solved simultaneously. The friction forces on the right hand side of the equation of motion need further explanation. Firstly, the method of implementing the friction is discussed first. Secondly, the driving force is explained. This latter term is implemented in a similar manner for conventional pigs and by-pass pigs.

*Friction force*

As explained in section 2.2.1.2, the friction is modeled using a static friction for low velocities and a dynamic friction for higher velocities. However, implementing this in a numerical code is not that trivial. To explain the difficulties, the friction during a stick-slip motion is evaluated. Consider a conventional pig inserted in a pipe with equal pressures at both sides of the pig. The net force in this case should be zero, implying that

the friction force is also zero. As soon as fluid enters the domain through the inlet, the pressure builds up. The pressure difference is not yet high enough to push the pig forwards. To make the resulting force zero, the friction should therefore be equal to the driving force. This continues until the pressure force overcomes the static friction force. Thereafter, the pig accelerates to a higher velocity accompanied by a lower dynamic friction. This process is illustrated in figure 2.18. Both a positive and negative force are shown. Besides, different values for the positive and negative frictions are used. As long as the pig attains a high velocity, the friction will be equal to the dynamic friction. However, in stick-slip motion the velocity will decrease towards zero. At low enough velocities the friction will increase again up to the static friction value. In the extreme case that the pig velocity becomes negative, the direction of the friction is reversed and a negative static friction force should be used. This situation is illustrated in figure 2.19.

As explained above, the two friction approaches associated with figure 2.18 and 2.19 will occur alternating. The first approach to change between the different friction forces did apply several if-statements. Unfortunately, this caused problems with the convergence because the code started to alternate between the different if-statements. To solve this problem, a smoothing method was used. In this method a combination of the two approaches may occur. This is best illustrated with a surface plot as shown in figure 2.20. The height of the surface indicates the friction force. The depending variables are the pig velocity and the driving force. In most situations, the friction force depends on the pig velocity as described above. Only for pig velocities close to zero and a driving force below the static friction force, the other approach is used. 2-D logistic function are used to create a smooth transition between the different domains. The formulas are shown in equation 2.82 to 2.84. The steepness of the transition can be set by adjusting the values of $c$. Figure 2.20 uses a finite amount of points to draw the surface. In the numerical model, the friction can obtain any value on the surface. By using this method the alternation between the if-statements was eliminated.

$$F_{vel} = -F_d^- + \frac{F_d^- - F_s^-}{1 + e^{-c_T(v_{pig} - v_T)}} + \frac{F_s^+ - F_s^-}{1 + e^{-c_T v_{pig}}} + \frac{F_d^+ - F_s^+}{1 + e^{-c_T(v_{pig} - v_T)}} \tag{2.82}$$

$$F_{drive} = -F_d^- + \frac{F_{drive} + F_d^-}{1 + e^{-c_S(F_{drive} + F_S^-)}} - \frac{F_{drive} - sign(F_{drive})\, F_d^+}{1 + e^{-c_S(F_{drive} - F_S^+)}} \tag{2.83}$$

$$D_{vel} = \frac{1}{1 + e^{-c_D(v_{pig} + v_S)}} - \frac{1}{1 + e^{-c_D(v_{pig} - v_S)}} \cdot \frac{1}{1 + e^{-c_D(F_drive + F_S^-)}} - \frac{1}{1 + e^{-c_D(F_{drive} - F_S^+)}} \tag{2.84}$$

where:
- $F_{vel}$ = Friction force as function of the velocity
- $F_{drive}$ = Friction force as function of the driving pressure
- $D_{vel}$ = Domain at which the $F_{vel}$ should be used
- $F_d^{+,-}$ = Dynamic friction force when moving with positive (+) or negative (-) velocity
- $F_s^{+,-}$ = Static friction force when moving with low positive (+) or negative velocity
- $F_{drive}$ = Driving force
- $v_{T,S}$ = Transition velocity between static-dynamic (T) or stick-slip (S) friction region
- $v_D$ = Transition velocity between velocity considered zero and non-zero
- $c_{S,T,C}$ = Steepness of transition curves

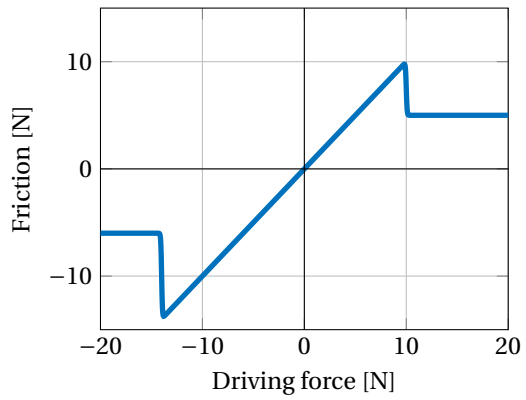


Figure 2.18: Friction as function of driving force

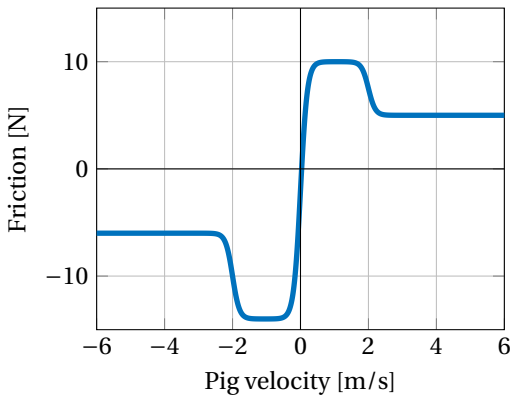


Figure 2.19: Friction as function of the pig velocity

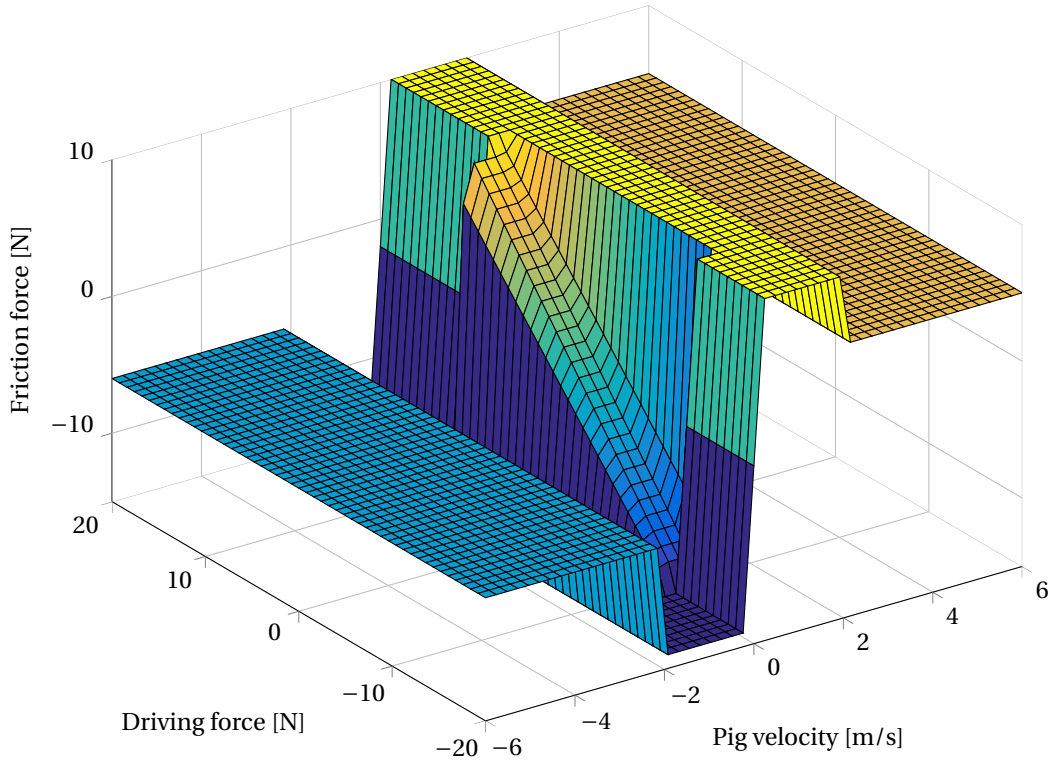


Figure 2.20: Friction as function of the pig velocity and the driving force

*Driving force*

The driving force on the pig is due to the pressure difference between the upstream and downstream side of the pig. For a conventional pig, the pressure upstream and downstream of the pig are not directly coupled. For a by-pass pig, the two pressures are coupled by means of the pressure drop relation suggested by Idelchik [23]. The pressures are in return coupled with the pig motion through the equation of motion of the pig (eq. 2.1). These coupled relations are solved simultaneously, which makes it a monotonic method. The coupling is incorporated in a similar manner as was done for the inlet and the outlet boundary. Consider again the governing equations as formulated in equation 2.67 and 2.68. At the boundary, one of the two variables should be prescribed whereas the other one follows from the governing equations. At the pig boundary, the time derivative of the velocity is prescribed. This is equal to the acceleration of the pig, which follows from the governing equation of the pig. Based on the known acceleration, also the other quantities on the pig boundary can be computed. For a conventional pig, the time derivative of the pressure is computed. For a by-pass pig, the coupling is more complex. One has to solve for a combination of quantities that also satisfy

the pressure drop relation suggested by Idelchik and the mass flux condition.

#### 2.2.2.5. Time marching method

In section 2.2.2.2 the discrete governing equations were written in a form in which the time derivative terms are combined in one vector and the other terms are combined in a flux vector. A detailed description of the flux term was given in the previous sections. For the sake of clarity, the Euler equation is stated again below:

$$\frac{\partial \mathbf{u}}{\partial t} + \mathbf{f}(\mathbf{u}, t) = \mathbf{0} \tag{2.77}$$

The first term represents the time derivative of the variable. One can use this derivative to compute the variable as a function of time. First, an initial solution should be defined that satisfies both the boundary conditions as well as the Euler equations. The solution at a next time step can be computed by integrating the equation in time. For the first time step, this is done using a first order Backward Differentiating Formula (BDF1). At subsequent time steps, a second order Backward Differentiating Formula (BDF2) is used. The time marching schemes are given equation 2.85 and 2.86 respectively.

$$\mathbf{u}_{n+1} = \mathbf{u}_n + \Delta t \mathbf{f}(\mathbf{u}_{n+1}, t_{n+1}) \tag{2.85}$$

$$\mathbf{u}_{n+1} = \tfrac{4}{3}\mathbf{u}_n - \tfrac{1}{3}\mathbf{u}_{n-1} - \tfrac{2}{3}\Delta t \mathbf{f}(\mathbf{u}_{n+1}, t_{n+1}) \tag{2.86}$$

BDF1 is first order accurate in time whereas BDF2 is second order accurate in time. The equation to solve is implicit and non-linear. Implicit since the flux term is computed based on the solution at the next time step. The goal is to find a solution at the next time step $\mathbf{u}_{n+1}$ such that the above equation is satisfied. This is done using a Newton-Raphson iteration method. To do so, the equation is first written in the following form:

$$\mathbf{g}(\mathbf{u}_{n+1}, \mathbf{u}_n, \mathbf{u}_{n-1}, t_{n+1}) = 0 \tag{2.87}$$

In the first iteration step, a guess about the solution is made. The first guess used here is the solution at the previous time step. This guessed solution will in general not satisfy the equation and a new guess should be made. This new guess is based on the Jacobian of the equation:

$$\mathbf{u}_{n+1}^{m+1} = \mathbf{u}_{n+1}^{m} - \frac{\mathbf{G}(\mathbf{u}_{n+1}^{m})}{\mathbf{G}'(\mathbf{u}_{n+1}^{m})} \tag{2.88}$$

where: $\mathbf{G}'(\mathbf{u}_{n+1}^{m})$ = Jacobian of $\mathbf{G}$ with respect to $\mathbf{u}_{n+1}$ and $t$

The next guess is computed in a similar way. This iteration process continues until the difference between two guesses is smaller than a certain threshold value. The latest guess is then used as the solution for the new time step. The solution at subsequent time steps is computed in a similar way.

*Order of accuracy*

Computing the terms of the discrete governing equations involves spatial integration. For this, a central differentiating scheme is used. This method is is second order accurate and is rather easy to implement. For the time marching method, a first order backward differentiating scheme (BDF1) is used for the first time integration step and a second order backward differentiating scheme (BDF2) is used for the subsequent steps.

### 2.2.3. Simplified numerical model

The numerical pigging model described above divides the pipeline in a certain amount of volumes. If only one element is used for the upstream and downstream domain, the model becomes comparable with the analytical stick-slip model. The comparison is even larger when the pressure in the downstream segment is always kept equal to the outlet pressure. The adapted numerical model will in the remainder of this report be referred to as the simplified numerical pigging model. The governing equation that describes the situation was derived in section 2.1.3.2 and is stated again below. For the analytical model extra simplifications regarding the pressure force and the friction were needed. When using the simplified numerical model, this is not necessary. The model can therefore be considered as an intermediate model compared to the analytical model and the full numerical pigging model.

$$M_{pig}\frac{dv_{pig}}{dt} = \left(p_{L,0}\frac{L_{L,0}}{L_{L,0}+x} + \frac{p_{L,0}}{\rho_{L,0}}\frac{\Delta m_{in}}{A(L_{L,0}+x)} - p_{out}\right)A - F_{friction} \tag{2.40}$$

# 3

# Experimental set-up

The flow loop in which the experiments were conducted is located at the Process & Energy building on the campus of the Delft University of Technical. The loop itself is already about 40 years old. In the beginning, when the loop was still located at the Shell lab in Amsterdam, the facility was merely used for experiments on slug flow, not for pigging experiments. Since 2015 the flow loop is located at its current location. Since then several modifications have been made. The flow loop used to consists of two long straight segments with a U-turn connecting them such that the inlet and outlet are at the same location. This first configuration allowed the simultaneous flow of both air and water, with the water tapped from and returned to the same reservoir. Due to difficulties with the U-turn in the pigging experiments, the second straight segment was uncoupled from the first. Besides, it was decided to focus this research on pigging experiments with air only. In the first section, the main characteristics of the flow loop as used for the pigging experiments of the current study are listed. In the subsequent section, the measurements devices are shortly described. The last part of this section is devoted to the characteristics of the pigs. Together they make up the total experimental set-up. In appendix B several photos are added to give an impression of the measurement equipment.

## 3.1. Flow loop characteristics

An overview of the flow loop is given in figure 3.2. The loop is built up from transparent perspex pipe segments with lengths of 2 $m$. Together they span a total length of roughly 62 $m$. Figure 3.1b shows a photo of the flow loop, where one can also see a pig inside. The air is tapped from a central system which is kept at a pressure of 8 $bar$ bar. A pressure reducing valve brings this down to 2 $bar$. The air then passes a flowmeter where the flow velocity can be controlled. More details are given in section 3.2.1. Just before entering the flow loop, the air flows through a pig-launcher. This part was designed to be able to insert the pigs. A photo is shown in figure B.5, whereas a design drawing is added to appendix B.1. The pig-launcher consist of a T-junction splitting up the pipes. By switching the valves, a pipe segment can be uncoupled from the flow loop in order to insert a pig while the fluid keeps flowing. Switching the same valves redirects the flow such that the pig is picked up and starts to move through the flow loop. At the end of the straight segment, a flexible tube is connected to the pipes. This tube is slightly larger than the nominal flow loop diameter. The tube ends in a pig catcher, which is simply a container with soft inner walls which ensures a soft landing. The air escapes to the atmosphere while the pig is caught in the pig catcher.

The individual pipes spanning the long straight segment are supported by small brackets. The brackets are mounted to large horizontal beams at a height of roughly 4 meters above the floor. Before starting with the experiments, the pipe segments were aligned as horizontally as possible. The process was as follows. First, the flow loop was closed and floated with water such that roughly half of the pipe was filled. It was made sure that the water surface was nowhere touching the top or bottom of the pipe. The water level was used to align the flow loop at 5 distinct places, located roughly 15 $m$ from one another. This was done using a measure around the pipe segments. The tolerance in the water level was measured to be roughly 2 $mm$. In between those locations, a laser and target were used to align the other parts. This was also done with an accuracy of roughly 2 $mm$. The local inclination is therefore below 0.01 $degr$, whereas the global overall inclination is even lower. In appendix B.1, several detailed photos of the flow loop and the aligning process are added.

The pipe segments are made of transparent PMMA, which is better known as perspex or plexiglas. Those pipes can be produced in two ways: extruded or moulded. Pipes produced in both manners are present in the flow loop. The mean outer and inner diameters of the pipes according to the manufacturer are 60 $mm$ and 52 $mm$, respecitvely. After contacting the manufacturer, tolerances of the inner and outer diameter were provided of $\pm$ 0.7 $mm$ and $\pm$ 0.8 $mm$. This implies that the inner diameter may vary between 52.7 $mm$ and 51.3 $mm$. This is in accordance with the observations made while measuring the inner diameter of several of the pipe segments. A difficulty caused by this variation is that it influences the friction between the wall and the pig. Within a pipe segment, the variation is continuous. However, from one pipe to another, sudden variations are present. More details on this are given in section 4.1.1. The pipe variation also had be taken into account for the pig design, as will be explained in section 3.3. A last aspect to mention regarding the pipes is the wall roughness. Roughness values of perspex are reported between 0.0015 $mm$ and 0.007 $mm$ [1]. However, on some of the pipe segments chalk deposit was observed which is expected to affect the value of the local roughness. It is recommended for future research that the pipe roughness is measured to obtain reliable values[2]. An overview of the main (average) characteristics of the flow loop is given in table 3.1.

In the overview of the flow loop as sketched in figure 3.2, also the measurement devices are indicated. The control station is next to the pig launcher. The first pressure sensor is located 74 $cm$ behind the pig-launcher. The second pressure sensor is located 41.4 meter further downstream. This is also the segment where three cameras are mounted. The flow loop segment within the field of view of the three camera's combined will in the remainder of this report be referred to as the measurement section. This location was chosen further downstream to eliminate the start-up effects. The end of the flow loop is 62 $m$ behind the first pressure sensor. An overview of the locations and field of view is listed in table 3.1.

[2] Removing the wax is why we perform pigging operations

[2] Obtained from `http://www.engineeringtoolbox.com/surface-roughness-ventilation-ducts-d_209.html`

(a) Pig launcher (b) Pig in the flow loop

Figure 3.1: Photos of the flow loop

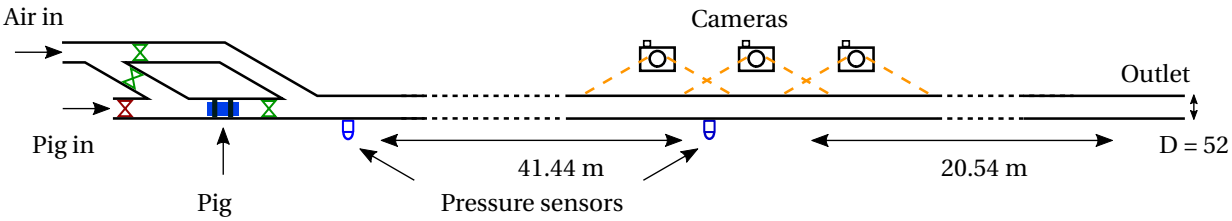


Figure 3.2: Sketch of the flow loop

Table 3.1: Properties of the flow loop

| **Property** | **Symbol** | **Value** | **Unit** |
|---|---|---|---|
| Inner diameter | $D$ | 52 | $mm$ |
| Total length | $L_{tot}$ | 62 | $m$ |
| Position pressure sensor 1 ** | $L_{p,1}$ | 0.74 | $m$ |
| Position pressure sensor 2 ** | $L_{p,2}$ | 42.18 | $m$ |
| Position F.O.V. cameras | $L_{fov}$ | 40 | $m$ |
| Width F.O.V. cameras | $\Delta L_{fov}$ | $\approx 7.5$ | $m$ |
| Maximum gas velocity | $v_{max,0}$ | 7.0 | $m/s$ |
| Exit pressure | $p_{out}$ | 1 | atm |
| Roughness ** | $\delta$ | 0.0015 - 0.007 * | $mm$ |
| Max. Reynolds number gas | Re | $\approx 16\,300$ | - |

* With respect to flow loop inlet
** Based on typical value for PVC and plastics [3]

[3] Obtained from `Engineeringtoolbox.com`

## 3.2. Measurement apparatus

The pigging operations are controlled and monitored using several devices. Each of these devices is shortly discussed below. After this, the data acquisition procedure is described.

### 3.2.1. Gas flow meter

For this research project, a new gas flowmeter was ordered (Bronkhorst - MASS-STREAM Series D-6300). A list of characteristics, in Dutch, as provided by the manufacturer is added to appendix B.2.1. The fluid flux ranges from 18 $lmin$ to 900 $l/min$, which corresponds to a bulk velocities in the flow loop of 0.14 $m/s$ and 7.06 $m/s$, respectively. The accuracy is said to be 2% of the maximum flux under calibration conditions. This calibration conditions are 3 $bar$ and 20 $°C$. The accuracy decreases with 2% per bar deviating from this. Since the upstream pressure of the flowmeter is 2 $bar$, the accuracy of the flow measurement is 4%.

The cross-sectional averaged velocity in the flow loop is computed by dividing the measured fluid flux with the cross-sectional area of the flow loop. When taking into account the accuracy of the flowmeter and the tolerance on the inner pipe diameter, the accuracy of the measured cross-sectional averaged velocity can be computed as follows:

$$v_{min} = \bar{v}(1-a) - 0.2825(1-a) \tag{3.1}$$

$$v_{max} = \bar{v}(1+b) + 0.2825(1+b) \tag{3.2}$$

where: $\bar{v}$ = Prescribed cross-sectional averaged velocity

$a = 0.0264$

$b = 0.0275$

This derivation is written out in appendix B.2.1. Next to this, leakage of air at pipe segment connections will reduce the flow velocity further downstream. To get an estimation of the leakage, the flow loop was first pressurized and then closed. The exponential reduction in the pressure as function of the time can be used to estimate the leakage. The measured pressure can be found in figure B.6 in appendix B.2.1. The pressure was increased up to 1.2 $bar$, which is a typical value for the upstream section during the pigging experiments. When combining this with the flow loop dimensions, the total mass can be computed. The same calculation are done after when the pressure has been decreased. Comparing the values gives the leakage in $kg/s$, which can be converted to a bulk velocity. At an over pressure of 1.2 $bar$, this turns out be 0.056 $m/s$. This leakage has the largest effect at low velocities. The minimum flow velocity during the experiments was 2 $m/s$, which corresponds to an extra error of 3%. This error will in general be lower since the leakage is likely to be spread over the flow loop. For further research it is recommended to measure the leakage in specific segments.

### 3.2.2. Pressure sensors

The pressures are measured using Validyne DP15 pressure transducers. A diaphragm inside the cubic device splits two small chambers, each of which is connected to the location over which the pressure should be measured. A pressure difference induces a deformation of the diaphragm, which results in a different electronic resistance. The used diaphragm has a range up to 0.86 $bar$. Although a pressure difference that high was never measured, it was still selected because of safety reasons. The voltage difference over the diaphragm is applied by a so-called carrier demodulator. This device delivers a second voltage output between -10 and 10 $V$. The formula of converting the voltage to a pressure depends on the configuration of the carrier demodulator and the diaphragm. It should therefore be calibrated first. The method of doing so is explained below.

*Calibration*

Both pressure sensors are calibrated by using a water column. A 10 meter long tube was filled with water and connected to the pressure sensor. At the other connection point a short tube was attached which was only partly filled with water. The pressure difference over the diaphragm can be calculated from the hydrostatic pressure difference. For the density of water and the gravitational constant, values of 998 $kg/m^3$ and

9.81 $m/s^2$, respecitvely were used. The long tube was placed on consecutive heights and the difference between the two water levels was registered. The tolerance of the measurements is less than a centimeter. This comes down to a variation of less than 100 $Pa$. The difference in pressure results in a different voltage output produced by the carrier demodulator. This demodulator was first set at a certain span and offset. The output voltage was measured using a standard multimeter. The measured pressures are plotted versus the voltage in figure B.7 in appendix B.2.2. The measured values show a linear relation between the measured voltage and applied pressure difference. A linear curve fit was therefore constructed using a least squares method. This method minimizes the sum of the squared errors, where the errors are defined as the difference between the curve fit and the measurement points. The obtained calibration curves are listed below the figures in the appendix B.2.2. They were fitted with a root mean square of the error of 132 $Pa$ and 174 $Pa$, respectively. Besides, also the 95% confidence bounds of the curve fits are given. Lastly, the manufacturer of the pressure sensors, Validyne, provides an accuracy of the DP15 pressure transducer of 0.25% of full scale. This comes down to a accuracy of 215 $Pa$.

*Tube connection*

The chambers inside the pressure sensor are linked with the flow loop via two tubes. The tubes are attached to a self-designed fitting connected to the pipe. The pressure in the tube will attain the same value as the static pressure inside the flow loop at that location. The tube connection creates a small irregularity in the pipe. The effect of this cavity on the measured static pressure is ignored. Photos of the tube and flow loop connection and the pressure sensors are shown in figure B.1. In table 3.2 the properties of air at 20 $degree$ and atmospheric pressure according to Engineeringtoolbox.com are given.

Table 3.2: Properties of air at 20 °C [4]

| **Property** | **Symbol** | **Value** | **Unit** |
|---|---|---|---|
| Density | $\rho$ | 1.205 | $kg/m^3$ |
| Dynamic viscosity | $\mu$ | $1.821 \cdot 10^{-5}$ | $kg/ms$ |
| Kinematic viscosity | $\nu$ | $1.511 \cdot 10^{-5}$ | $m^2/s$ |

### 3.2.3. Video recordings

The pigging operations was obtained with three GoPro cameras. They were mounted roughly 40 $m$ downstream of the inlet. The field of view of the cameras is in the remainder referred to as the measurement section. Each camera is detached to a arm which in return is mounted to the large beams, as shown in figure B.4b in appendix B.1. They are separated in such a way that part of the individual fields of view overlap. A code was written in Matlab to stitch the three individual recordings to one wide recording. The approach taken is shortly described below. Next to this, a method to synchronize the recordings in time was designed. The cameras are turned on using the same remote controller. However, there is still a mismatch of roughly one second in the starting time. The synchronization method is also shortly described. Finally, with the recordings both synchronized and stitched, a pig detection routine can be performed. A flowchart of the whole process is provided in figure 3.4. The images in that flowchart are stretched vertically to make them more readable.

Before continuing, some details of the GoPro cameras will be given. The lens of the camera creates a fish-eye image. The individual images are captured with a rolling shutter with a shutter speed depending on the frame rate. The output is an MPEG4 file compressed using h.264. The fish-eye effect can be removed with a program provided by GoPro. When loaded in Matlab, matrices are formed with dimensions equal to the chosen resolution. Besides the resolution, also the frame rate must be set. A trade-off between the two had to be made since a higher resolution goes along with a lower frame rate. The framerate was set to 120 frames per second and the resolution to 720p.

[4] Obtained from `Engineeringtoolbox.com`

*Stitching*

First of all, the images are rotated such that the flow loop is horizontal. This is done by clicking on two points at the left and right side of the image which should be horizontal. Based on this, a rotation angle can be computed, which is used in the remainder of the procedure. Next, the stitching can begin. The field of view of the middle camera overlaps at the right and left side with the neighbouring cameras. The image in the overlapping region is roughly the same. Objects in that region can therefore be used to correlate the images and perform the stitching. However, one should take some aspects into account. A discrepancy occurs due to a difference in the angle with which the cameras are looking at the region. This discrepancy is minimized when the object is very thin and oriented parallel to the lens of the camera. For stitching the images at a depth equal to the flow loop, the object should be positioned in the same plane. Two unique figures were therefore cut from a cardboard and placed on top of the flow loop in the overlapping regions. as can be seen in the flowchart in figure 3.4. When running the Matlab code, this part of the image can be selected manually in one of the recordings. Next, a cross-correlation between the selected part and the recording of the other camera is computed to find where both images overlap. The procedure is exactly the same for both overlapping regions. With the known overlap position, it is rather easy to stitch the three images to one wide image. As soon as this is done, one can narrow down the total field of view to the flow loop only. The final result is a small but wide window, covering approximately 8 $m$ of the flow loop. In the flowchart, one can see the results of this. A final thing thing to do in this stage is to determine the pixel distance. This is done by clicking on specific parts within the image where the location is known. Dividing the actual distance in meters between two locations by the pixel distance gives a pixel distance in the unit length per pixel. For the camera position used during the experiments, this turned out to be approximately 0.244 $cm$ per pixel.

*Synchronizing*

To synchronize the recordings in time, three led lamps are switched on simultaneously. When this happens, a sudden light increase in the light intensity is observed. This can be detected by looking at part of the individual images aimed at the lamps and sum over the pixel intensities of that region. For every recording, this certain increase is detected in a specific frame. When knowing the shift, the recordings can be synchronized. Furthermore, the time at which the lamps are turned on is registered. It is therefore possible to synchronize the recordings not only with one another, but also with the other measurements.

*Pig detection*

As soon as the stitching and synchronizing have been performed, a pig detection routine can be started. The goal of this is to detect to centre of the pig on each individual frame. This is done as follows. First, only a limited amount of frames is selected on which the pig is visible, called the pigging frames. Next, an average background is selected from several images in which no pig is visible. This average background is subtracted from the pigging frames. Due to the presence of a pig, there will be a larger difference in light intensities at locations of the pig in comparison with other locations. The differences are gathered in one matrix. Next, the matrix is converted to a binary matrix. Whether a value becomes zero or one depends on the threshold. This should mean that all values become zero except at the location of a pig. However, due to noise, a somewhat distorted cluster of ones will be formed. Using some build-in tools from Matlab, this cluster is smoothed. For instance by filling up 'holes' in the cluster and by removing ones that are surrounded by a single other one only. Next, the area weighted centroid of the cluster of ones is computed. Sometimes, an erroneous centroid is determined. For instance if, due to people passing by, the light intensity changes also on another location. Because some information onabout the motion of the pig is known, limitations on the founded centroid can be set. One does for example know that the centroid should always move in one direction and cannot jump over to large distances. Another problem is caused by the brackets supporting the pipes, since they block the field of view. An option was therefore build in that allows one to adjust or remove a found centroid by hand. At the end of the procedure, a centroid is found for a range of frames. In the output video, the centroids are traced. This final video shows the stitched and synchronized recording of the three GoPro cameras reduced in size and it shows the motion of the detected pig. Using the pixel distance, the pig position in meters with respect to the inlet of the flow loop can be determined. In addition to this, the position of the pig as a function of time is known since the measurements are synchronized in time, as explained before. Finally, by multiplying the frame rate with the distance covered by the pig between two frames, also the average velocity of the pig in between the two snapshots is known. Together with the flow and pressure measurements, this gives a detailed description of the pig motion when moving through the measurement section.

*Accuracy*

As mentioned above, a threshold is used as a criteria for the difference in light intensities to determine whether the value at that pixel location should be turned into a one. Around the centroid of the pig, this threshold will likely be reached. However, around the boundaries, the boundary is rather blurry both due to the scattering of light as well as the shutter speed. Moreover, the blurriness depends on the actual velocity of the pig and on the angle at which the pig is looked at. Figures 3.3a and 3.3b Show a snapshot of a pig moving at a low and high velocity, respectively. For interpretation of the results, it is important to have an idea on how accurate the pig can actually be detected. The estimation of the pig detection accuracy is based on visual observation. First, a frame is freezed. By zooming in into the pig, the blur around the pig boundaries is enlarged. Next, a pixel left and right of the blurred region are selected. The number of pixels in between the two selected ones is an indication of accuracy of the detection. For low pig velocities (1 $m/s$), the blur consists of roughly 5 pixels, which comes down to 1.2 $cm$. At high velocities, the number of pixels in the blurred boundary region can reach up to 20 pixels, which comes down to 4.8 $cm$.

(a) Pig at low velocity

(b) Pig at high velocity

Figure 3.3: Frames to show blurriness depending on velocity

### 3.2.4. Data acquisition

The pigging operations are controlled and monitored using devices discussed above. The flowmeter, pressure sensors and led lamps are connected to a computer by means of a National Instruments USB 6008 DAQ device (see appendix B.2.3). The device converts continuous inputs into discrete signals with a resolution of 12 bits. For the pressure sensors, this implies that the maximum change in pressure to be measured is 21 $Pa$, which is much smaller than the accuracy of the sensor itself. The control of the three devices is incorporated in one script written in Labview, National Instruments. A dashboard allows one to set and store the input and output of the devices. Since the sample time of the pressure sensors and the flowmeter are different, two different data sets are created. These sets are synchronized and coupled, resulting in a .txt file containing the following information:

- Sample number sensors
- Voltage output sensor 1
- Voltage output sensor 2
- Measured percentage of maximum fluid flux
- Lamp off (=0) or on (=5)

Next to the above mentioned devices, three GoPro cameras are recording the pigging operation. These cameras need to be turned on with a remote control. The synchronization with the other measurements is done based on the led lamps, as explained before. A nice feature to mention is that the sample rate is chosen such that the ratio is a certain integer. This allows one to couple the pig location as detected from the video recordings with the output from the gas flowmeter and pressure sensors.

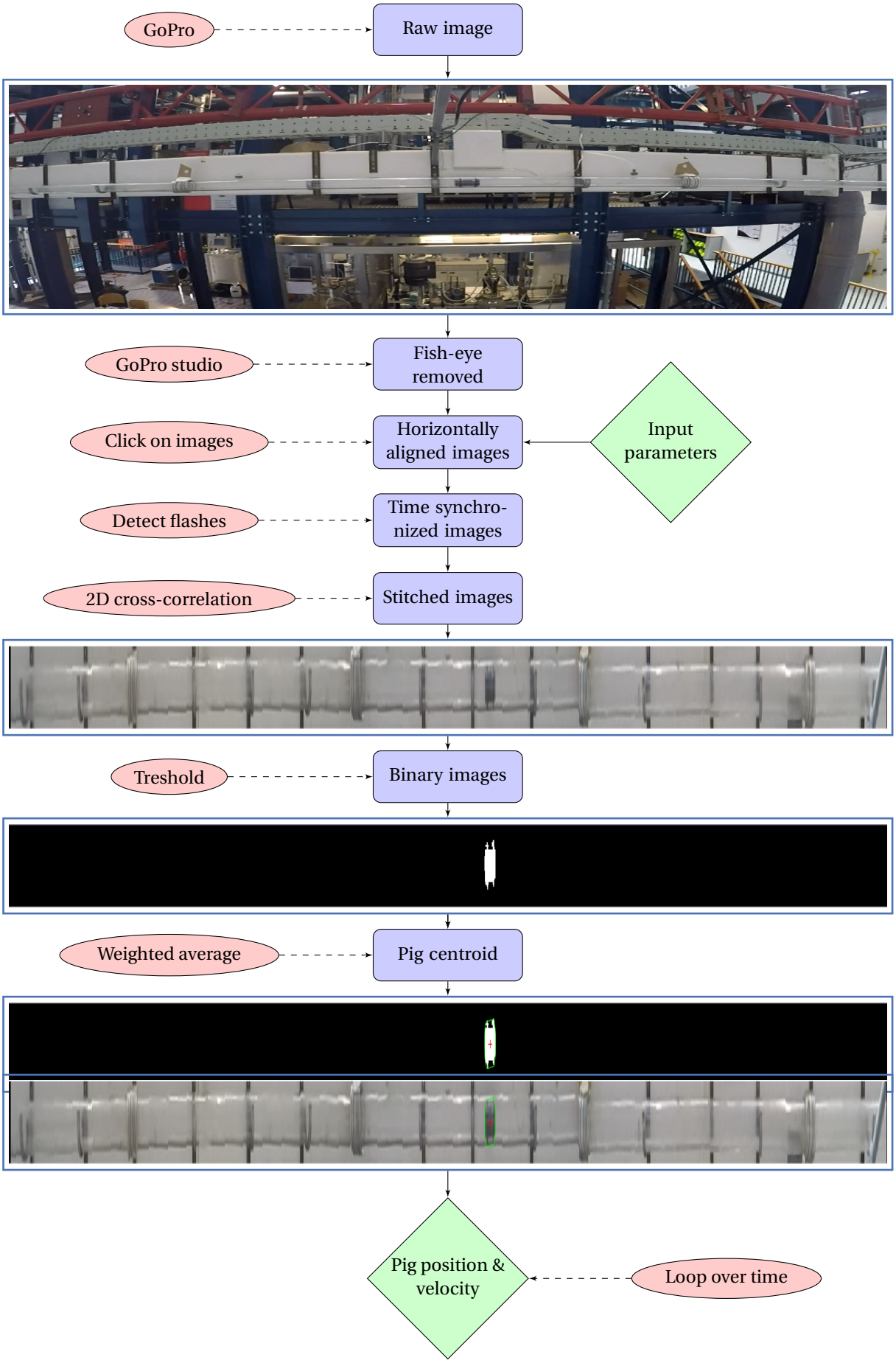


Figure 3.4: Flowchart of the video analysis process

### 3.2.5. Static friction

To get an idea of the friction between the pig and the wall, a simple static friction experiment was carried out. The pig was inserted in a short pipe segment. A string rope was inserted through the by-pass hole from the back through the front. This rope was guided over a cylinder and a bucket was attached. This bucket was slowly filled with water until the pig started sliding. The filled bucket was weighted with a balance that has a range from 0 to 5 $kg$. This mass was converted to a force, which should represent the static friction. This process was repeated several times for one specific configuration to reduce the error. In addition, this test was performed several times in between the actual pigging experiments. By doing so, insight in the consequence of wear on the friction was obtained. The results of this are given in the next chapter. Some photos of the measurement setup are shown in appendix B.3.2.

### 3.2.6. Data analysis

A typical pressure measurement result is shown in figure 3.5a. The steady state pressure drop was first subtracted from the measured pressure to get a better indication of the driving pressure. On the right vertical axis, also the velocity is shown. When a the pig passes a pressure sensor, the measured pressure rises rapidly. On the contrary, when the pig exits the flow loop a sudden decrease in the pressure is measured. These discontinuities are marked manually in the plot for each pigging run, as indicated by the red dashed vertical lines. When combining the time differences with location distances, an average travel time can be computed. Since the upstream sensor is located roughly 62 $m$ away from the outlet, there is a certain delay between the time the pig actually leaves the flow loop and the time the pressure drop decreases. This delay is equal to the distance divided by the speed of sound, which is roughly 0.2 $s$. When comparing the pigging runs for different configurations, average values will be used. The range taken into account in determining these averages starts 1 $s$ after the first discontinuity and ends 1 $s$ before the last discontinuity.

In figure 3.5a, two black lines are added to indicated when the pig is in the field of view of the cameras. Zooming in into this segments results in figure 3.5b. Now, the pig velocity is shown instead of the fluid velocity. The pressure measurements and the pig detection have already been synchronized in time. A first observation is that there is a certain time shift between the pressure sensors. This is again explained by distance between the sensors. When comparing the pig velocity with the pressure, one can see that the pressure drops as soon as the pig accelerates, which is expected.

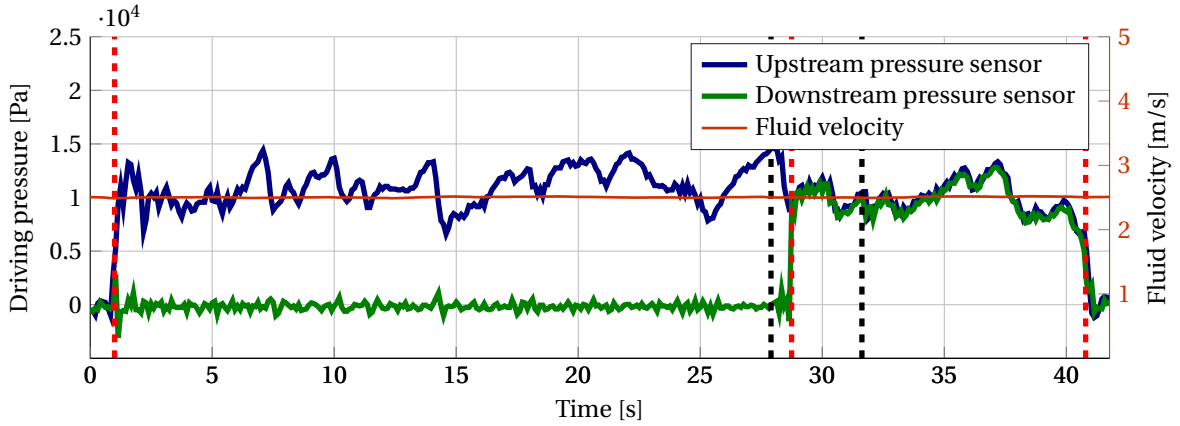


(a) Complete prun

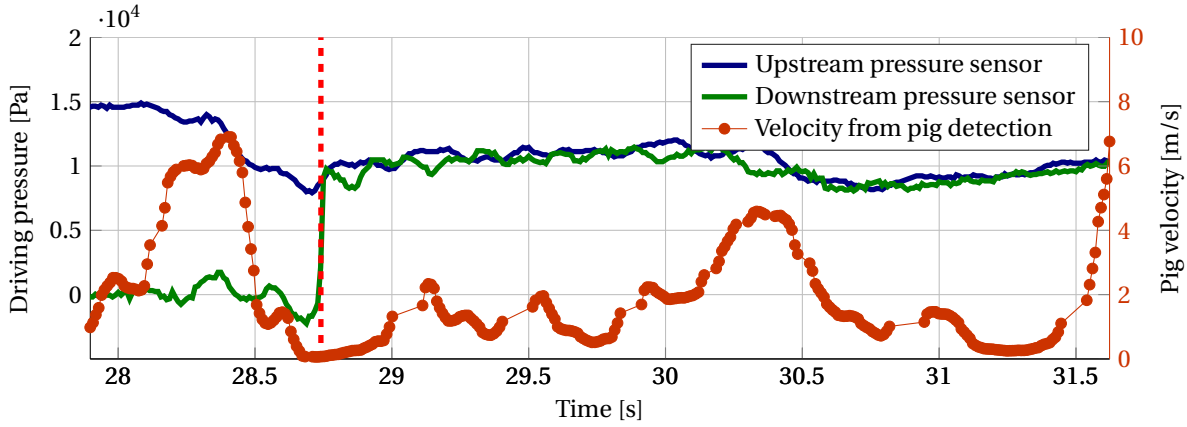


(b) Measurement section

Figure 3.5: Typical measurement results

## 3.3. Pig characteristics

In the introduction, several types of pigs were mentioned. A commonly used one is the so-called mandrel pig, which consist of a core where element can be mounted on to depending on the operation to perform. The design of the pigs used for the experiments in this research has been based on that type of pig. In this section, a description of the pigs used during the experiments will be given. This includes the configuration, dimensions and materials.

### 3.3.1. Dimensions

Two different pig configurations were extensively tested. Both pigs are build up from the following components:

- Core
- Sealing disks
- Clamping disks
- Rings
- Nuts

A 3D drawing and an exploded view of pig in configuration 2 with all the components are shown in figure 3.6. Five different core elements have been produced: one without a by-pass hole and four with a by-pass hole ranging from 1% to 8%. The other components can be moved over the outer ends of the core. The sealing disks are mounted to ensure that the inner diameter is completely sealed. They are clamped tight by the clamping disks. The nuts are screwed over the screw-thread to hold everything together. Rings can be placed in between the nuts to align the outer edge of the core with the end of the nut.

A large collection of sealing disks, clamping disks and rings was manufactured. Possible variation are the outer diameter, the thickness, the rounding and the material. The modular design then allows one to quickly change between different configurations. For example, if it was decided that the friction was too high, a sealing disk with less oversize, a thinner sealing disk or a sealing disk made from another material could be chosen. It turned out that even a small variation in the configuration can drastically change the behaviour of the pig. A more extensive description of the observed phenomena can be found in section 4.1.1.

For the parameter study, two configurations were selected. Some requirements on these configurations were that: (1) the pig remains horizontally aligned, (2) the pig does not move in a shaking manner and (3) the friction is such that the pig can move through the flow loop for a variety of fluid velocities. The dimensions of the two configurations are given in the 2D sketched in figure 3.7. The given mass holds for the % by-pass pigs. The mass lowers with 3 $gram$ per % by-pass hole. In appendix B.3.1 a more detailed table with the pig properties is provided.

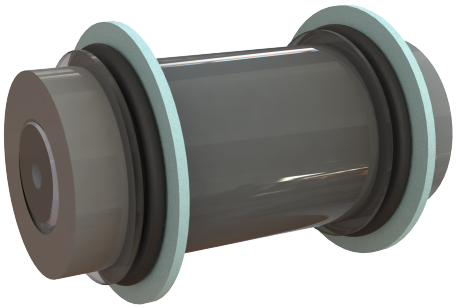

(a) Pig configuration 2

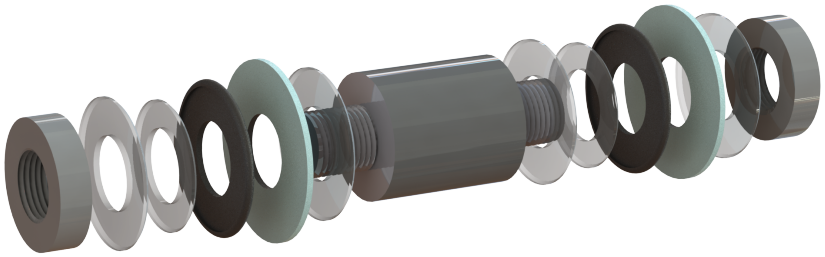

(b) Exploded view configuration 2

Figure 3.6: Part of recordings to show blurriness depending on velocity

### 3.3.2. Sealing properties

To build up enough pressure, it is essential that the pig seals the pipe properly. To ensure this, the sealing disks should first of all be impermeable. Next to this, one should makes sure that the seals cover the whole inner pipe circumference. They should therefore have a certain oversize, where the variation in the inner pipe diameter are taken into account. The two pig configurations have a different compression behaviour, which is illustrated in figure 4.3. The seals in configuration 1 are compressed in the radial direction. In industry, sealing disks deformed in a similar way are referred to as scraper disks [3]. Since the used material is rather flexible, the variation in friction is limited during diameter variations. Furthermore, the clamping disks can be relatively large in comparison to the inner pipe diameter. This prevents tilting of the pig. A downside of the flexible seals is that severe wear occurs. They had to be replaced after roughly every 6 runs. The seals in configuration 2 show a bending deformation. This is comparable with what is referred to in industry as cone disks [3]. The material itself is much harder and shows very good wear properties. A downside is that more space is required for the seals to bend, which increases the chance of the pig being tilted. From the pressure measurements, an estimation of the friction was obtained. This is described in more detail in section 4.1.2 in the next chapter. The average frictions for the two configurations are already listed in table 3.3. This table also provides other important properties regarding the sealing.

Table 3.3: Properties of pig configurations

| **Property** | **Configuration 1** | **Configuration 2** | **Unit** |
|---|---|---|---|
| Material sealing disk 1 | EPDM | Para rubber | - |
| Hardness sealing disk 1 | 35 * | 45 | *Shore A* |
| Outer diameter sealing disk 1 | 57 | 57 | *mm* |
| Thickness sealing disk 1 | 4 | 2 | *mm* |
| Material sealing disk 2 | EPDM | EPDM | - |
| Hardness sealing disk 2 | 35 | 35 | *Shore* |
| Outer diameter sealing disk 2 | 55 | 48 | *mm* |
| Thickness sealing disk 2 | 4 | 4 | *mm* |
| Average friction | 25.68 | 41.3 | *N* |

* The hardness is measured according Shore 00 standards. A comparable Shore A value is given here to compare with the other material

** The edges are rounded to space for the sealing disks to bend backwards

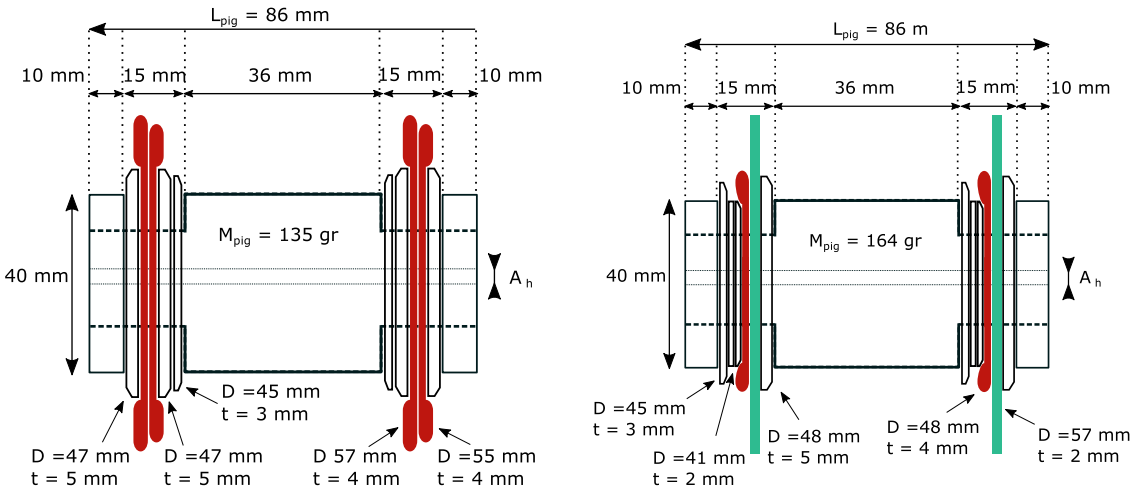


(a) Configuration 1 (b) Configuration 2

Figure 3.7: Dimensions of the pigs used for the parameter study

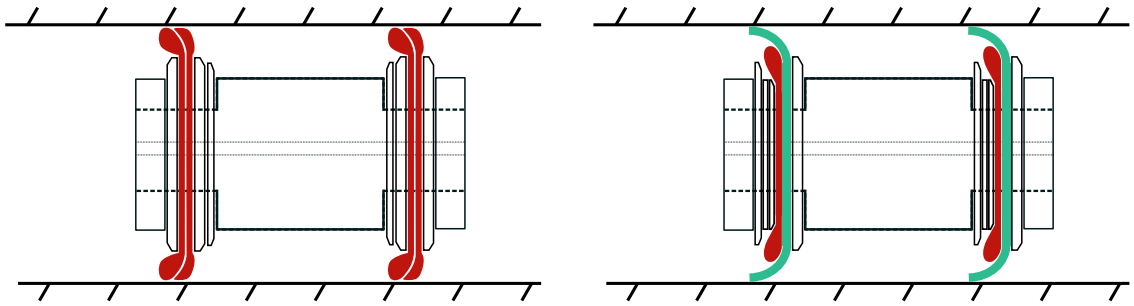

(a) Configuration 1 (b) Configuration 2

Figure 3.8: Compression of the pigs used for the parameter study

# 4

# Results

The main focus of this research is on the pigging experiments. A large amount of runs was conducted with varying pig configurations. Based on the findings, two configurations were selected for an extensive parameter study. The results are described in the first section of this chapter. In the second section, a comparison between the experimental results and results from the models are given. The comparison starts with comparing the mean quantities. At the end, also a comparison of the dynamic behaviour is made.

## 4.1. Experimental results

This section start with some general observation of the pigging runs. These observations already gave insight in the several phenomena playing a role in the behaviour of pigs. A more detailed insight in the behaviour was obtained from the parameter study with two pig configurations. The results of 72 pigging runs were used in the analysis of configuration 1. For configuration 2, 60 runs were included. The parameter study first concentrates on the global quantities. Secondly, an analysis of the local behaviour is given which focuses on a subset of the pigging runs.

### 4.1.1. General observations

The modular pig design allows for quick changes in the pig lay-out. A large number of pigging runs were performed to see the effect of changes in the configuration. It was observed that small changes could lead to a significantly different behaviour. Here, some of these observations are shortly discussed.

*Tilting*

Due to gravity, the bottom side of the sealing disks will in general be more compressed in comparison with the top side, resulting in a higher wall friction at the bottom side. Likewise, an irregularity in the flow loop may cause part of the sealing disk to be compressed more, yielding a higher wall friction on that specific part of sealing disk. As a consequence, the pressure acting at the upstream side of the pig will tend to tilt the pig over its front sealing disks. A schematic view of this is shown in figure 4.1a. The tilting has several implications. First of all, the by-pass hole is no longer aligned with the pipeline, which effects the pressure drop. Secondly, when the pig is tilted strongly, the clamping disks may come in contact with the pipe wall. As mentioned in the previous section, the pipe diameter may suddenly vary at pipe segment connections. The clamping disk may hit these extrusions and experience a sudden impulse force. To diminish this impact force, the clamping disks were rounded. Thirdly, when the upstream pressure varies because of a different pig velocity, also the tendency to tilt changes. This can cause the pig to start vibrating. Lastly, because of tilting the local area of the pipe that should be sealed increases. When the sealing disks are not stiff enough. they may collapse and result in leakage. A schematic view of this phenomena is shown in figure 4.1b.

The tilting tendency of the pig can be decreased by using stiffer sealing disks. This can be attained by using either another material, another thickness or by using clamping disks with a larger outer diameter. However, making the sealing disks stiffer also increases the friction. Furthermore, when increasing the outer diameter of the disks also the chance of hitting the wall increases. A trade-off should therefore be made. The pigs used for the parameter study showed good performance with respect to all aspects described above.

*Stick-slip*

A phenomenon observed during almost all runs was the so-called stick-slip behaviour. This entails the sudden acceleration and deceleration of the pig. When a pig has zero velocity, the upstream pressure will increase. When a certain pressure difference is reached, the pig quickly accelerates. The driving pressure quickly drops and due to friction the pig pig decelerates back to zero velocity. The same process then starts over. It is believed that this stick-slipping motion is triggered by a difference in the inner pipe diameter. Furthermore, the friction when the pig has zero velocity and when the pig is moving, is different. This is referred to as static friction and dynamic friction, respectively. The effect of a reduced inner diameter and higher static pressure add up since low velocities are expected at sections where the inner pipe diameter is decreased. The difference between the static and dynamic friction was larger for the pigs in configuration 1. Figures and show the measured pressures for configuration 1 and 2, respectively, with the same bulk velocity and by-pass area. The peaks are caused by a pig sticking at a pipe segment which has locally a smaller pipe diameter. The local friction at those segments is higher than the average friction and is referred to as the static friction. One can see that the relative peaks in the pressure are larger in comparison with the mean pressure for configuration 1 than for configuration 2. This might be caused by the difference in deformation when the pig has no velocity or when it is moving. In configuration 1, a rather different deformation is observed whereas the deformation of the seals in configuration 2 stays practically the same. It is recommended to investigate the friction phenomena in more detail in a future research project.

As a results of the larger difference between the static and the dynamic friction, also the stick-slip behaviour observed during the pigging runs with configuration 1 was more pronounced. Another observation was that stick-slip behaviour is more pronounced at low bulk velocities. In those cases there is a clear dis-

tinction between the sticking and slipping part. The slipping distance seems to increase when the pig is further downstream. For higher bulk velocities, there is also a variation in the velocity. However, it was seldom observed that the pig velocity drops down to zero, as was observed at lower bulk velocities. This can be explained by the fact that the pressure decrease upstream of the pig is less significant for high bulk velocities due to inflow of air during the slipping part. Next to this, it also takes more time to built up the pressure at a low bulk velocity. Since the stick-slip phenomenon was so dominant, several attempts were made to model this behaviour. The approaches were discussed in section 2 and a comparison with the experimental results is given in the next section.

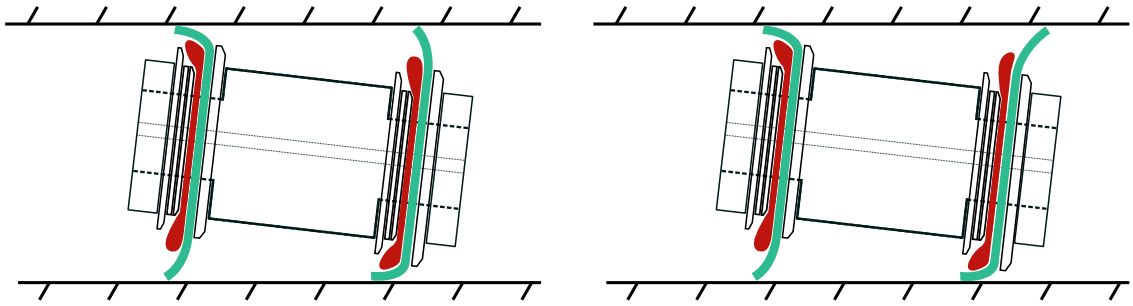

(a) Pig configuration 2 when tilted

(b) Pig configuration 2 when no longer sealed

Figure 4.1: Difficulties with the sealing disks

*Repeatability*

The fact that small changes may lead to quite different behaviour made it difficult to repeat experiments. Obviously, exact repeats of the pigging runs cannot be achieved. Instead, two configurations were chosen which showed rather similar behaviour for a large range of velocities. Look again at figure 4.2 where the measured pressure of two runs with the same pig configuration and the same bulk velocity is plotted in one figure. Figure 4.2a shows the runs in configuration 1 whereas figure 4.2b shows the runs in configuration 2. Although the signals show local variation, the average values are quite similar. The analysis of the measurement data was therefore first focused on average quantities. The analyzing process was explained in section 3.2.6.

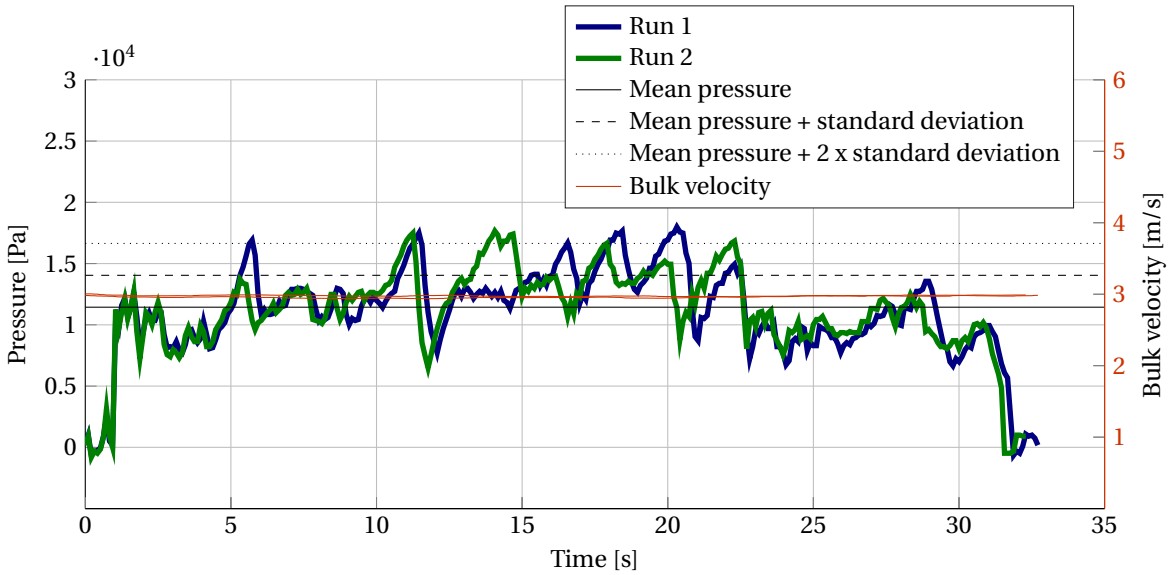


(a) Configuration 1

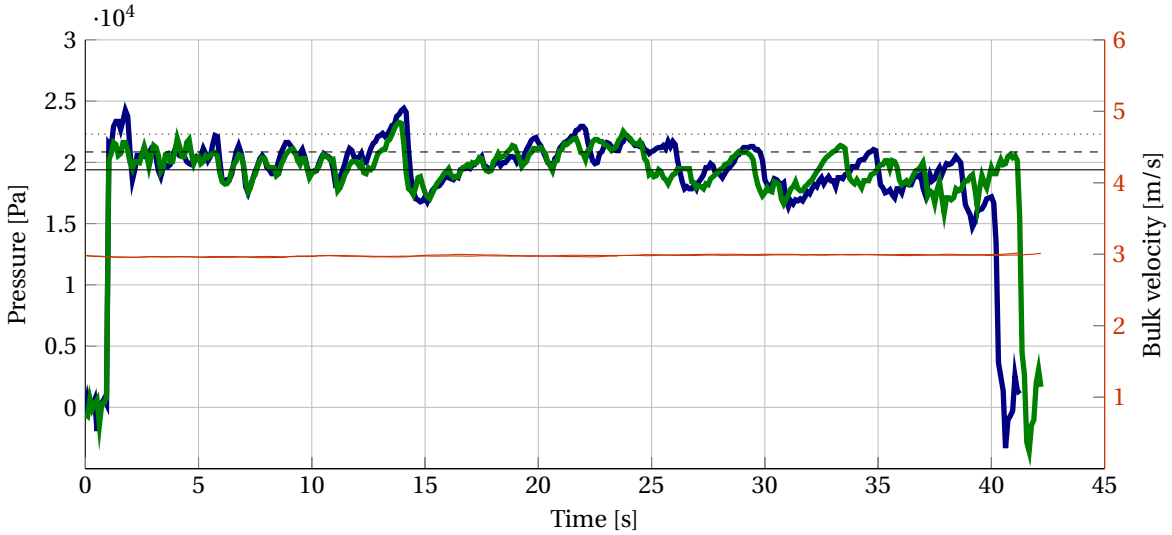


(b) Configuration 2

Figure 4.2: Pressure measurement of two runs with the same by-pass area at a bulk velocity of 3 $m/s$

### 4.1.2. Friction

The friction is an important input parameter to model the pig motion and should therefore be analyzed in more detail. As mentioned before, the friction between the pig and the wall will vary during a run due to local variations. Besides this, it will also vary from run to run since the seals suffer from wear. This is particularly true for the seals used in configuration 1. To get an estimation of the friction and the change in this friction, two methods were applied.

*Friction from pressure measurements*

From the pressure measurements, an average pressure drop over the pig during a pigging run is computed. This should be balanced by the friction. Multiplying the average pressure drop with the cross-sectional area gives the average friction, as was shown in section 2.1.2. In configuration 1, the seals were replaced multiple times. One average pressure was therefore computed. In configuration 2, the seals were only dismounted when another by-pass area was being tested. For each series a separate average friction factor was computed. Since the friction was computed during the pigging tests, they are a measure of the dynamic friction. All

values are listed in table 4.1.

When looking at the time series of a pressure measurement, clear peaks are observed. These peaks are associated with the static friction. The peak heights do unfortunately vary strongly. Besides, the width between peaks is not constant. An estimation of the static pressure was therefore made manually. Consider again figure . Together with the measured pressure, also the mean pressure and the mean pressure plus one and two times the standard deviation of the pressure are shown. For configuration 1 the peaks gather around the line of the mean pressure plus twice the standard deviation. That value was therefore chosen as a representation of the static friction and used in the models. For configuration 1, the mean pressure plus one time the standard deviation seems to better agrees with the pressure peaks and was therefore used as an estimation of the static friction.

*Static friction measurement*

To get an idea of the friction of the pig during the runs, a simple friction test was constructed, as mentioned in section 3.2.5. The tests were performed in between consecutive pigging runs to be able to analyze the influence of wear. Since the seals in configuration 1 had to be replaced more frequently, the approach was different in comparison with the static friction test of configuration 2.

Consider figure 4.3a. The total number of runs that are performed with the same set of sealing disks is shown on the x-axis. The solid lines represent the results from the static friction measurement. The dots are placed halfway between two runs to indicate the moment at which the static friction measurement took place. The error bars show the standard deviation of the measurements. In the same figure, also the dynamic friction as obtained from the pressure measurements during a run is shown. The static friction measured in between the runs turned out to be lower than the dynamic pressure during the runs. A possible explanation is the deposit of wax in the flow loop, which increases the pig wall friction. Another explanation is that the inner diameter of the pipe segment used for the static pressure measurement is larger than the mean diameter of the flow loop. Although the exact values may not be realistic, the change in the measured friction after consecutive runs gives insight in the influence of wear. One can see that the measured static friction drops significantly after one run. In the follow-up test, the decrease in friction is only limited. This trend is observed in both the static measurement and from the dynamic analysis. The sudden drop of the friction after the first run is explained by the deformation of the sealing disks when moving through the flow loop. Before the first run, the seals looked clean and smooth. After the first run, the seals showed substantial wear. However, this was not much larger after consecutive pigging runs. A photo of the sealing disks after a pigging runs is shown in figure C.1a in appendix C.

The seals used in configuration 2 could withstand the wear much better. A photo of the pig in after a pigging run is shown in figure C.1b in appendix C. The same seals were used during all pigging runs. They were only dismounted after the runs with a specific by-pass area were completed. The static measurements were performed before and after the set of test with 1% and 2% by-pass area. The number of pigging runs performed with the same sealing disk in between two static friction test was therefore much larger. Consider figure 4.3b. The solid lines do represent the static friction measurement results whereas the points on the dashed lines represent the dynamic friction computed from the pressure measurement during the pigging runs. Only the dynamic friction in the runs before and after the static measurement are shown. The static measurement again under-predicts the dynamic friction values. More important is the trend in the friction. The friction turned out to stay on average unchanged after a set of pigging runs. Only when the seals were removed and mounted on another pig core, a change in the average pressure was measured. This is the reason that three different values of the friction are used associated with each by-pass ratio.

Table 4.1: Properties of pig configurations

| **Property** | **Dynamic friction** | **Standard deviation** | **Static friction** * | **Unit** |
|---|---|---|---|---|
| Configuration 1 | 4 | 5.90 | 31.59 | $N$ |
| Configuration 2 (0 % by-pass) | 40.34 | 3.65 | 43.99 | $N$ |
| Configuration 2 (1 % by-pass) | 44.38 | 4.59 | 48.97 | $N$ |
| Configuration 2 (2 % by-pass) | 39.26 | 2.88 | 42.13 | $N$ |

* The static friction stated here is equal to the dynamic friction plus the standard deviation

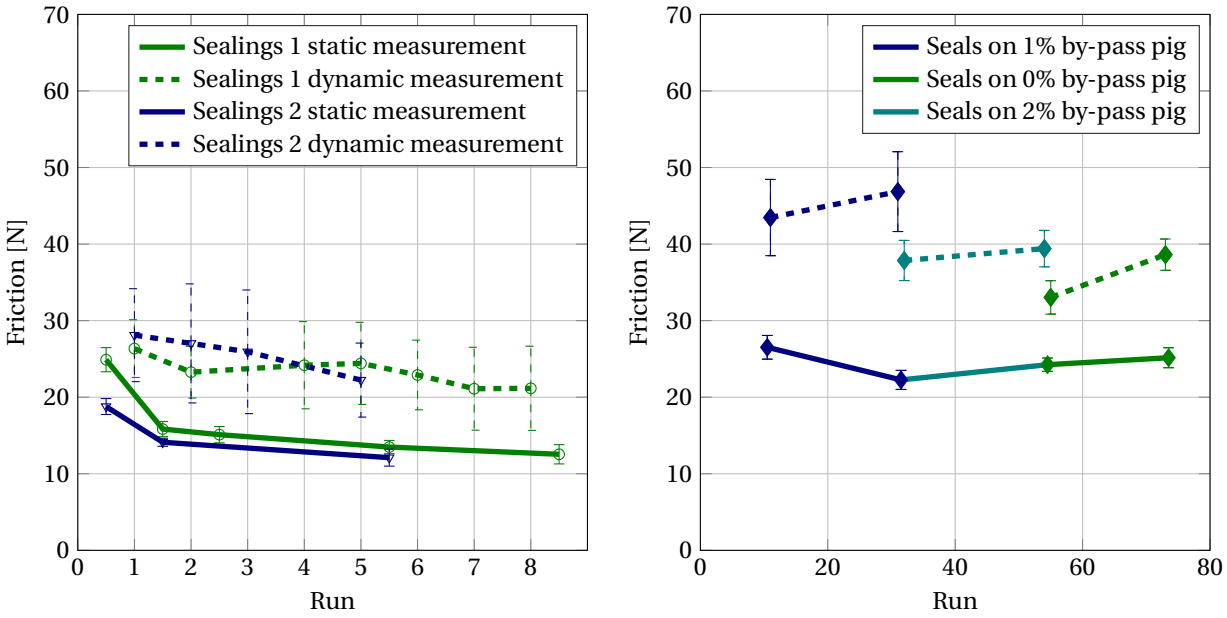


(a) Configuration 1

(b) Configuration 2

Figure 4.3: Estimations of the static and dynamic pressure

### 4.1.3. Global behaviour

An analysis is made on the averaged pressure, the standard deviation of the pressure and the average velocity.

#### 4.1.3.1. Pressure

*Mean pressure*

For each pigging run, a time averaged driving pressure was computed. Figure 4.4 shows the average driving pressure as a function of the pig velocity. The graph on the left and right correspond to configuration 1 and 2, respectively. One can see that the friction is in both cases independent of the average pig velocity. When comparing the configurations, one can see that the mean driving pressure of configuration 2 is larger than that of configuration 1. Moreover, the variation in the measured pressure is larger for configuration 1. This is in accordance with visual observations. The motion of the pig in configuration 1 showed a strong stick-slip behaviour whereas the motion of the pig in configuration 2 seemed to be smoother. Furthermore, the friction of the sealing disks in configuration 1 slowly decreases for consecutive runs. This is reflected in the spreading of the mean pressure. The outlier at 2.5 $m/s$ in figure 4.4a can be caused by damaged sealing disks, which results in a tilted pig and an increase in the friction.

*Standard deviation of pressure*

Time series of the pressure measurements revealed that the peaks in the pressure are higher in configuration 1 than in configuration 2. Since the stick-slip motion is also more pronounced in configuration 1, the pressure fluctuations can serve as an indication of the intensity of stick-slip behaviour. In figures 4.5a and 4.5b the standard deviation of the pressure are shown for configurations 1 and 2, respectively. Several features can be derived from these figures. Comparing the two configurations, one can see that the standard deviation of the driving pressure is indeed somewhat higher for configuration 1 than for configuration 2. Since the mean driving pressure is lower in configuration 1, the relative fluctuations are even higher in configuration 1 than in configuration 2. When comparing the standard deviation with respect to the pig velocity, one can see that there is no real dependency on the pig velocity. Although the stick-slip behaviour is more pronounced at low pig velocities, this does not result in a higher standard deviation of the pressure. This means that the standard deviation can not be used to compare the intensity of stick-slip behaviour at different velocities. A last important observation is that the standard deviation does not seem to depend on the by-pass area ratio. Or stated differently: the pressure fluctuations are not reduced for higher by-pass area ratios. The reduction was expected since the by-pass hole allows pressure from the upstream pocket to be released to the downstream

pocket. This could smooth the pressure fluctuations induced by the sudden acceleration and deceleration of the pig. However, this was not reflected in the pressure measurements. A possible explanation is that the by-pass area ratio is only 1, 2 or 4%. The opening areas might be too small for the pressure to escape during a typical stick-slip period. Further research on the influence of larger by-pass areas should be done to be able to really compare the influence of a by-pass hole on the stick-slip behaviour.

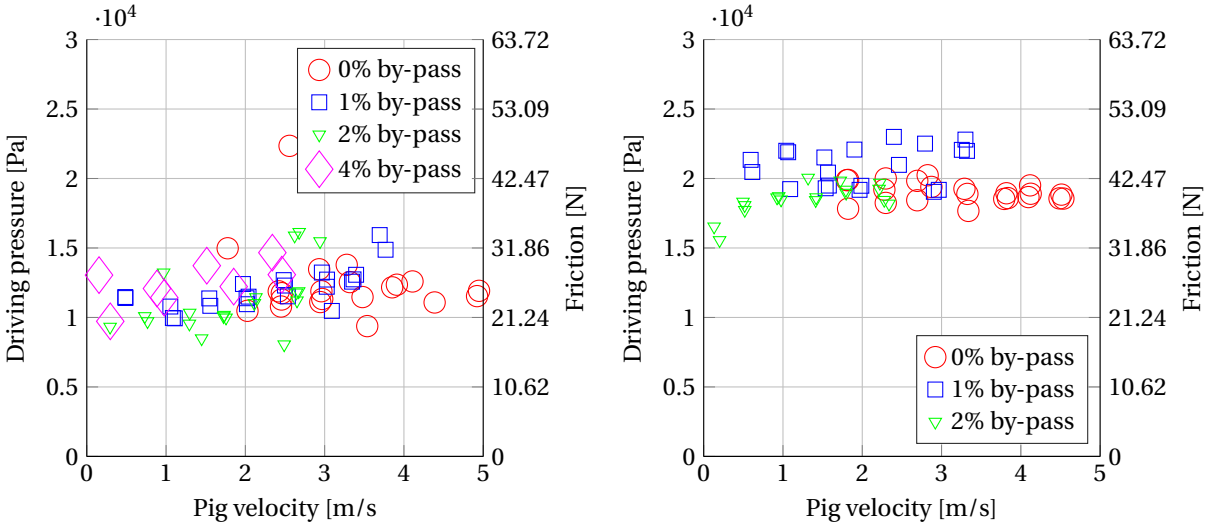


(a) Configuration 1

(b) Configuration 2

Figure 4.4: Driving pressure as function of the fluid velocity

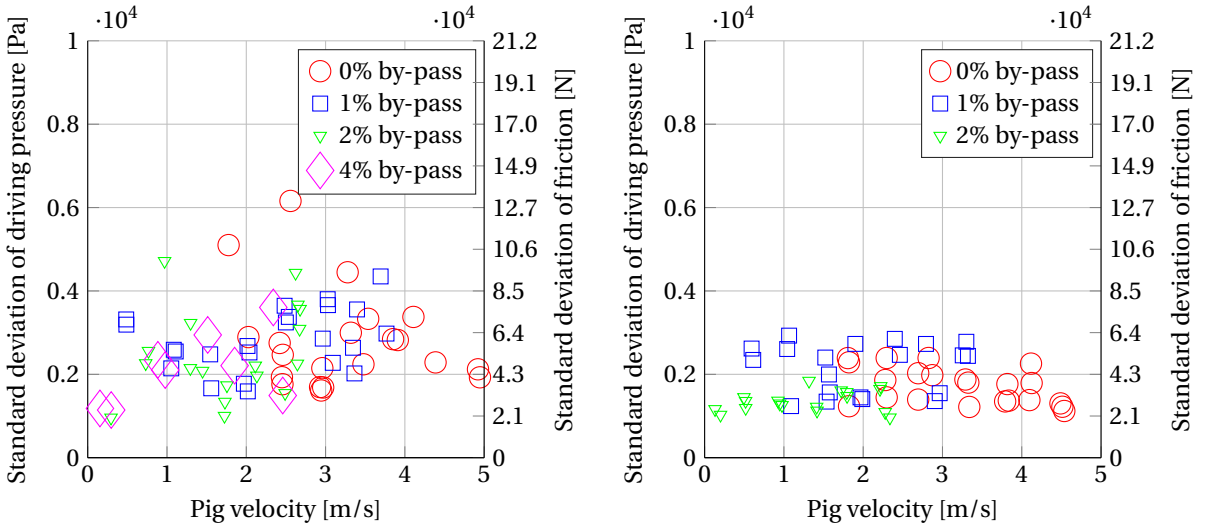


(a) Configuration 1

(b) Configuration 2

Figure 4.5: Standard deviation of driving pressure as function of the pig velocity

### 4.1.3.2. Pig velocity

One of the main reasons for using by-pass pigs is the ability to adjust the pig velocity. The flow velocity can be kept at the nominal production rate whereas the pig travels through the pipeline at a lower velocity. The reduction in velocity is depending on the reduction in pressure drop, which is depends on the by-pass area ratio. Figure 4.6 shows the pig velocity versus the flow velocity for both configurations 1 and 2. Different colours and symbols are used for different by-pass area ratios.

The red markers represent the pigging runs with 0% by-pass. These should in theory be equal to the bulk velocity. That theoretical line is shown in gray. One can see that the measured average velocity is somewhat lower. The mean of the differences for configuration 1 and configuration 2 is 2.9% respectively 6.7%. The discrepancy can be due to various reasons. Due to leakage of the flow loop, the bulk velocity just upstream of the pig might be lower. Because the upstream pressure in configuration 2 is higher, the leakage of the flow loop is larger. This would explain why the discrepancy is larger for configuration 2 than for configuration 1. Another possible reason is the occurrence of leakage at the pigs. If the sealing disks do not completely seal the inner pipe wall, some fluids may by-pass. This yields a lower pig velocity. Yet another explanation is the error in the velocity measurement. The average pig velocity is computed as the total length divided by the total time. For the length, the distance between the first pressure sensor and the exit is used. For the time, the difference between the pressure increase and decrease observed by the upstream pressure sensor is used. Since the pressure drop when the pig leaves the flow loop is observed later than the actual moment the pig leaves the flow loop, an error in the time difference is introduced. The error is equal to the length divided by the speed of sound, which comes down to roughly 0.2 $s$. The influence of this error increases for higher pig velocities. This would explain why the deviation of the measured and theoretical pig velocity increases for higher pig velocities.

The other markers represent the pig velocity for a specific by-pass ratio. One can see that they all lay on straight lines. Above it was shown that the friction does not depend on the velocity. The friction is balanced by the force exerted due to the pressure drop. For a certain by-pass area, this pressure drop is achieved at a specific relative velocity. If the bulk velocity is higher, the pig should move at a velocity equal to the difference between the bulk velocity and the required relative velocity. Therefore increasing the bulk velocity results in an equal increase in the pig velocity. This explains why the measured velocities lay on a straight line of 45 $degr$. The black lines in the plot are shown to indicate the theoretical steady state velocity, where the pressure drop coefficient suggested by Idelchik [23] is used. The lines were obtained by using the approach described in section 2.1.2. The solid black lines were constructed by using the mean friction. For the dashed lines, the mean pressure plus or minus the standard deviation were used. It can be seen that a variation in the friction has a much larger influence on the pigs with a larger by-pass area. This is explained by the larger steepness of the pressure drop formula for low by-pass areas. The comparison is described in more detail in section 4.2.1, where also the results of other models are included.

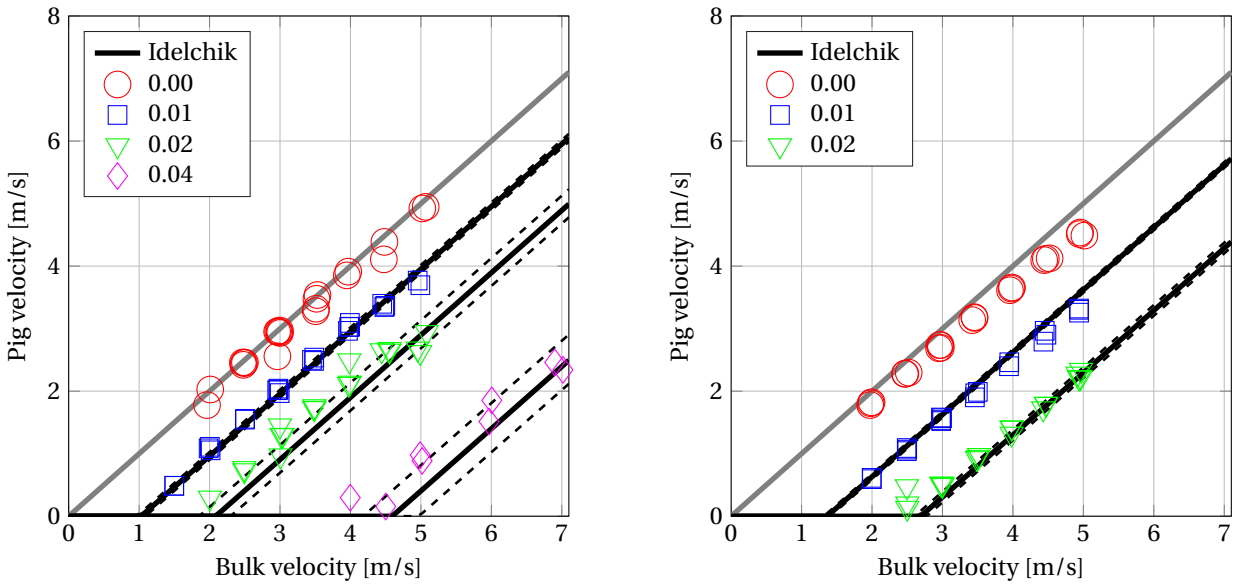


(a) Configuration 1

(b) Configuration 2

Figure 4.6: Pig velocity as function of the bulk velocity

### 4.1.4. Local behaviour

A closer look has been taken to a subset of all experiments. The second configuration with 0% by-pass has been chosen because the analytical model is constructed for conventional pigs. Besides, this subset of runs showed good repeatability.

#### 4.1.4.1. Pressure

A typical plot of the measured pressure as function of time is shown in figure 4.7a. The red lines indicate when the pig passes either the upstream sensor, the downstream sensor or exits the flow loop. The black lines show when the pig enters the measurement domain where the cameras are mounted. Two regions can be distinguished where the pressure follows a certain pattern: (1) the moment after the pig launching and (2) when the pig is further downstream. Zooming in at the period around launching results in figure 4.7b. A rather smooth sinusoidal variation of the pressure is measured which decays in time. This fluctuation is caused by the initial launching of the pig. The pig quickly accelerates and overshoots the equilibrium velocity. The equilibrium velocity is the velocity at which the friction and pressure are in balance. Because of the overshoot, the pressure is reduced. The pig velocity subsequently decreases below the equilibrium velocity, causing an increase in the pressure and the pressure increases. These oscillations would slowly damp out in time if the pipe was perfect. The velocity of the pig would be equal to the equilibrium velocity. However, variations in the inner pipe diameter cause variations in the friction, which result in changes in the pig velocity. Those inner diameter variations are present throughout the whole flow loop. An increase in the pressure indicates that the pig velocity is low and the friction is high, whereas a drop in the pressure indicates an acceleration of the pig caused by a widening of the flow loop. Zooming in at the period when the pigs enters the measurement section gives figure 4.7c. Again, a sinusoidal oscillation is observed. Just before entering the measurement domain, a peak in the pressure is seen. The velocity of the pig will be low. The situation is comparable with the launching situation. Once the friction has been overcome, the pig will accelerate quickly. The velocity for that specific run is shown in red in figure 4.8. Once can indeed see that the pig has a high velocity when entering the field of view of the cameras. Due to an overshoot, a decrease in the pressure is observed. A similar damped oscillation of the pig velocity around the equilibrium velocity will take place, which is accompanied by a similar oscillation of the pressure. However, variations in the inner pipe diameter cause difference with this ideal situation. Every time the pig velocity reduces to zero can be seen as a new initial condition for the pig launching. This is supported by the observation that the frequency of the oscillation after launching are higher than the frequency when the pig is further downstream. This is explained by the fact that the pocket upstream of the pig is much smaller at the period of launching. The same reduction in pressure will be caused by a smaller displacement of the pig. These findings have led to the analytical stick-slip motion as described in section 2.1.3. A comparison between the model and the observation is given in the section 4.2.

The pressure plots also show some other interesting features, which are less related to the pigging behaviour but still worth mentioning. A first aspect to note is the lag between the pressure measured by the sensor at the inlet and the sensor at the measurement section. When looking at the zoomed-in pressure plot during launching, one can see that the downstream sensor is lagging behind. When the pig is at the measurement section, the upstream sensor lags behind. This was expected because the time it takes for a fluctuation to reach a pressure sensor is lowest for the closest sensor. A second aspect to note are the pressure fluctuations just before launching the pig and when the pig leaves the flow loop. The fluctuations just before launching are caused by a distortion of the flow when the valves of the pig launcher are switched. When the pig exits the pipeline, a dip in the measured pressure is observed due to the expansion of the gas which used to be behind the pig. It will take a short period for the flow to find a new steady-state.

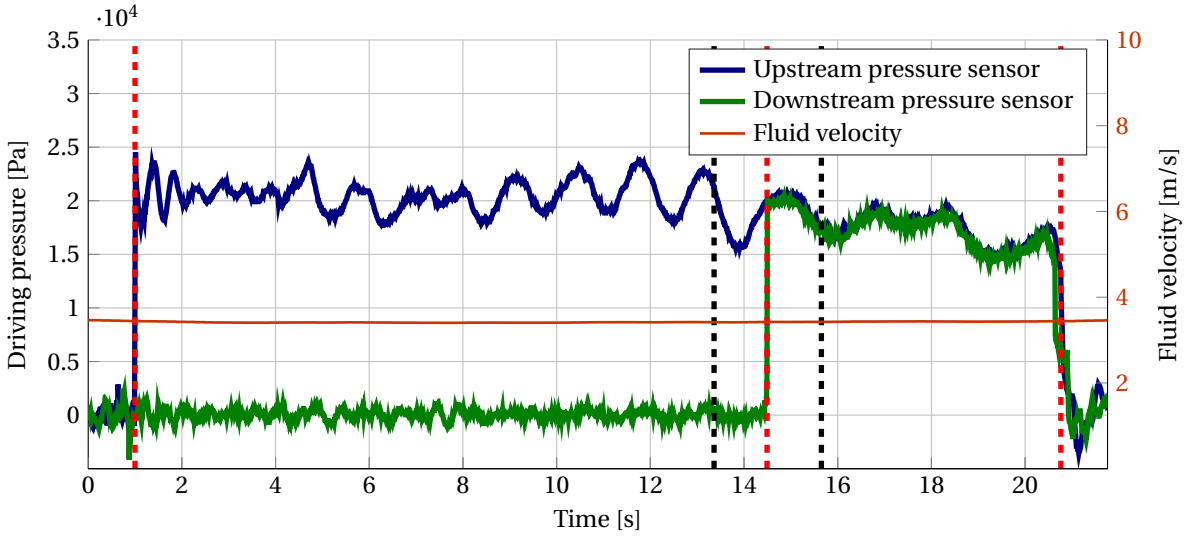


(a) Complete run

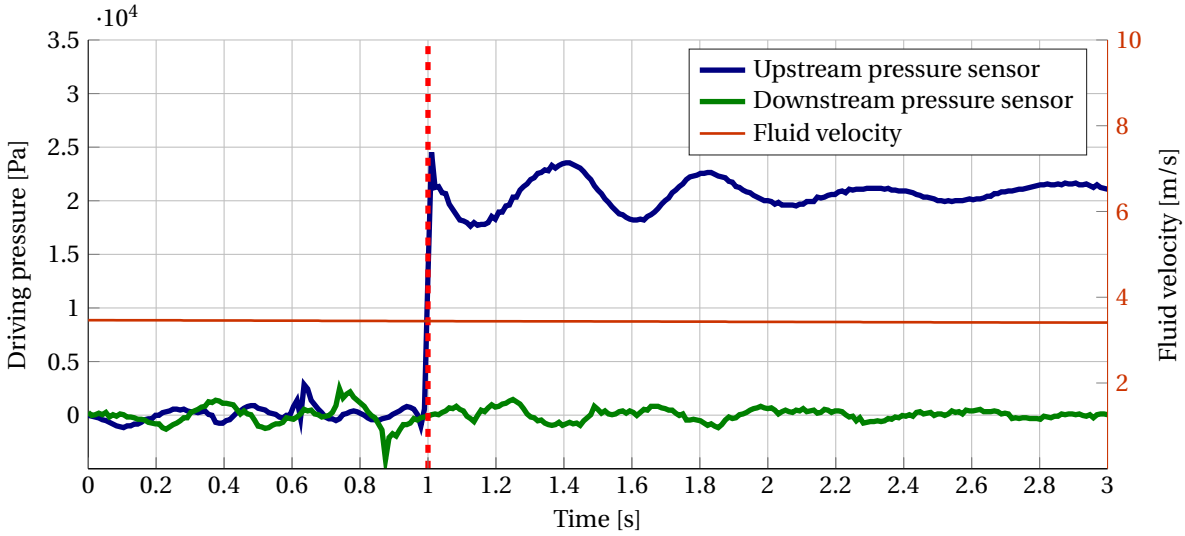


(b) Measured pressure at the time of launching

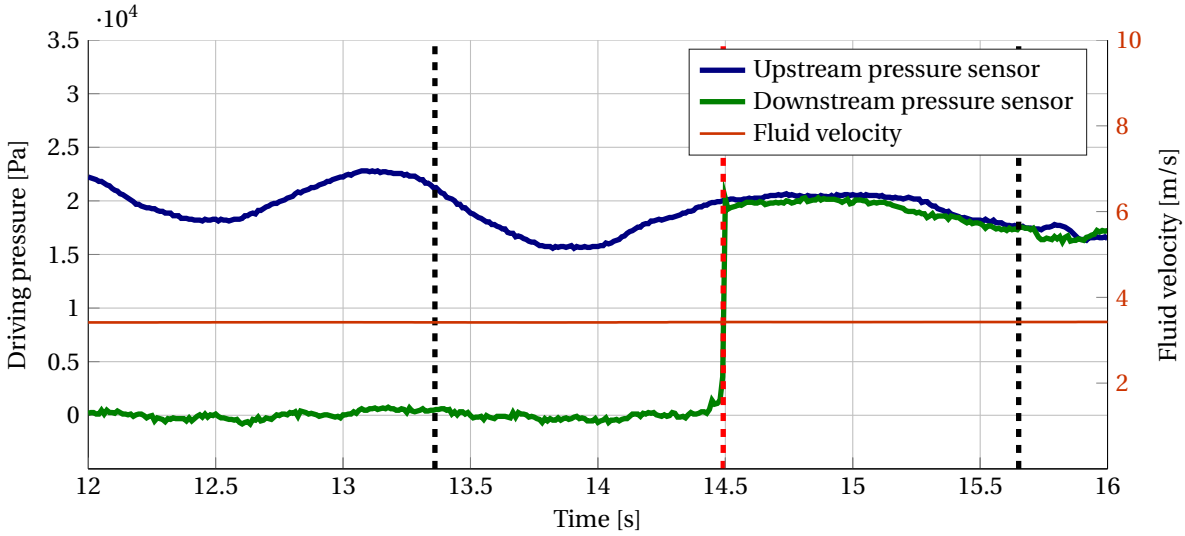


(c) Measured pressure when the pig is at the measurement section

Figure 4.7: Pressure measurement of a 0% by-pass pig in configuration 2 at a bulk velocity of 3 $m/s$

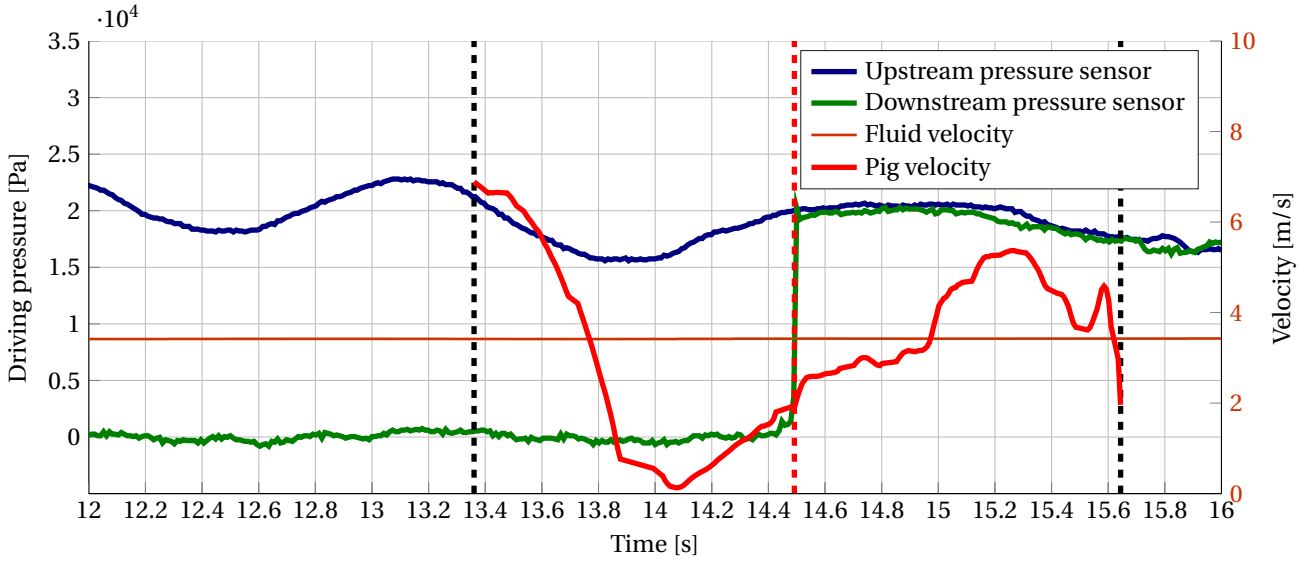


Figure 4.8: Pressure and velocity measurement of a 0% by-pass pig in configuration 2 at a bulk velocity of 3.5 $m/s$

### 4.1.4.2. Pig velocity

The local pig velocity can be determined based on the video recordings. The detection method was described in section 3.2.3. It turns out that the local pig velocity can be significantly larger than the average pig velocity. Figure 4.8 shows both the pressure and the pig velocity. The relation between the pressure and pig velocity was discussed in the previous section. An increased friction just ahead of the measured section, probably caused by a reduction in the pipe diameter, results in a low pig velocity. Approximately halfway the measurement section there is a second reduction. The velocity in between these two points can become relatively large. Figure 4.9 shows the velocity of the pig as a function of the location in the measurement section for two different bulk velocities. One can see that the maximum velocity can become twice as large as the bulk velocity. This is caused by the stick-slip behaviour. The pig detection method was applied for all pigging runs with 0% bypass in configuration 2. The results of this analysis is shown in figure 4.10. Several features can be noticed. First of all, the maximum velocity (filled dots) is significantly larger than the average velocity (open dots). The increase is relatively larger for low bulk velocities. From this limited set of observations, it seems that the maximum velocity increases approximately linearly with the bulk velocity. The large maximum velocity is explained by the stick-slip phenomenon. The total velocity of the pig after acceleration can be seen as a sum of the equilibrium velocity and an overshoot due to the acceleration from zero. The acceleration is caused by the increased friction which has to be overcome and it is similar for all runs. The corresponding impact of the overshoot on the maximum velocity is therefore relatively larger for a low bulk velocity. This is the reason for the higher ratio of the maximum velocity over the mean velocity at low bulk velocities. The reason why the maximum velocity is lower at the highest bulk velocity is that the pig did not stick around the measurement section. The quick acceleration after the sticking was therefore not seen on the videos.

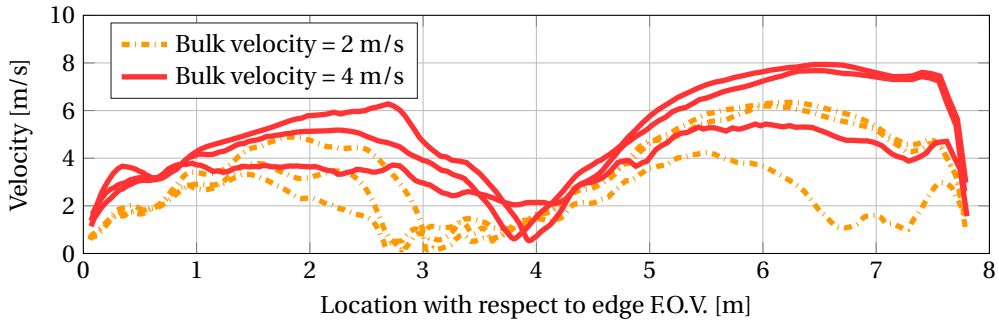


Figure 4.9: Pig velocity as function of the location within the field of view of the cameras

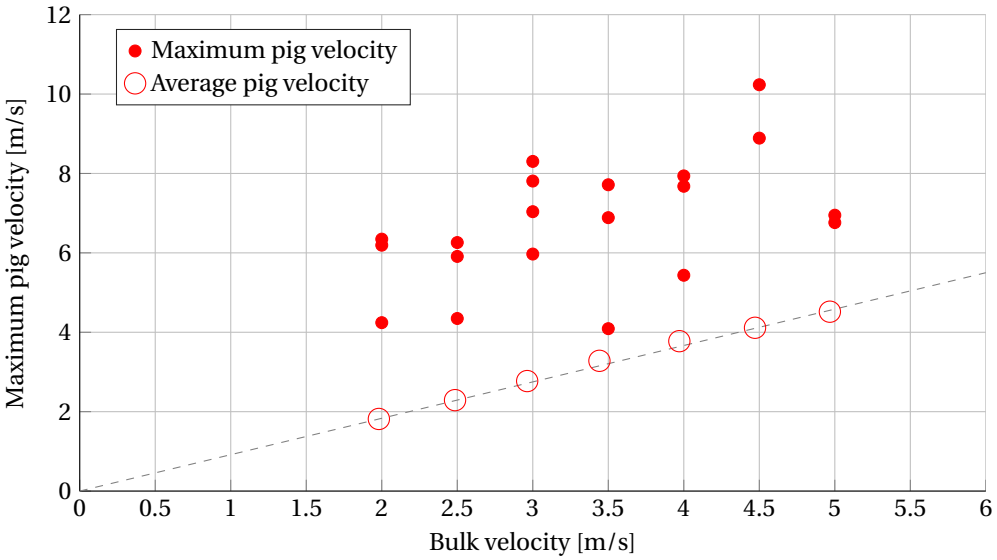


Figure 4.10: Maximum pig velocity in the measurement section and average pig velocity of the complete run

### 4.1.5. Static pressure drop

Models aimed at simulating the motion of by-pass pigs need to include a formula to relate the upstream pressure to the downstream pressure. Based on that, the driving pressure is computed. This is commonly done by using a pressure drop coefficient to compute the driving pressure [8, 14, 15, 19, 21]. This also holds for the numerical pigging model as described in section 2.2. In that specific model, a formula for the pressure drop over an orifice as suggested by Idelchik [23] is adopted. The formula is stated in equation 2.15 and was discussed in section 2.1.2.2. The reason for using the pressure drop coefficient for an orifice is that a moving pig with a simple by-pass hole has strong analogies with an orifice. A static pressure drop measurement was performed to check whether this formula can indeed accurately predict the pressure drop coefficient for the pigs used in the experiments. Static here means that the pig was placed inside the pipe in between two points connected to a pressure sensor. The distance between two points was 1.50 $m$. The pig was placed a slightly upstream of the centre point, since the entrance effects are assumed to span over a shorter distance than the exit effects. The measured pressure drop together with the formula suggested by Idelchik is plotted versus the velocity in figure 4.11a. The pressure drop is made dimensionless with the dynamic pressure in the by-pass hole. The results are plotted versus the Reynolds number in the by-pass hole in figure 4.11b. It can be seen that the curves follow a similar trend. The deviations at low Reynolds numbers were expected since the formula provided by Idelchik hold only for the higher Reynolds number regime. The lowest Reynolds numbers correspond to the regime where transition between laminar and turbulent flow is believed to take place. A possible reason for the small over-predictions of the pressure drop in the higher Reynolds number regime is the error in the fluid velocity. Furthermore, the actual dimensions of the pig might slightly differ from the presumed dimensions. The suggested formulas can nevertheless be used as a good predictor of the pressure drop over the pigs used in this research.

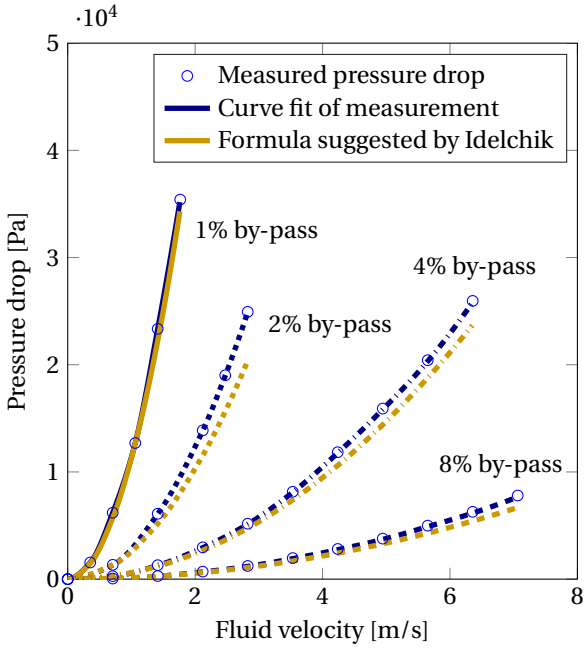


(a) Pressure drop

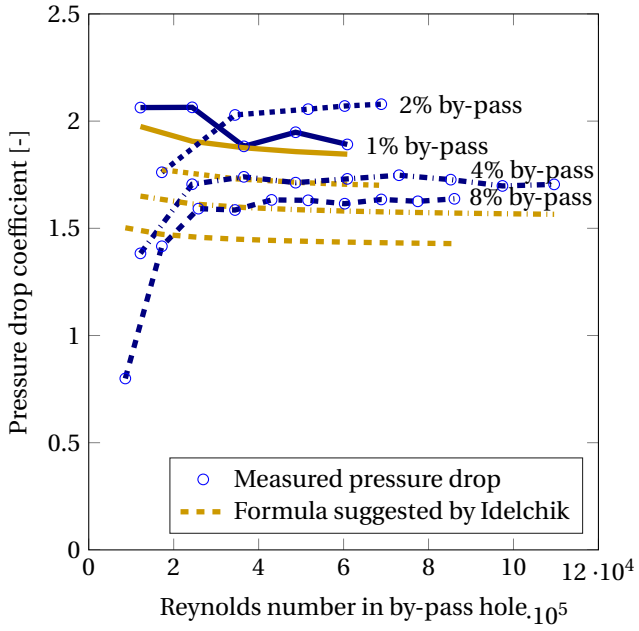


(b) Pressure drop coefficients

Figure 4.11: Static pressure drop measurement

## 4.2. Comparison between experimental & modelling results

The results from the experiments were compared with different pigging models. First, a comparison of the average velocity is given. Second, a closer look is taken in the local behaviour. That analysis was limited to a subset of the experiments, namely the runs of configuration 2 with a 0% by-pass area. At the end a brief parameter study of the numerical pigging model is made.

### 4.2.1. Average pig velocity

The average velocity obtained from the experiments is compared with the simulations from three different models: (1) the analytical by-pass pigging model, (2) the numerical pigging model and (3) the Dynamic Multiphase Flow Simulator OLGA. This latter commercial package is often used in the oil and gas industry to model pipe flow. The software package includes a module on pigging simulations which has been used to simulate the pigging experiments. The simulations were carried out by an expert from Shell Global Solutions International BV (M. Fransen, priv. comm., August 2016). Below, some input parameters of the three model are given. Those were chosen to represent the actual pigging experiments as close as possible.

*Input parameters*

The OLGA model (version 2014.2) is given in appendix A.3. The mass flux is varied each simulation and lies between 0.0043 and 0.020 $kg/s$. This corresponds to the range of flow velocity as used in the pigging experiments. The pipeline details, such as length, elevation and material, mimic the situation in the lab one-to-one. The pipe wall roughness was taken as $5 \times 10^{-5}$ m. Each computational cell is 0.25 $m$ in length, which was verified to be a decent grid size. The bypass pig enters the flow loop at the first pipe section and exits at the last one. The friction force between the pig and the wall was set at 26 $N$. This corresponds to the average friction of the by-pass pigs in configuration 1 as obtained from the pressure measurements. The leakage factor in OLGA is taken equal to the bypass area, whereas the pig length is not taken into account. Some of the other input parameter are listed in table A.1 in appendix A.3. Unfortunately, it is not known what method is used to compute the pressure drop over the pig.

The friction in the analytical by-pass pigging model was slightly adjusted. Instead of the average friction of all runs, the average friction of the runs with the same by-pass area was used. This had only a small effect on the final results since the friction was approximately the same. The density and viscosity were set to respectively 1.2 $kg/m^3$ and $1.81 \cdot 10^5$ $kg/(ms)$. The roughness of the wall inside the by-pass hole was set at $5 \cdot 10^{-6}$ $m$.

The input parameters in the numerical pigging model are similar. Also three different values for the friction were used. Both the dynamic and static friction were set to these values. The timestep and grid size were chosen such that convergence was reached. A length of 4 $m$ was added in front of the start position to simulate the volume of the pig launcher. At the end, a segment of 2 $m$ was attached. The pressure at the right boundary was set equal to the outlet pressure of 1 $bar$. At the inlet, the velocity was prescribed. The numerical integration scheme was explained in section 2.2. The average velocity was computed in a similar method as was done during the experiments, i.e. dividing length by time.

*Results*

Figures 4.12 shows the average pig velocity versus the bulk velocity. Instead of all measured average velocity, the mean velocity of the runs performed at the same velocity and with the same by-pass area is used. The similarity between the experimental and numerical results is very good, especially for the 0 % and 1 % by-pass runs. The small discrepancy can be explained by the difference between the input values and the actual conditions. The discrepancy becomes larger at lower pig velocities. This was expected since the formula for the pressure drop coefficient does no longer accurately represent the actual pressure drop coefficient in the low Reynolds number region. The similarity stays however reasonable. This result is even more remarkable when taking into account that the during the experiments severe stick-slip behaviour was observed. The numerical pigging model and the simulation with OLGA models predict a steady-state velocity motion. Moreover, the analytical by-pass pigging model is even based on a steady-state motion. It turns out that the average pig velocity of a pigging run where stick-slip motion takes place can be accurately predicted with a steady-state model. This statement can be reversed if it is assumed that steady-state models do accurately predict steady-state situations (this is not proven here). The conclusion would then be that stick-slip motion does not affect the average pig velocity.

A last point to mention is the lower limit of the bulk velocity to the drive a by-pass pig forward. According to the analytical by-pass pig model, a certain flow velocity is required to overcome the friction. This same limit corresponds to the lowest velocities that had to be applied in the experiments to drive the pig forward. The numerical pigging model and the OLGA model predict a similar velocity limit.

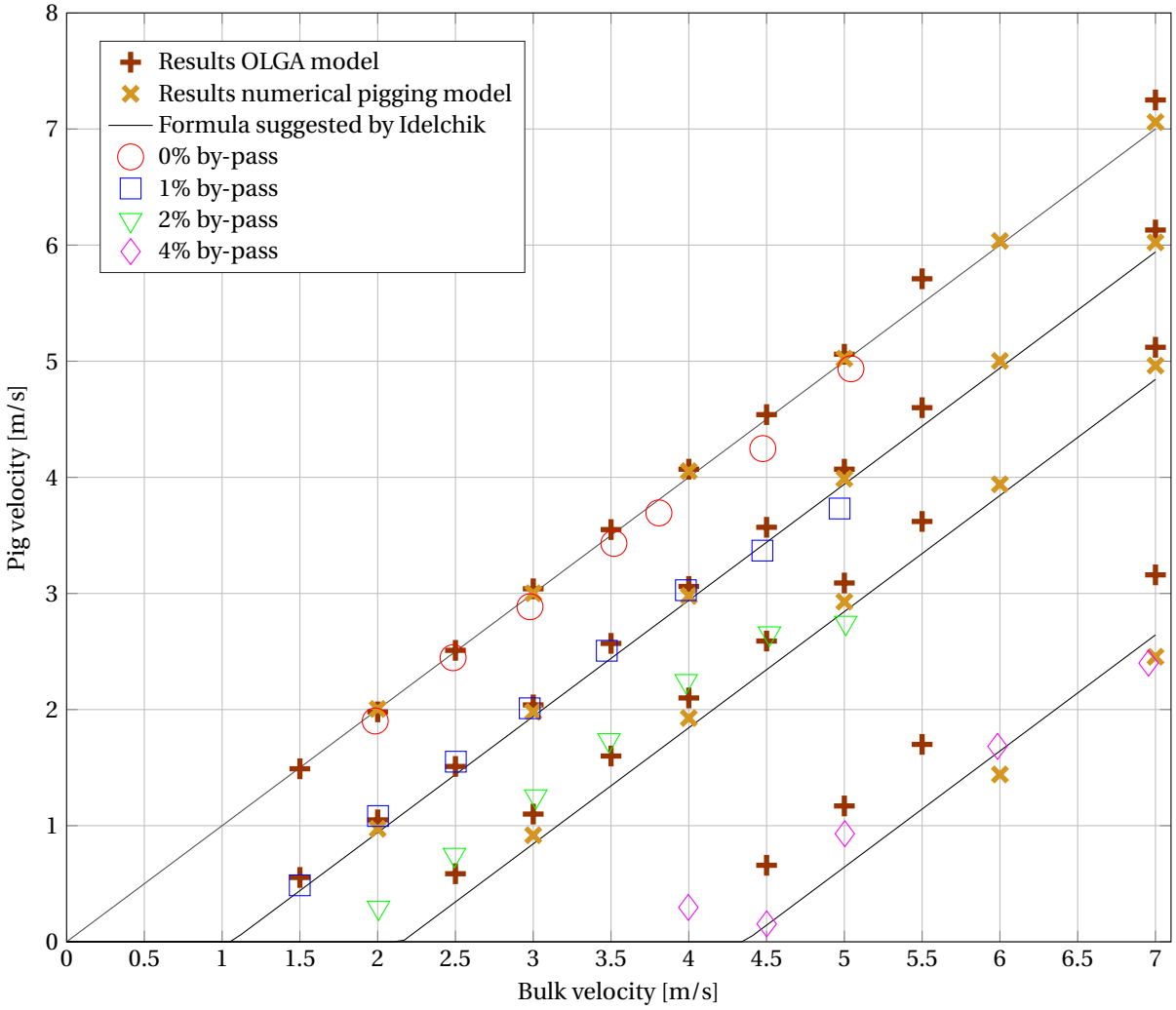


Figure 4.12: Comparison between measured and predicted average pig velocity

### 4.2.2. Local characteristics

The local pig behaviour can significantly differ from the steady-state behaviour. A discussion on the local velocity and pressure fluctuations as deduced from the measurements was provided in section 4.1.4. Several characteristics of the behaviour were mentioned. This section shows to what extent the models can capture the same characerstics. The models used are (1) the numerical pigging model, (2) the simplified numerical model and (3) the analytical stick-slip model. Again, only the runs performed with a pig in configuration 2 and 0% by-pass are considered.

#### 4.2.2.1. Pressure

A comparison between the experimental results and model predictions is made based on two complete runs. The bulk velocity of the first run is 2 $m/s$ whereas the bulk velocity during the second run is 4 $m/s$ . The numerical pigging model considers a flowloop which again starts 4 meter ahead of the initial position of the pig and ends 2 meter behind the actual exist. These lengths were not accurately measured. The other

parameters were taken to represent the flowloop as accurate as possible. Both the dynamic and static friction were set at the average friction of the whole subset in consideration and not taken the same as the average pressure of that specific run. The simplified numerical pigging model was initialized with almost the same input parameters. The only difference was the static friction, which was set at a value 9 % higher than the dynamic friction. In section 4.1.3.1 it was shown that the peaks in the pressure are around this value. The same frictions were used in the analytical stick-slip model. Also this model requires a length upstream of the pig initial position, which was set to 4 $m$. The other parameters were chosen according to the flowloop dimensions. The reason for not setting the static value in the numerical pigging model at this value is that the pig velocity will reach a steady-state for which the effect of the higher static friction is not noticable. A stick-slip behaviour can be enforced when higher ratios of the static over dynamic friction are used. An analysis of the main parameters playing a role in occurrence of stick-slip in the numerical pigging model is given in section 4.2.3.

The simulated and the measured pressures are shown in figure 4.13a and 4.14a, corresponding to a bulk velocity of 2 $m/s$ and 4 $m/s$, respectively. These figures show that the simulated pressure of the simplified numerical pigging model and or the analytical stick-model are in the same range as the measured pressure. The measured pressure shows some larger extremes caused by variations in the inner pipe diameter. However, the general trend is surprisingly similar. Especially since the static and dynamic pressures used in the models are computed from the average of all pigging runs and not only of this specific run. Next to the range, also the frequencies and the steepness of the curves are similar. The frequency of the measured pressure is highest directly after launching the pig and it then slowly smoothens out. Exactly the same is predicted with the models.

Enlarged plots of the fluctuations in the pressure around the time of launching the pig are shown in figure 4.13b and 4.13b for bulk velocities of 2 $m/s$ and 4 $m/s$ respectively. The results of the simulations are shifted to the left since they represent the pressure at the left boundary. The pressure sensor is located a bit downstream and only measures the increased pressure once the pig has passed. The acutal time shift was not computed. When comparing the results, also the numerical pigging model can be considered since the pig behaviour is determined by the initial conditions and not yet by the stick-slip behaviour. The simulation performed with the pigging model agrees best with the measured pressure. The fluctuations are in the same range. Besides, it is nice to see that the simulated pressure does not decay linearly in time. The same is also seen in the measurement. The reason for this is the local variation in the pressure. Pressure waves traveling through the domain cause local variations in the pressure. These fluctuations are not present in the simpler models since a uniform pressure at both side of the pig is assumed. Another consequence of this assumption is that the peaks are larger. The local pressure behind a pig which is accelerating will decrease because of the expansion of the gas behind the pig. This results in a lowered driving pressure. The computed velocity in the simplified numerical model and the analytical stick-slip model will be higher since they do not take this effect into account. The discrepancy between the measured pressure and the pressure computed with the analytical model is largest. This is caused by the fact the values at the start of the acceleration are used through the first oscillation. The values at the end of that oscillation are used for the subsequent oscillation. The model uses an equivalent spring based on the length of the upstream section, as explained section 2.1.3. The relative change of this section during an oscillation is lower when the upstream section is larger. The analytical model therefore approaches the simplified numerical model when the pig is further downstream, as can also be seen in the graphs.

Lastly, the influence of the bulk velocity is analyzed by comparing figures 4.13 and 4.14, corresponding to 2 $m/s$ and 4 $m/s$ respectively. The fluctuations in the pressure after launching are larger for higher bulk velocities. This follows from the measurements as well as from the simulations. This can be explained by the larger absolute overshoot of the pig velocity with respect to the equilibrium velocity. The frequencies are however the same. Also this is observed in both the experiments as well as in all simulations. The fluctuations in the measured pressure when the pig is further downstream can not be compared reasonable based on only these plots. However, figure 4.5 in section 4.1.3.1 showed that the standard deviation of the pressure does not depend on the pig velocity. This implies that the fluctuations in the pressure will on average not be different when the pig is further downstream. The same conclusion could be drawn based on simulations with the analytical stick-slip model and the simplified numerical pigging model. These models also suggest that the frequency of the pressure fluctuations is the same. The main conclusion of this analysis is that the bulk velocity has effect on the pressure fluctuations just after launching, but that a similar influence is not expected when the pig is further downstream.

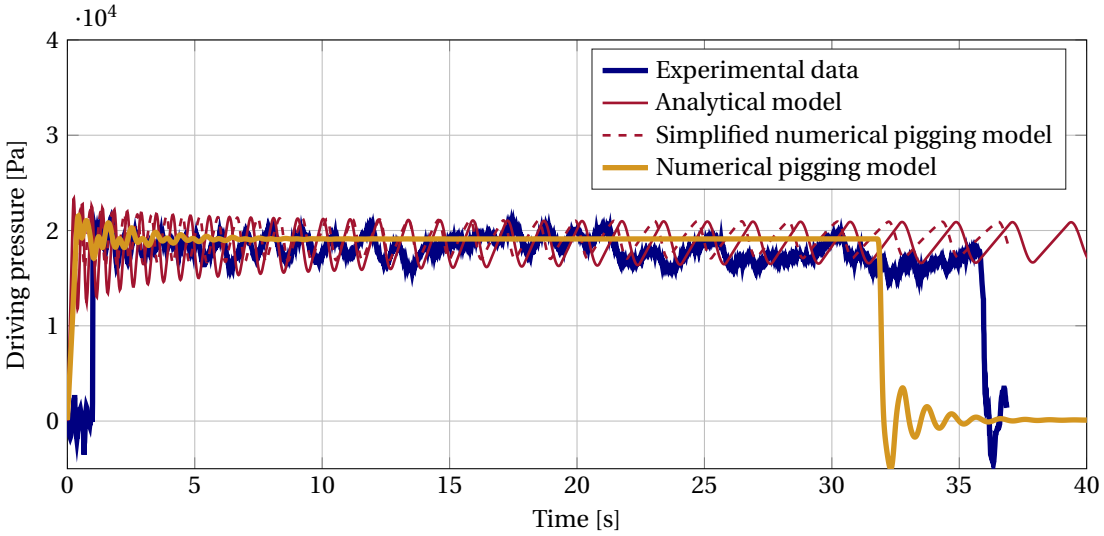


(a) Upstream pressure as function of time during the complete run

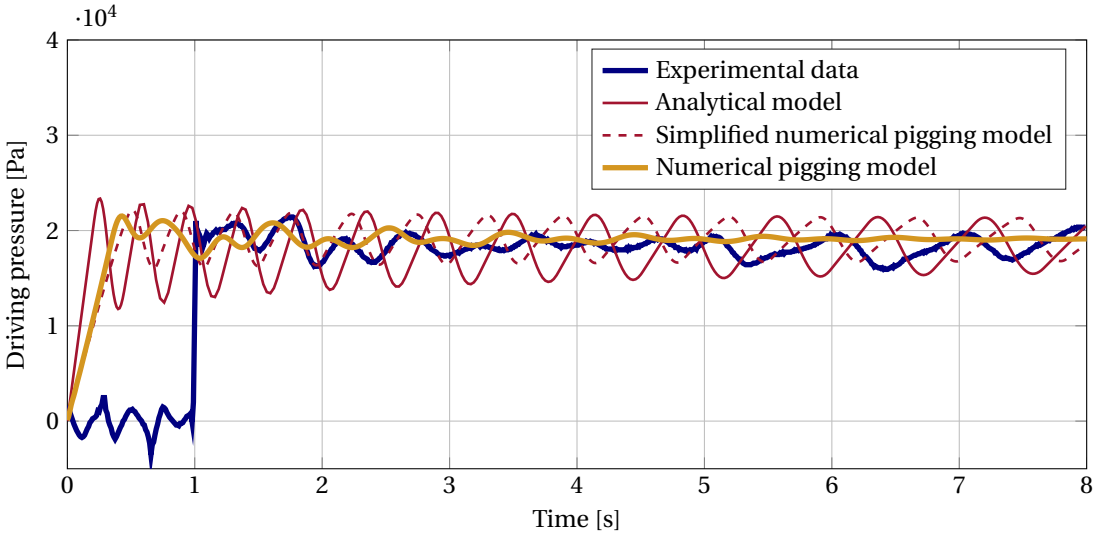


(b) Upstream pressure as function of time at the moment of launching

Figure 4.13: Upstream pressure of 0 % by-pass pig in configuration 2 at a bulk velocity of 2 $m/s$

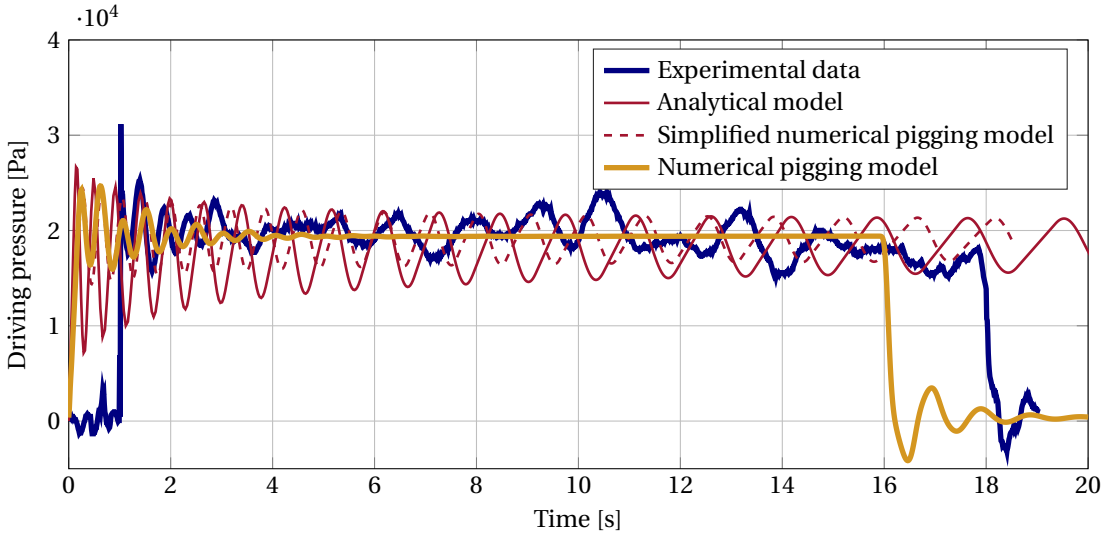


(a) Upstream pressure as function of time during the complete run

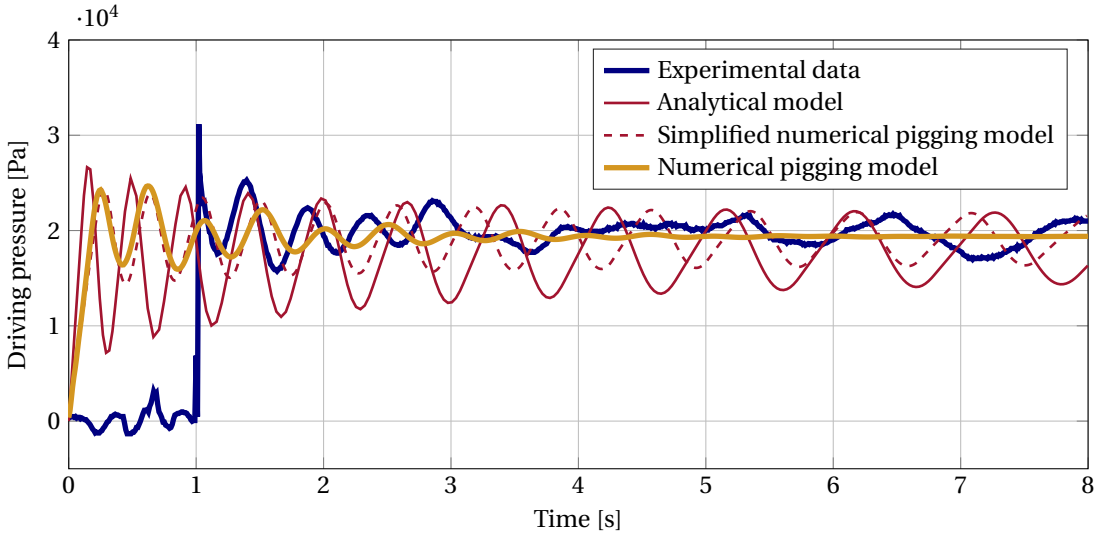


(b) Upstream pressure as function of time at the moment of launching

Figure 4.14: Upstream pressure of 0 % by-pass pig in configuration 2 at a bulk velocity of 4 $m/s$

#### 4.2.2.2. Maximum velocity

*Comparison*

The maximum velocity can become significantly larger than the mean velocity because of the stick-slip effect, as was shown in figure 4.10 in section 4.1.4.2. Simulations with the the numerical pigging model and the analytical stick-slip model were performed to see whether the maximum velocity can be predicted accurately. During the experiments, the pigs tended to stick just before the measurement section. This situation is comparable with the launching of a pig from that same location. The simulations are therefore started with an upstream length of 44 $m$. By doing so, also the results of the numerical pigging model can be included. For the analytical stick-slip model the results of starting the simulation at the inlet would be same. The maximum pig velocity obtained from these simulation are plotted together with measured maximum velocity in figure 4.15.

The black lines show the results of the analytical stick-slip model. The curves are described by equation 2.50 stated in section 2.1.3.4. For the computations, three different ratios of the static friction over the dynamic friction are used. This was done to show the influence of the static friction on the maximum velocity. The higher this factor, the higher the computed maximum velocity. A factor of 1 was used for the solid line.

For the dashed line above, the static friction as obtained from the measurements was used. This seems to be a good estimation of the maximum velocity. Higher factors of the static over the dynamic friction over-predict the maximum pig velocity.

The simulations with the numerical pigging model are also carried out with a dynamic friction equal to the average friction and a static friction corresponding to the peaks seen in the experiments. The higher static friction results also here in a higher maximum velocity. The result is not as regular because the local variations of the pressure upstream and downstream of the pig.

It is questionable whether this part of the flowloop is representative for this rest of the flowloop. Nothing can be said about the maximum velocity of the complete run. Furthermore, the dynamic friction in this part might be different from the average friction values as used in the computations. However, the order of magnitude shows reasonably good agreement. Furthermore, the trend in the maximum velocity as function of the bulk velocity is comparable. This approach could therefore be used to get an estimation of the maximum velocities during a pigging run where stick-slip is encountered. A larger factor of the static over the dynamic friction should be used when one wants to compute an upper limit of the pig velocity. It would be even more accurate to compute the maximum velocity by using the local friction around the section where an estimation of the maximum velocity is made. However, this is very time consuming and not practical in reality.

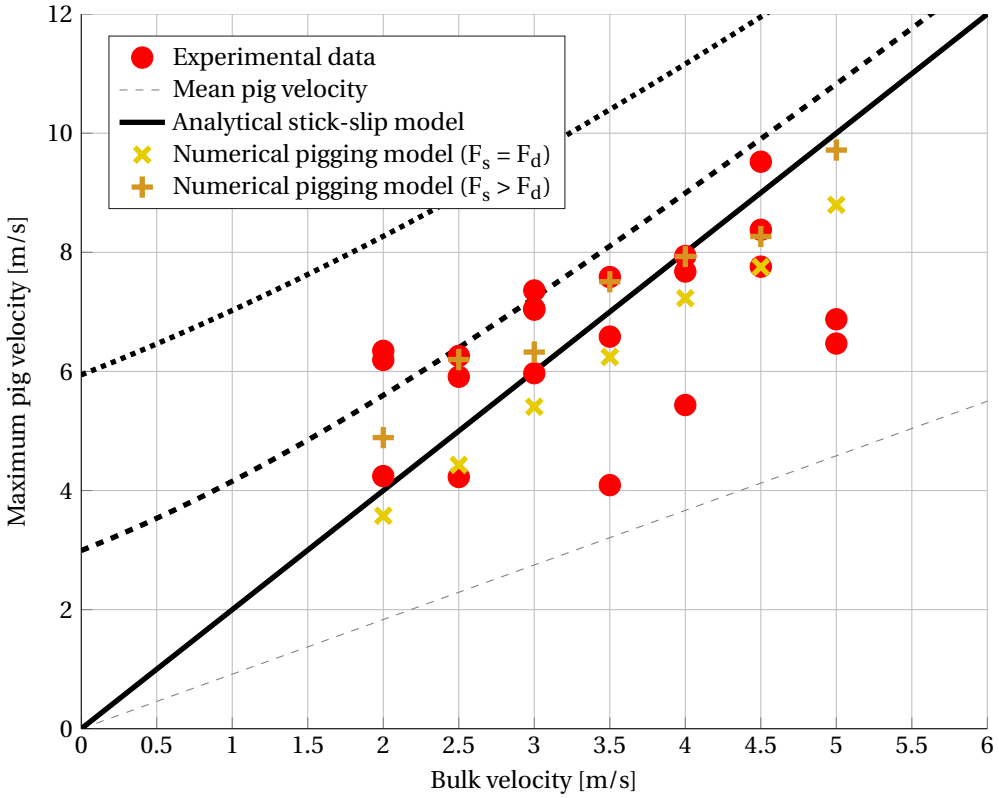


Figure 4.15: Comparison between measured and predicted maximum pig velocity

*Predictions*

In the previous section is was shown that simulations of the stick-slip models agree reasonably well with the measurement data. This holds for the pressure throughout the complete runs as well as for the velocity within the the measurement section. The models were therefore used to get an idea of the velocity in the segments outside the field of view of the cameras. Plots of simulations performed with the simplified numerical model and the analytical stick-slip model are shown in figure 4.16 and 4.17 for bulk velocities of 2 $m/s$ and 4 $m/s$. As a reference, also the maximum pig velocity as obtained from the recordings is indicated. Besides, results of simulations with the numerical pigging model when using the same frictions has been added as

a reference. These simulations do not show a stick-slip behaviour. The next section discusses how that can actually be enforced.

We now consider the results of the analytical stick-slip model and the simplified numerical pigging model. The simulations show comparable results. The deviation can again be explained by the extra assumption made in the analytical model. In that simplification it is assumed that the parameters do not vary during a slipping cycle. The predicted velocities are therefore somewhat larger. When the pig moves through the pipeline, the amplitude of the velocity slowly increases. The increase is more significant at lower bulk velocities. This is explained by the relatively higher influence of the static over dynamic friction factor. The frequency slowly decreases over time. This is explained by the larger volume upstream of the pig. The length of this segment is explicitly included in the computation of the equivalent stiffness, equation 2.46. The stiffness factor determines the frequency. This shows that the frequency should increase when the upstream segment is larger. The main findings of these simulations is that, according to the two models, a larger pig velocity will be encountered at the end of the flowloop. Besides, the frequency is decreased. This leads to a larger slipping distance per stick-slip cycle. These findings hold for both the pressure measurements and to visual observations.

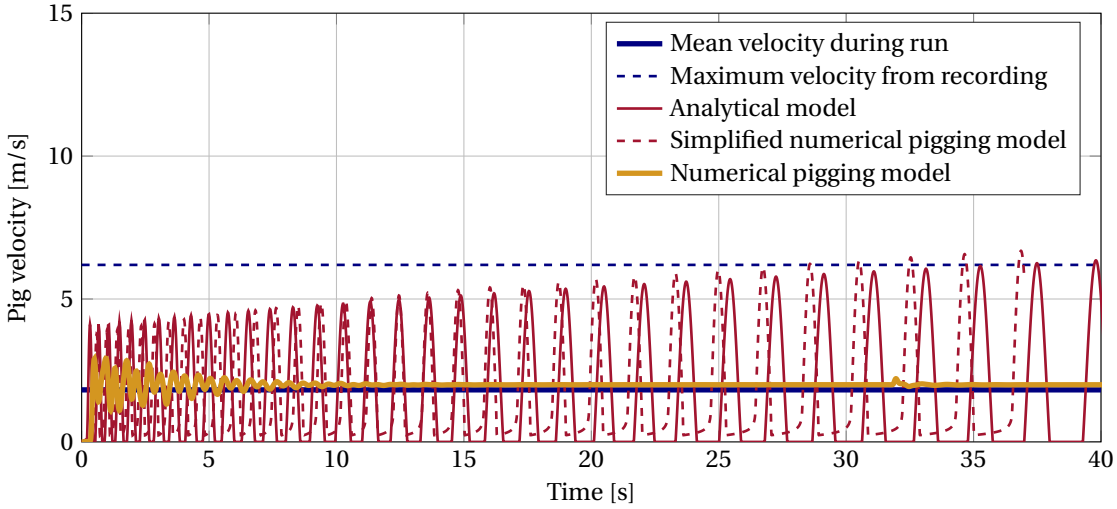


(a) Pig velocity as function of time during complete run

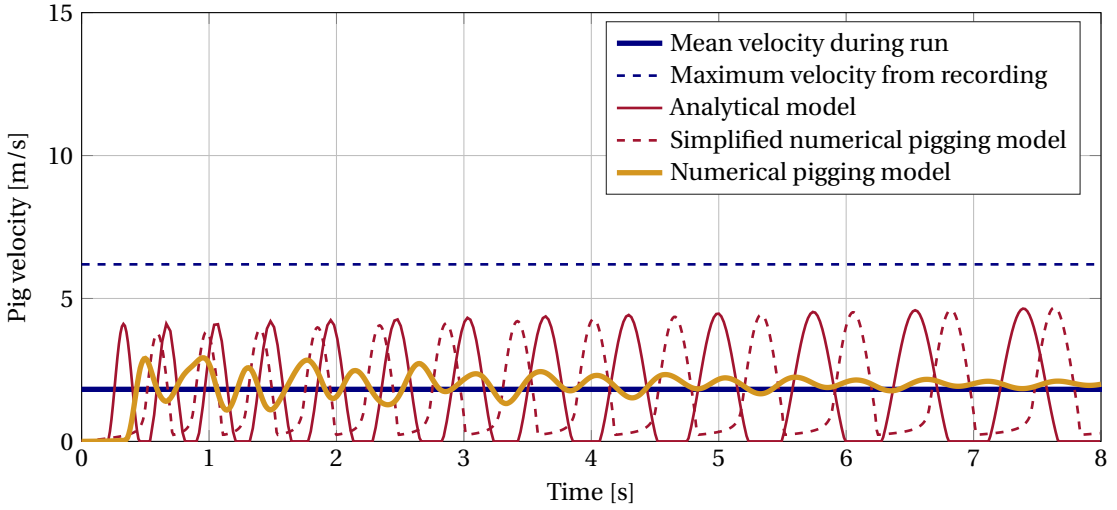


(b) Pig velocity as function of time just after the moment of launching

Figure 4.16: Velocity prediction of 0 % by-pass pig in configuration 2 at a bulk velocity of 2 m/s

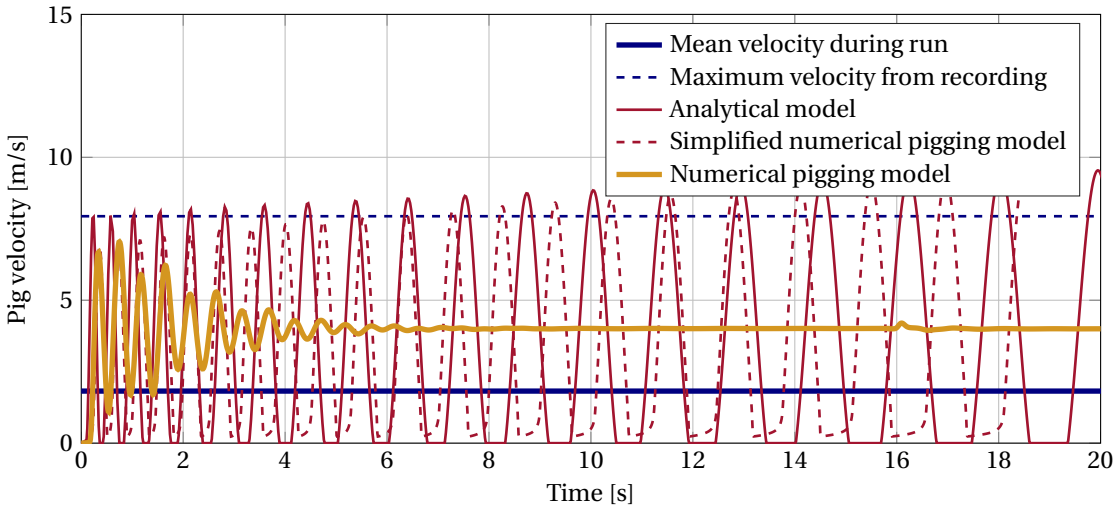


(a) Pig velocity as function of time during complete run

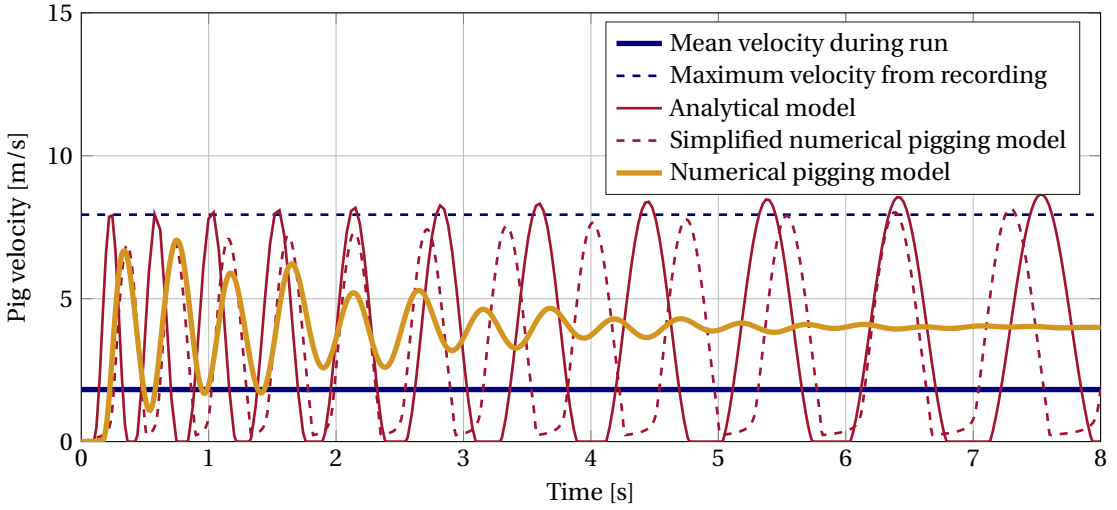


(b) Pig velocity as function of time after the moment of launching

Figure 4.17: Velocity prediction of 0 % by-pass pig in configuration 2 at a bulk velocity of 4 m/s

### 4.2.3. Numerical pigging model

The numerical pigging model shows on oscillation of the pig velocity after launching. This oscillations damps out when using the same value for the static as well as the dynamic friction. However, a stick-slip motion can be enforced when a different value for each of the friction forces is taken. In section 2.2.2.4 the method of modeling the friction was discussed. A transition velocity must be chosen which marks the transition between the static and dynamic friction. If the velocity drops below this value, the friction increases to the static friction, as was visualized in figure 2.19. Whether or not a stick-slip motion is encountered therefore largely depends on the following factors:

- Ratio of the static and dynamic friction
- Bulk velocity
- Transition velocity between static and dynamic friction

A small parameter study was carried out to show the influence of the static to dynamic friction ratio and the bulk bulk velocity. The transition velocity was set at 1 $m/s$. The other parameters were set according to the dimensions of the flowloop and the properties of the pig in configuration 1 (dynamic friction = 40.34 $N$) with

a 0% by-pass area. Figure 4.18 shows a scatter plot which indicates whether or not a stick-slip motion was encountered in the simulations. As one can see, the probability of encountering a stick-slip motion increases for a larger ratio between the static and dynamic friction as well as for a lower bulk velocity. This was also observed in the pigging experiments.

To show the difference between simulations with and without a stick-slip motion, the time series of four runs are shown in figure 4.19. The pressure at the inlet boundary and the pig velocity of the same run are plotted side by side. The bulk velocity of all shown runs was 4 $m/s$. Figure 4.19 ($a$) shows the situation where the friction ratio $F_s/F_d$ is 1. One can see that the oscillation damps out relatively fast. The friction ratio in the subsequently shown time series are increased step by step. A higher friction ratio increases the length of the oscillatory motion. The friction ratio of the last time series was 1.24. This corresponds to a static friction of 50 N. The stick-slip motion is maintained throughout the who pipeline. This is accompanied with a fluctuating behaviour of the pressure upstream.

It is very interesting to see the similarity with the measured pressure during the pigging experiments. The time series of the simulation is plotted on top of the pressure measurement with the same conditions in figure 4.20. One can see that a very similar trend is obtained. Both graphs show a higher amplitude oscillating in the beginning, which is related to the oscillating motion. A certain offset was used since the pressure according the numerical model was taken at the inlet boundary whereas in the experiments the pressure sensor is behind the pig launcher. A more detailed model of the pig launcher should be made to obtain a better synchronization. Further downstream, a second frequency can be distinguished. This frequency is related to the stick-slip behaviour. A sudden pressure drop is observed associated with a quick acceleration of the pig. As the pig velocity drops back to zero, a linear increase of the upstream pressure is observed. The higher peaks from the numerical model are explained by the higher static friction factor necessary to force a stick-slip motion. In the experiments, the stick-slip motion is enhanced by variations in the inner pipe diameter. However, even though these variations are not present in the current numerical pigging model, a stick-slip motion can be forced which gives comparable results as in the experiments. An extension of the numerical pigging model is advised which incorporates the influence of variations in the inner pipe diameter.

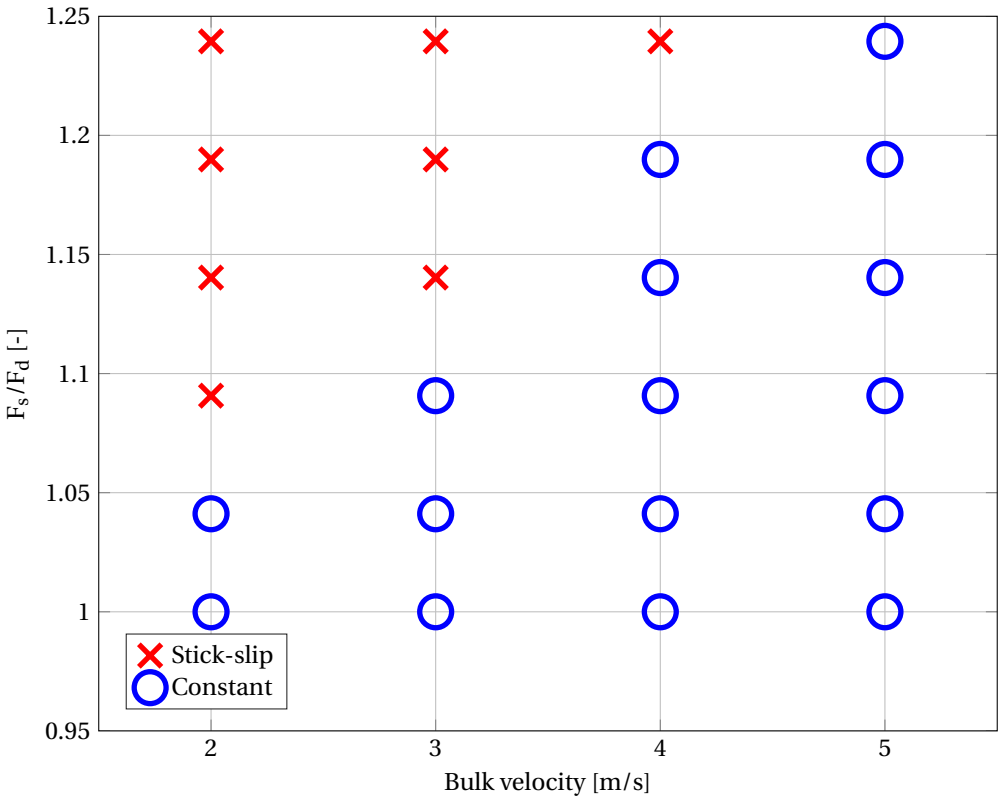


Figure 4.18: Overview of occurrence of stick-slip as a function of the friction ratio and the bulk velocity

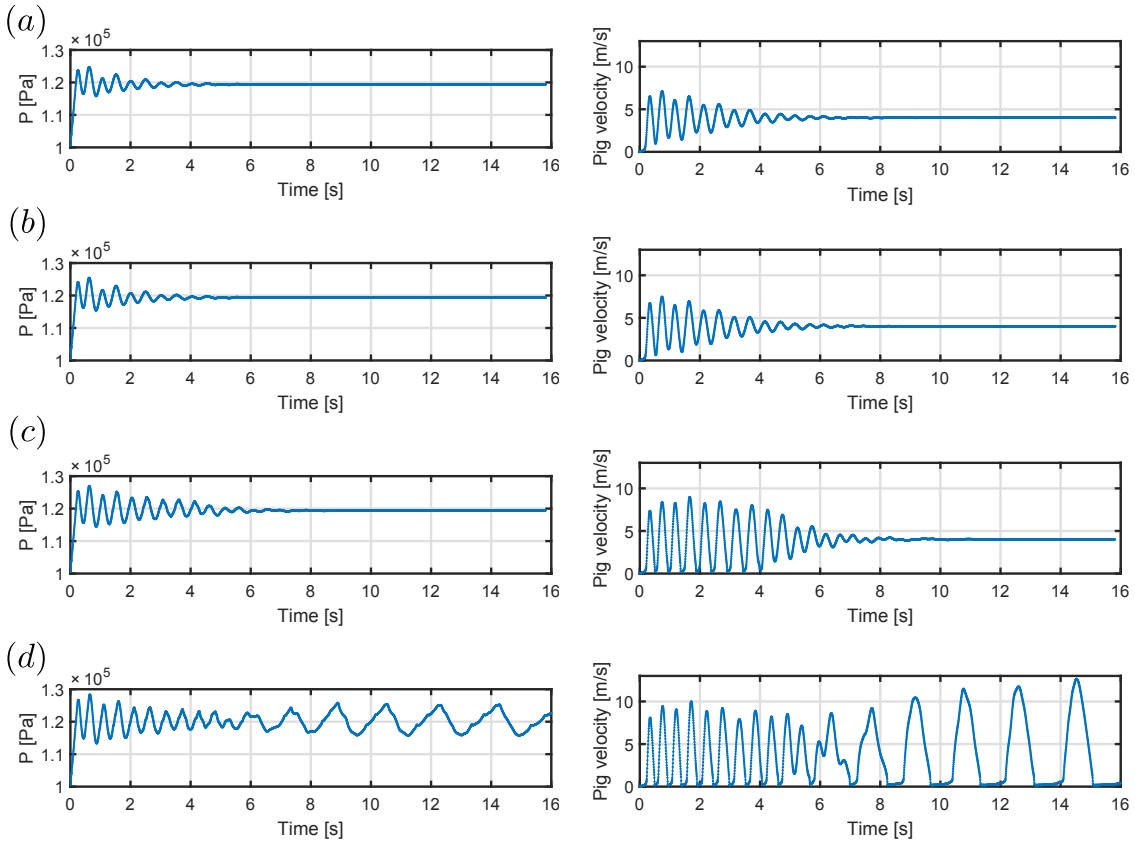


Figure 4.19: Time series of the pressure (a) and the pig velocity (b)

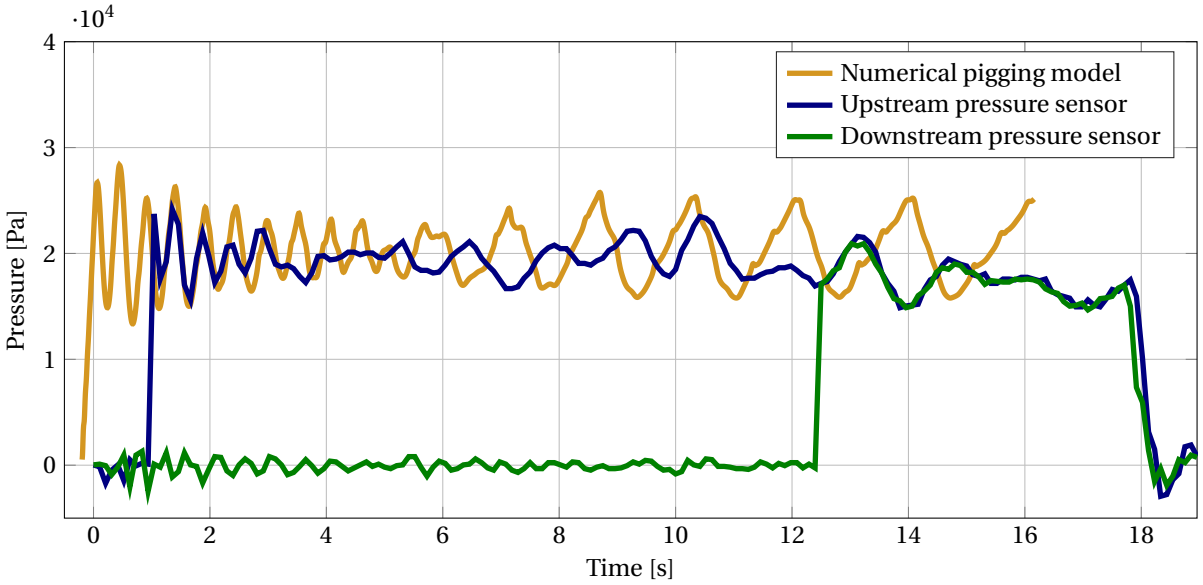


Figure 4.20: Time series of the pressure from the experiments and from the numerical simulation

# 5

# Discussion

The results and a discussion on these results were given in the previous chapter. This chapter discusses some more general issues which were faced during the experiments and which are worth noting.

*Experiments*

Selecting a pig configuration suitable for conducting the parameter study was rather difficult. It was desirable to have the friction as low as possible such that also pigs with a large by-pass area could be included in the parameter study. This can be obtained by decreasing either the oversize, the thickness of the sealing or the outer diameter of the sealing disks. However, when this is done also the stiffness of the sealing disks decreases. This in return causes the pig to start tilting and suffer from leakage. When the latter happens, a large reduction in the driving pressure is observed and the pig probably will get stuck. It happened several times that the flowloop had to be dismantled to remove a stuck pig. These problems led to the decision to use sealing disks with a higher stiffness such that the influence of the leakage was limited. A consequence of this was that the 8 % by-pass pig could not be used since the pressure drop over the pig was not large enough to overcome the friction.

A second difficulty experienced with the sealing disk of configuration 1 was the effect of wear. It was shown in section 4.1.2 that the friction slowly decreases every time that the seals are used again. One could instead replace the sealing disks every run. However, also this does not guarantee that the friction during each pigging run would remain the same. Also the strength at which the bolds are tightened influences the friction. Besides this, the dimensions of the sealing disks may slightly differ. They were fabricated with a self-made tool. This tool had some variations in the alignment of the inner diameter and the outer diameter. After each run it was checked whether the sealing disks were still intact.

The terms dynamic and static friction are used throughout this report. The distinction between the two is based on the observation that the friction is higher when the pig has no velocity, whereas it drops as soon as it starts moving. This distinction is also made in the commercial package OLGA, where a factor for the reduction of the friction as function of the velocity can be inserted. Next to the influence of the velcoity, there is also the effect of a varying pipe diameter. This effect is believed to be even stronger. During the experiments it was observed that the pig tends to get stuck at specific locations. This was seen as an increase in the pressure. The higher friction at these lcoations are caused by a reduction in the pipe diameter. The variations in the pipe diameter as a function of the pipe length are unknown. Besides this, neither one of the models can include the effect of the local pipe diameter. They can however include the effect of a difference in the static and dynamic pressure. This possibility is used to mimic the effect of variations in the pipe diameter. To do so, the static friction is set to a value comparable with the height of the pressure peaks. Although this is actually the effect of a variation in the pipe diameter, it is in this report referred to as the static friction. A similar note should be made on the dynamic friction. This is the friction experienced when the pig is sliding. Variations in the pipe diameter will however cause the friction to be different per location. Furthermore, the dynamic friction is computed as the time average friction during a pigging run. During a run with severe stick slip there are large periods that the pig is stuck. An approximation of the dynamic friction based on the measured

pressure will therefore yield too high values of the dynamic friction.

The measured pressure fluctuations show no reduction at higher by-pass area ratios. A reduction was expected since the by-pass hole allows pressure from the upstream pocket to be released to the downstream pocket. This could smooth the pressure fluctuations induced by the sudden acceleration and deceleration of the pig. However, this was not reflected in the standard deviation of the pressure measurements. A possible explanation is that the by-pass area ratios of 1, 2 of 4 % are too small for the pressure to escape during the typical stick-slip period. Further research on the influence of a larger by-pass area is needed.

*Simulations*

In the simulations it was tried to model the actual pigging experiments as accurate as possible. However, certain discrepancies will always be present. It was already mentioned that it is not (yet) possible to include the effect of local pipe diameter variations. Another difference is the length before and after the flow inlet. The pig is in reality launched from the pig launcher. It then passes a valve and a T-junction. These will change the local friction on the pig and thereby the pig motion. In the simulations, it was simply assumed that there is a certain length upstream of the initial position of the pig. This length was chosen based on an educated guess of the volume of the flowloop. However, the effect of the valve and T-junction ae not included.

The agreement between the measured average velocity and the simulated average velocity was very good. The differences between the simulations are limited. This was expected since the simulated pigging operations are rather simple. Besides this, a small discrepancy between the analytical by-pass model and the numerical pigging model was expected since both models use the same formula to compute the pressure drop. Simulations of other pigging conditions should be performed to compare the different models. It would be interesting to see how the models compare with actual pigging operations.

*Link to industry*

The experiments are carried out in a laboratory environment. The conditions in industry might be significantly different. It is therefore doubtful whether the same phenomena as found in the lab experiments are encountered in industry as well. Both the pig and the pipeline can differ in size by an order of magnitude. The pigs are a lot heavier and made from other materials. The sealing disks are normally made from polyurethane, which is much harder than the sealing disks used in the experiments. This results in much larger forces on the pipe wall. This is allowed in industry since the pipelines are much stronger and the working pressure is a lot higher. Related to this is a rule of thumb often used in industry. This rule of thumb aims at predicting the driving pressure as function of the diameter of the pipe and the type of the pig [25]. Both the formula and the graph to select a certain pig type are given in figure 5.1. The pig in configuration 1 and 2 would correspond to a K-factor of respectively 6 and 10. The formula to compute the required driving pressure is based on the assumption that the friction between the wall and the pig is constant for a certain pig type. As just mentioned, the friction between the wall and the pig in the experiments is much smaller than in industry. The formula to predict the driving pressure is therefore meaningless in our case. And even for large scale pigs it is doubtful whether it can be used. Many factors playing a role are not taken into account, for example the material and the oversize of the sealing disks. It is nevertheless used in industry.

A last important difference to mention is the presence of wax in industrial pipelines. The wax can form a layer in between the pig and the pipe wall that lubricates the friction. This can cause the friction to drop dramatically. Such a lubrication layer was not present in the experimental set-up. A wax type material could be inserted. However, it is difficult to spread this evenly over the flowloop and keep the distribution constant. Differences in the spreading would yields a different friction per pigging run, which makes it much harder to compare different pigging runs. However, since lubrication is believed to play a large role in the friction, it is recommended for future research to include the effect of wax deposit.

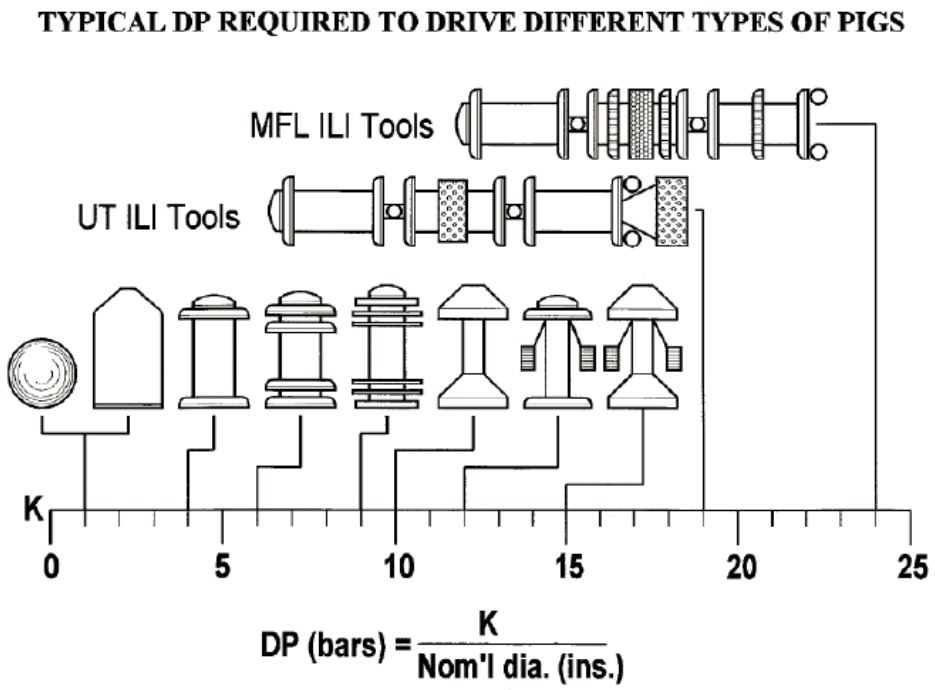


Figure 5.1: K factor corresponding to a certain pig type [1]

[1] Obtained from Cordell [25]

# 6

# Conclusions

The results from new pigging experiments as presented in this thesis have given insight in the behaviour of both conventional pigs and by-pass pigs traveling through straight gas pipelines. The influence of a changing by-pass area and a changing bulk velocity was analyzed by means of an extensive parameter study. This parameter study was subsequently be used to compare and verify the following five pigging models: (1) the analytical by-pass model, (2) the analytical stick-slip model, (3) the numerical pigging model, (4) the simplified numerical pigging model and (5) the commercial package OLGA. The analysis was first focused on the averaged quantities over complete pigging runs. Next, also the behaviour of the local quantities was analysed for a subset of all runs. The main findings of the current research are listed on the next page. Note that the conclusions are limited to situations comparable to the experimental set-up.

*Conclusions on global behaviour:*

- Small changes in the pig configuration may lead to significantly different pig motion. The nature of the pig motion is largely dependent on the friction between the pig and the wall and on the alignment of the pig with the pipeline. The friction is determined by the oversize of the sealing disks, the contact area of the sealing disks with the wall, the material of the sealing disks and the size of the clamping disks. The alignment of the pig and the pipeline depends on the length of the pig, the weight of the pig and the stiffness of the sealing disks.
- A typical behaviour observed during all pigging runs is the so-called stick-slip motion. This motion is characterized by a short period in which the pig has no velocity followed by a short period in which the pig quickly moves forward. The upstream pressure rises when the pig has no velocity whereas the pressure drop quickly decreases as soon as the pig slips forward.
- The stick-slip behaviour is triggered by variations in the inner pipe diameter which cause the friction to vary locally. Moreover, the stick-slip motion is more pronounced at low bulk velocities and when the ratio of the static over the dynamic friction is larger.
- Results of the current study show no dependency of the average friction on the pig velocity.
- The standard deviation of the pressure can be used as a measure of the intensity of stick-slip behaviour when comparing different pig types traveling at the same velocity. However, it cannot be used to compare the stick-slip intensity of the same pig at different bulk velocities.
- The current study shows no change in the intensity of the stick-slip behaviour when the by-pass area is changed from 0 % to 1, 2 or 4 %.
- The stick-slip motion has large influence on the local behaviour. However, the variations cancel out when one considers the time averaged quantities only. Steady-state models can therefore still be used to predict the average velocity.
- The average velocity is strongly dependent on the by-pass area. The velocity of pigs with no by-pass approaches the bulk velocity and decreases for increasing by-pass area ratio. All situations can be computed accurately with each of the pigging models when using a friction force deduced from the pressure measurements. Also the lower limit of the bulk velocity to push a by-pass pig forward can be estimated well with all models.

*Conclusions on local behaviour:*

- Graphs of the pressure fluctuations show a distinction between the pig behaviour after launching and when the pig is further downstream. The behaviour at the time around launching of the pig is dominated by the initial condtions. The local behaviour when the pig is further downstream is dominated by variations in the inner pipe diameter.
- The maximum pig velocity during a pigging operation where stick-slip is observed is significantly larger than the average pig velocity. The ratio of the maximum velocity over the average velocity increases for lower bulk velocities and for a higher fraction of the static friction over the dynamic friction. The maximum pig velocity and the slipping distance increase if the length upstream of the pig increases whereas the frequency decreases with an increasing upstream length.
- An estimation of the maximum velocity at a location further downstream can be made by virtually launching the pig from that location. All stick-slip models show reasonable agreement with the experiments.
- A larger bulk velocity results in larger pressure fluctuations after launching. However, it does not result in larger pressure fluctuations when the pig is further downstream.
- The numerical pigging model is capable of simulating the local pressure fluctuations that travel through the domain. The measured pressure fluctuations around launching of the pig are therefore best simulated with the numerical pigging model. The discrepancy is largest for the analytical stick-slip model. This discrepancy is decreased when the volume upstream of the pig is enlarged.
- Characteristics of the pressure fluctuations during a pigging operation can be estimated reasonably well with the analytical stick-slip model. The dynamic friction should be chosen based on the average pressure drop whereas for the static friction a value that corresponds to the pressure peaks should be used. Agreement is reached on both the range of the fluctuations as well as the frequency.
- The numerical pigging model predicts the pig motion to reach a steady-state when the same friction for the dynamic and static friction is used. Stick-slip motion, however, can be enforced in the numerical model by adjusting the friction function of the pig.

# 7

# Recommendations

This research has given several insights in the behaviour of both conventional pigs and by-pass pigs. However, it also left some questions unanswered. It is believed that the current experimental set-up forms a good basis for extending the experimental work. With the flowloop up and running, many more pigging experiments can be conducted to investigate different types of pigs. It is recommended to focus these studies on the following aspects:

- Behaviour of pigs with by-pass area ratio's larger than 4 %, with the focus on its influence on the stick-slip behaviour.
- The motion of by-pass pigs with different pressure drop characteristics. One can think of pigs with an extra disk to block the by-pass fluid or pigs with irregularities in the by-pass hole.
- Smart pigs that are able to monitor the pressure and velocity on-board. The on-board measurements can subsequently be used to control the pig motion. A first project on this has already been finished successfully. This work could be extended.
- Pigging experiments in two-phase flow. The required equipment to allow the simultaneous flow of air and water is already available. Adjustments on the current flowloop are however required.
- Influence of wax deposit at the inner wall.

Results from the experiments can again be used to verify the performance of the numerical pigging model under comparable conditions. The further development of the numerical pigging model is an ongoing task carried out in parallel with the experiments. The following extensions of the current pigging model are recommended:

- Other pressure drop correlations corresponding to a different by-pass geometry.
- Variations in the inner pipe diameter, which influence the friction of the pig. The results are usefull in analysing the stick-slip behaviour.
- Non-straight pipe segments. This tasks is not straightforward, since many different pipe geometries are possible. One should select geometries which are of most interest

The results of the current study show good agreement with the experiments. The numerical model can therefore be used to perform a numerical parameter study that extends the experimental parameter study. Pigging conditions which are outside of limits in the experimental set-up can quickly be simulated with numerical simulations. Some parameters which are of particular interest are: (1) the ratio of the static over the dynamic pressure, (2) the outlet pressure and (3) larger pipe dimensions.

The findings of the current study are limited to situations comparable with the experimental set-up used in this study. The pigging behaviour in other environments could be quire different. Recommendations for further research on phenomena which cannot be measured with the current experimental set-up are:

- Stick-slip behaviour of pigs in pipelines of industrial size
- Characteristics of the pig wall friction of pigs typically used in industry
- Characteristic behaviour of pigs around non-straight pipe segment or other irregularities

# Bibliography


[1] R. Davidson. *An introduction to pipeline pigging*. Gulf Professional Publishing, 1995.

[2] J. Cordell & H. Vanzant. *The pipeline pigging handbook*. ISBN: 0-9717945-3-7. Clarion Technical Publishers & Scientific Surveys Ltd., 3rd edition, 2003.

[3] J. Quarini & S. Shire. A review of fluid-driven pipeline pigs and their applications. *Journal of Process Mechanical Engineering*, 221(1):1–10, February 2007. Proceedings of the Institution of Mechanical Engineers, Part E.

[4] A. Entaban & A. Ismail & M. Jambari & P. Ting & K.M. Amin & C.C. Ping & S. Zou & G. Van Spronsen. Bypass pigging - a 'simple' technology with significant business impact. In *IPTC - International Petroleum Technology Conference*, number 16905, Beijing, China, March 2013.

[5] H.L. Wu & G. Van Spronsen & E.H. Klaus & D.M. Stewart. By-pass pigs for two-phase flow pipelines. In *Proceedings of the 1996 75th Annual Convention of the Gas Processors Association*, number 45096, pages 262–266, Denver, CO, USA, March 1996. Gas Processors Association.

[6] N. Money & D. Cockfield & S. Mayo & G. Smith. Dynamic speed control in high velocity pipelines. *Pipeline and gas journal*, pages 30–38, August 2012.

[7] A. Singh & R.A.W.M. Henkes. Cfd modeling of the flow around a by-pass pig. In *Proceedings of the 8th North American Conference on Multiphase Technology*, pages 229–243, Banff, Canada, June 2012. BHR Group.

[8] A.O. Nieckele & A.M.B. Braga & L.F.A. Azevedo. Transient pig motion through gas and liquid pipelines. *Journal of Energy Rescources Technology, Transactions of the ASME*, 123(2-4):260–268, December 2001.

[9] B.N.J. Persson. *Sliding Friction*. ISBN: 3-540-63296-4. Springer, 1998.

[10] G. Tan & D. Wang & S. Liu & H. Wang & S. Zhang. Frictional behaviors of rough soft contact on wet and dry pipeline surfaces: With application to deepwater pipelaying. *Science China Technological Sciences*, 56:3024–3032, December 2013.

[11] X. Zhu & D. Wang & H. Yeung &S. Zhang & S. Liu. Comparison of linear and nonlinear simulations of bidirectional pig contact forces in gas pipelines. *Journal of Natural Gas Science and Engineering*, June 2015.

[12] T.T. Nguyen & S.B. Kim & H.R. Yoo & Y.W. Rho. Modeling and simulation for pig flow control in natural gas pipeline. *KSME International Journal*, 15(8):1165–1173, August 2001.

[13] D.K. Kim & S.H. Cho & S.S. Park & Y.W. Rho & H.R. Yoo & T.T. Nguyen & SB. Kim. Verification of the theoretical model for analyzing dynamic behavior of the pig from actual pigging. *KSME International Journal*, 17(9):1349–1357, September 2003.

[14] T.T. Nguyen & S.B. Kim & H.R. Yoo & Y.W. Rho. Modeling and simulation for pig with bypass flow control in natural gas pipeline. *KSME International*, 15(9):1302–1310, Septembe 2001.

[15] T.T. Nguyen & H.R. Yoo & Y.W. Rho & S.B. Kim. Speed control of pig using bypass flow in natural gas pipeline. In *2001 IEEE International Symposium on Industrial Electronics Proceedings (ISIE 2001)*, volume 2, pages 863–868, Pusan, South Korea, June 2001.

[16] F. Esmaeilzadeh & D. Mowla & M. Asemani. Mathematical modeling and simulation of pigging operation in gas and liquid pipelines. *Journal of Petroleum Science and Engineering*, 69(1-2):100–106, November 2009.

[17] S.T. Tolmasquim & A.O. Nieckele. Design and control of pig operations through pipelines. *Journal of Petroleum Science and Engineering*, 62(3-4):102–110, September 2008.

[18] M. Saeidbakhsh & M. Rafeeyan & S. Ziaei-Rad. Dynamic analysis of small pigs in space pipelines. *Oil and Gas Science and Technology*, 64(2):155–164, March 2009.

[19] M. Lesani & M. Rafeeyan & A. Sohankar. Dynamic analysis of small pig through two and three-dimentional liquid pieline. *Journal of Applied Fluid Mechanics*, 5(2):75–83, 2012.

[20] M. Mirshamsi & M. Rafeeyan. Dynamic analysis of pig through two and three dimensional gas pipeline. *Journal of Applied FLuid Mechanics*, 8(1):43–54, 2015.

[21] M. Mirshamsi & M. Rafeeyan. Dynamic analysis and simulation of long pig in gas pipeline. *Journal of Natural Gas Science and Engineering*, 23:294–303, March 2015.

[22] F.M. White. *Fluid Mechanics*. ISBN: 978-0-07-128645-9. Mcgraw-Hill, 6th edition, 2008.

[23] I.E. Idelchik & A.S. Ginevski i. *Handbook of hydraulic resistance*. ISBN: 978-1-56700-251-5. Begell House, Redding, CT, 4th edition, 2007.

[24] M. Mirshamsi & M. Rafeeyan. Speed control of pipeline pig using the QFT method. *Oil and Gas Science Technology*, 67(4):693–701, July 2012.

[25] J.L. Cordell. Conventional pigs - what to use and why. Pipes and Pipelines International, 1992.

# A

# Models

## A.1. Analytical model

### A.1.1. Friction factors

The expression below give an approximation for the Darcy friction factor. The fanning friction factor is equal to 1/4th of the Darcy friction factor.

For laminar flow regime:

$$f_D = \frac{64}{Re} \tag{A.1}$$

The Colebrook-White equation, valid for the turbulent flow regime:

$$\frac{1}{\sqrt{f_D}} = -2\log_{10}\left(\frac{\varepsilon}{3.7D_h} + \frac{2.51}{Re\sqrt{f_D}}\right) \tag{A.2}$$

The Haaland equation, valid for the turbulent flow regime:

$$\frac{1}{\sqrt{f_D}} = -1.9\log_{10}\left[\left(\frac{\varepsilon/D}{3.7}\right)^{1.11} + \frac{6.9}{Re}\right] \tag{A.3}$$

The Serghide's solution, valid for the turbulent flow regime:

$$\frac{1}{\sqrt{f_D}} = \left(A - \frac{(B-A)^2}{C-2B+A}\right) \tag{A.4}$$

where: $A = -2\log_{10}\left(\frac{\varepsilon}{3.7D} + \frac{12}{Re}\right)$

$B = -2\log_{10}\left(\frac{\varepsilon}{3.7D} + \frac{2.51A}{Re}\right)$

$C = -2\log_{10}\left(\frac{\varepsilon}{3.7D} + \frac{2.51B}{Re}\right)$

Re = Reynolds number

$= \frac{\rho UL}{\mu}$

$\varepsilon$ = Roughness height

$\varepsilon/D$ = Relative roughness height

Churchill relation:

$$\zeta_{friction} = 2\left(\left(\frac{8}{Re}\right)^{12} (A+B)^{-1.5}\right)^{1/12} \tag{A.5}$$

where: $A = \left(2.457 \ln\left(\left(\left(\frac{7}{Re}\right)^{0.9} + 0.27\frac{\varepsilon}{D}\right)^{-1}\right)\right)^{16}$

$B = \left(\frac{37530}{Re}\right)^{16}$

$Re = \frac{\rho u D}{\mu}$

## A.2. Numerical model

### A.2.1. Continuous governing equations

*Extended Euler equations*

Rewriting conservative form of Euler equations to the primitive form:

$$\frac{\partial \mathbf{u}}{\partial t} + \mathbf{A}\frac{\partial \mathbf{u}}{\partial x} = \mathbf{s}_u \tag{A.6}$$

$$\frac{\partial \mathbf{u}}{\partial \mathbf{w}}\frac{\partial \mathbf{w}}{\partial t} + \mathbf{A}\frac{\partial \mathbf{u}}{\partial \mathbf{w}}\frac{\partial \mathbf{w}}{\partial x} = \mathbf{s}_u \tag{A.7}$$

$$\frac{\partial \mathbf{w}}{\partial t} + \left(\frac{\partial \mathbf{u}}{\partial \mathbf{w}}\right)^{-1}\mathbf{A}\left(\frac{\partial \mathbf{u}}{\partial \mathbf{w}}\right)\frac{\partial \mathbf{w}}{\partial x} = \left(\frac{\partial \mathbf{u}}{\partial \mathbf{w}}\right)^{-1}\mathbf{s}_u \tag{A.8}$$

$$\frac{\partial \mathbf{w}}{\partial t} + \mathbf{P}^{-1}\mathbf{A}\mathbf{P}\frac{\partial \mathbf{w}}{\partial x} = \mathbf{P}^{-1}\mathbf{s}_u \tag{A.9}$$

$$\frac{\partial \mathbf{w}}{\partial t} + \mathbf{B}\frac{\partial \mathbf{w}}{\partial x} = \mathbf{s}_w \tag{A.10}$$

where: $\mathbf{P} = \begin{bmatrix} 1/c^2 & 0 \\ u/c^2 & \rho \end{bmatrix}$

$\mathbf{P}^{-1} = \begin{bmatrix} c^2 & 0 \\ -u/\rho & 1/\rho \end{bmatrix}$

$\mathbf{B}(x,t) = \mathbf{P}^{-1}\mathbf{A}\mathbf{P} = \begin{bmatrix} u & \rho c^2 \\ 1/\rho & u \end{bmatrix}$

*Decoupled Euler equations*

The transformation from the variable **w** to another variable, **q**, is done by means of a transformation matrix:

$$d\mathbf{q} = \mathbf{S}^{-1}d\mathbf{w} \tag{A.11}$$

$$d\mathbf{w} = \mathbf{S}d\mathbf{q} \tag{A.12}$$

Substituting this into the equation yields:

$$\mathbf{S}\frac{\partial \mathbf{q}}{\partial t} + \mathbf{B}\mathbf{S}\frac{\partial \mathbf{q}}{\partial x} = \mathbf{0} \tag{A.13}$$

$$\tag{A.14}$$

The transformation matrix **S** should be chosen such that the matrix in front of the spatial derivative becomes decoupled. The first step in constructing this transformation is finding the eigenvectors of **B**:

$$\mathbf{B}\mathbf{v}_i = \lambda_i \mathbf{v}_i \tag{A.15}$$

$$[\mathbf{B} - \mathbf{I}\lambda_i]\,\mathbf{v}_i = \mathbf{0} \tag{A.16}$$

$$\begin{bmatrix} u-\lambda_i & \rho c^2 \\ 1/\rho & u-\lambda_i \end{bmatrix} \mathbf{v}_i = \mathbf{0} \tag{A.17}$$

where: $\lambda_i$ = eigenvalue

$\mathbf{v}_i$ = eigenvector corresponding to i-th eigenvalue

This can be solved if the determinant of the matrix is zero. Plugging the eigenvalues back into the equations gives the corresponding eigenvectors. The results are:

$$\lambda_1 = u + c \qquad : \mathbf{v}_1 = \begin{bmatrix} +\rho c \\ 1 \end{bmatrix} = \begin{bmatrix} (p+\hat{p})/c \\ 1 \end{bmatrix}$$

$$\lambda_2 = u - c \qquad : \mathbf{v}_2 = \begin{bmatrix} -\rho c \\ 1 \end{bmatrix} = \begin{bmatrix} -(p+\hat{p})/c \\ 1 \end{bmatrix}$$

A property of the eigenvectors is that these are orthonormal. This is used for the decoupling. Let the columns of the transformation matrix $\mathbf{S}$ be equal to the eigenvectors:

$$\mathbf{S} = \begin{bmatrix} \rho c & -\rho c \\ 1 & 1 \end{bmatrix} = \begin{bmatrix} (p+\hat{p})/c & -(p+\hat{p})/c \\ 1 & 1 \end{bmatrix} \tag{A.18}$$

$$\mathbf{S}^{-1} = \tfrac{1}{2} \begin{bmatrix} 1/(\rho c) & 1 \\ -1/(\rho c) & 1 \end{bmatrix} = \tfrac{1}{2} \begin{bmatrix} c/(p+\hat{p}) & 1 \\ -c/(p+\hat{p}) & 1 \end{bmatrix} \tag{A.19}$$

After substituting this into the equation and multiplying with the transformation matrix again, the matrix equations are decoupled:

$$\mathbf{S}\frac{\partial \mathbf{q}}{\partial t} + \mathbf{B}\mathbf{S}\frac{\partial \mathbf{q}}{\partial x} = \mathbf{0} \tag{A.20}$$

$$\frac{\partial \mathbf{q}}{\partial t} + \mathbf{S}^{-1}\mathbf{B}\mathbf{S}\frac{\partial \mathbf{q}}{\partial x} = \mathbf{0} \tag{A.21}$$

$$\frac{\partial \mathbf{q}}{\partial t} + \Lambda\frac{\partial \mathbf{q}}{\partial x} = \mathbf{0} \tag{A.22}$$

$$\tag{A.23}$$

The new variable can be computed using equations A.11:

$$d\mathbf{q} = \mathbf{S}^{-1} d\mathbf{w} \tag{A.24}$$

$$= \tfrac{1}{2} \begin{bmatrix} 1/(\rho c) & 1 \\ -1/(\rho c) & 1 \end{bmatrix} \begin{bmatrix} dp \\ du \end{bmatrix} \tag{A.25}$$

$$= \begin{bmatrix} \frac{du}{2} + \frac{dp}{2\rho c} \\ \frac{du}{2} - \frac{dp}{2\rho c} \end{bmatrix} \tag{A.26}$$

Substituting yields the following two, decoupled, equations:

$$\frac{\partial}{\partial t}(dp+\rho c du)+(u+c)\frac{\partial}{\partial x}(dp+\rho c du)=0 \tag{A.27}$$
$$\frac{\partial}{\partial t}(dp-\rho c du)+(u-c)\frac{\partial}{\partial x}(dp-\rho c du)=0 \tag{A.28}$$

The above transformation was done using the quasi-linear form as shown in equation 2.60. Exactly the same result would be obtained if the transformation was done based on equation 2.58. The eigenvalues are the same, whereas the transformation matrix, which is composed of the eigenvectors, looks as follows:

$$\mathbf{T}=\begin{bmatrix}\rho/c & -\rho/c\\ \rho(1+u/c) & \rho(1-u/c)\end{bmatrix} \tag{A.29}$$
$$\mathbf{T}^{-1}=\tfrac{1}{2}\begin{bmatrix}(c-u)/\rho & 1/\rho\\ -(u+c)/\rho & 1/\rho\end{bmatrix} \tag{A.30}$$

The above transformation matrices can be found in a quick way by using the transformation matrix **P** that relates **u** and **w**. This is done using the following identities:

$$\mathbf{T}=\mathbf{PS} \tag{A.31}$$
$$\mathbf{T}^{-1}=\mathbf{S}^{-1}\mathbf{P}^{-1} \tag{A.32}$$

Now look back at the decoupled equations 2.63 and 2.64. The first equations states that the variable $dp+\rho c du$ does not change over the line $u+c$, whereas the second equation states that the variable $dp-\rho c du$ does not change over the line $u-c$. Variables which remain constant over a certain line are often referred to as invariants and corresponding lines as their characteristics. The velocity at which the information travels equals to respectively $u+c$ and $u-c$.

*Splitted Euler equations*

Below, the primitive form of the Euler equations is restated:

$$\frac{\partial \mathbf{w}}{\partial t}+\mathbf{B}\frac{\partial \mathbf{w}}{\partial x}=\mathbf{c}_w \tag{A.33}$$

The Jacobian flux matrix **B** can be decoupled in the following way:

$$\mathbf{B}=\mathbf{S}\Lambda\mathbf{S}^{-1} \tag{A.34}$$
$$=\begin{bmatrix}\rho c & -\rho c\\ 1 & 1\end{bmatrix}\begin{bmatrix}u+c & 0\\ 0 & u-c\end{bmatrix}\begin{bmatrix}\frac{1}{\rho c} & \frac{1}{2}\\ \frac{-1}{\rho c} & \frac{1}{2}\end{bmatrix} \tag{A.35}$$
$$\tag{A.36}$$

Plugging this back into the Euler equations yields:

$$\frac{\partial \mathbf{w}}{\partial t}+\mathbf{S}\Lambda\mathbf{S}^{-1}\frac{\partial \mathbf{w}}{\partial x}=\mathbf{c}_w \tag{A.37}$$
$$\frac{\partial \mathbf{w}}{\partial t}+\begin{bmatrix}\rho c & -\rho c\\ 1 & 1\end{bmatrix}\begin{bmatrix}u+c & 0\\ 0 & u-c\end{bmatrix}\begin{bmatrix}\frac{1}{2\rho c} & \frac{1}{2}\\ \frac{-1}{2\rho c} & \frac{1}{2}\end{bmatrix}\begin{bmatrix}\frac{\partial p}{\partial x}\\ \frac{\partial u}{\partial x}\end{bmatrix}=\mathbf{c}_w \tag{A.38}$$
$$\frac{\partial \mathbf{w}}{\partial t}+\mathbf{S}\mathscr{L}=\mathbf{c}_w \tag{A.39}$$

where: $\mathscr{L}_w = \Lambda \mathbf{S}^{-1} \frac{\partial \mathbf{w}}{\partial x}$

$$= \begin{bmatrix} u+c & 0 \\ 0 & u-c \end{bmatrix} \begin{bmatrix} \frac{1}{\rho c} & \frac{1}{2} \\ \frac{-1}{\rho c} & \frac{1}{2} \end{bmatrix} \begin{bmatrix} \frac{\partial p}{\partial x} \\ \frac{\partial u}{\partial x} \end{bmatrix}$$

This is split into contributions due to left and right flowing waves:

$$\mathbf{S}\mathscr{L}_w = \begin{bmatrix} \rho c & -\rho c \\ 1 & 1 \end{bmatrix} \begin{bmatrix} u+c & 0 \\ 0 & u-c \end{bmatrix} \begin{bmatrix} \frac{1}{\rho c} & \frac{1}{2} \\ \frac{-1}{\rho c} & \frac{1}{2} \end{bmatrix} \begin{bmatrix} \frac{\partial p}{\partial x} \\ \frac{\partial u}{\partial x} \end{bmatrix} \tag{A.40}$$

$$= \mathbf{S}\Lambda^{+}\mathbf{S}^{-1}\frac{\partial \mathbf{w}}{\partial x} + \mathbf{S}\Lambda^{-}\mathbf{S}^{-1}\frac{\partial \mathbf{w}}{\partial x} \tag{A.41}$$

$$= \mathbf{S}\mathscr{L} - W^{+} + \mathbf{S}\mathscr{L} - w^{-} \tag{A.42}$$

$$= \begin{bmatrix} \rho c & -\rho c \\ 1 & 1 \end{bmatrix} \begin{bmatrix} u+c & 0 \\ 0 & 0 \end{bmatrix} \begin{bmatrix} \frac{1}{\rho c} & \frac{1}{2} \\ \frac{-1}{\rho c} & \frac{1}{2} \end{bmatrix} \begin{bmatrix} \frac{\partial p}{\partial x} \\ \frac{\partial u}{\partial x} \end{bmatrix} + \begin{bmatrix} \rho c & -\rho c \\ 1 & 1 \end{bmatrix} \begin{bmatrix} 0 & 0 \\ 0 & u-c \end{bmatrix} \begin{bmatrix} \frac{1}{\rho c} & \frac{1}{2} \\ \frac{-1}{\rho c} & \frac{1}{2} \end{bmatrix} \begin{bmatrix} \frac{\partial p}{\partial x} \\ \frac{\partial u}{\partial x} \end{bmatrix} \tag{A.43}$$

$$\tag{A.44}$$

The total equation therefore is as follows:

$$\frac{\partial \mathbf{w}}{\partial t} + \begin{bmatrix} \rho c & -\rho c \\ 1 & 1 \end{bmatrix} \begin{bmatrix} u+c & 0 \\ 0 & 0 \end{bmatrix} \begin{bmatrix} \frac{1}{\rho c} & \frac{1}{2} \\ \frac{-1}{\rho c} & \frac{1}{2} \end{bmatrix} \begin{bmatrix} \frac{\partial p}{\partial x} \\ \frac{\partial u}{\partial x} \end{bmatrix} + \begin{bmatrix} \rho c & -\rho c \\ 1 & 1 \end{bmatrix} \begin{bmatrix} 0 & 0 \\ 0 & u-c \end{bmatrix} \begin{bmatrix} \frac{1}{\rho c} & \frac{1}{2} \\ \frac{-1}{\rho c} & \frac{1}{2} \end{bmatrix} \begin{bmatrix} \frac{\partial p}{\partial x} \\ \frac{\partial u}{\partial x} \end{bmatrix} = \mathbf{c}_w \tag{A.45}$$

Exactly the same can be done for the conservative form. This is most simple done by using the transformation matrix **P**.

## A.3. OLGA model

The OLGA model consists of a closed inlet, a mass source, a pipeline, a (bypass) pig, and an outlet. A sketch is shown below. In table A.1 some input parameters are listed. The formula used within OLGA to compute the friction between the pig and the wall is given in equation A.46.

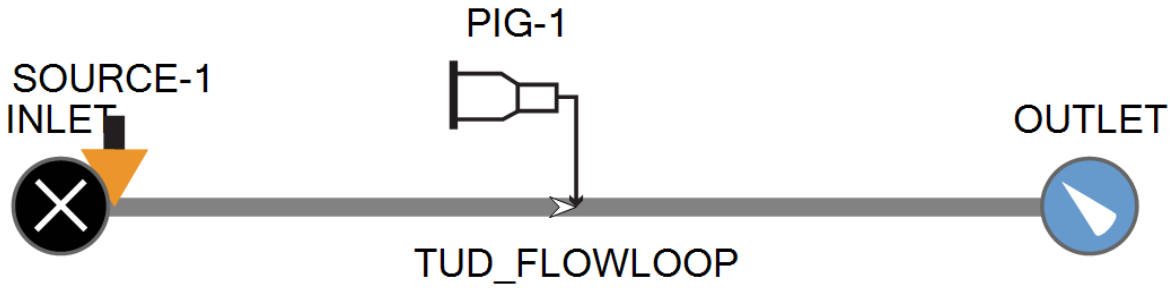


Figure A.1: Olga model (M. Fransen, priv. comm., August 2016)

Table A.1: Input parameters of the OLGA model

| **Parameter** | **Value** | **Unit** |
|---|---|---|
| Static force | 26 | $N$ |
| Wall friction | 0 | $Ns/m$ |
| Mass | 0.135 | $kg$ |
| Leakage factor | 0 - 0.01 - 0.02 - 0.04 | – |

$$f_W = \left(F_0 + f_w \cdot V_{pig}\right) \cdot sign\left(V_{pig}\right) \tag{A.46}$$

where: $f_W$ = Total friction

$F_0$ = Static friction

$f_w$ = Factor accounting for the decrease in friction at higher velocities, set at 0

$V_{pig}$ = Pig velocity

# B

# Experimental setup

## B.1. Flowloop characteristics

(a) Exploded view configuration 1

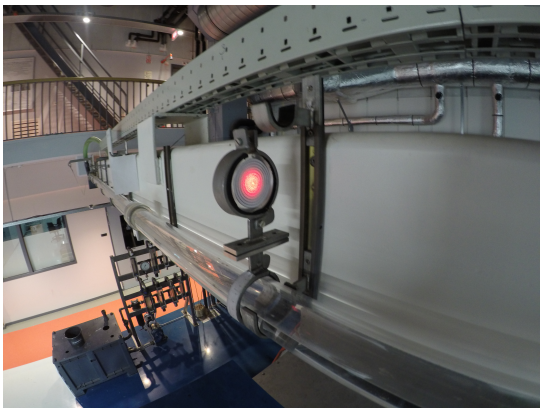

(b) Exploded view configuration 2

Figure B.1: Laser and target used to align the flowloop

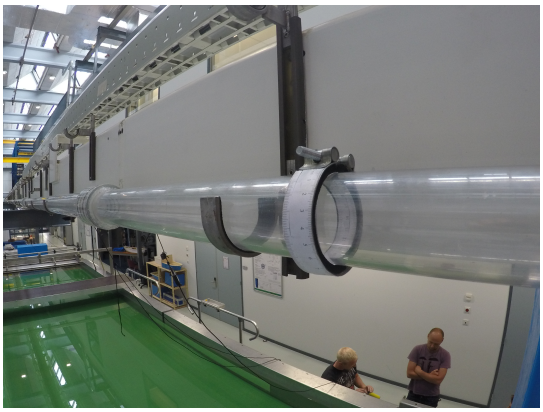

(a) Water level measure

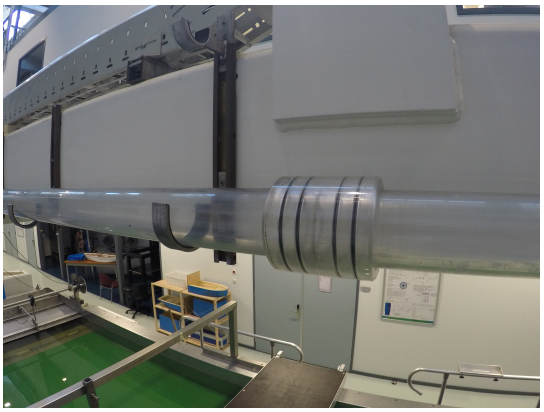

(b) Connection between two pipe segments

Figure B.2: Close-ups of pipeline

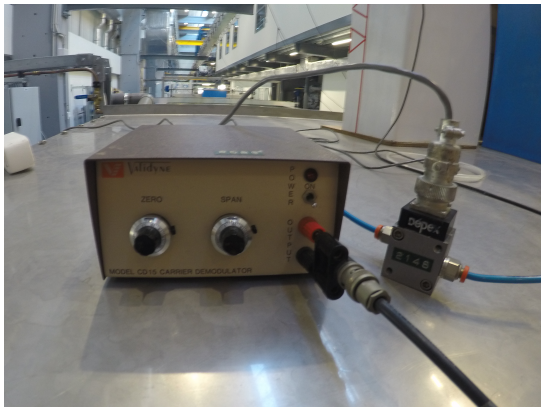


(a) Carrier demodulator (left) and pressure transducer (right)

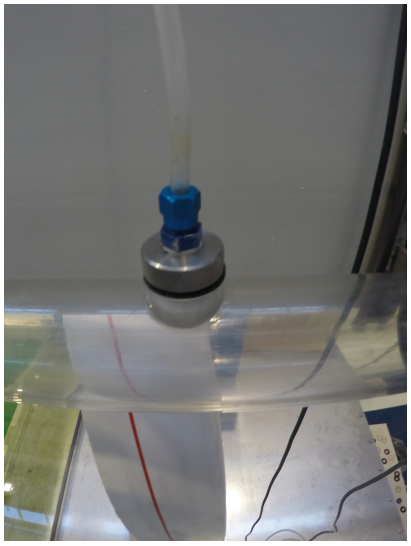

(b) Connection between a pressure tube and the flowloop

Figure B.3: Close-ups of pressure sensor components

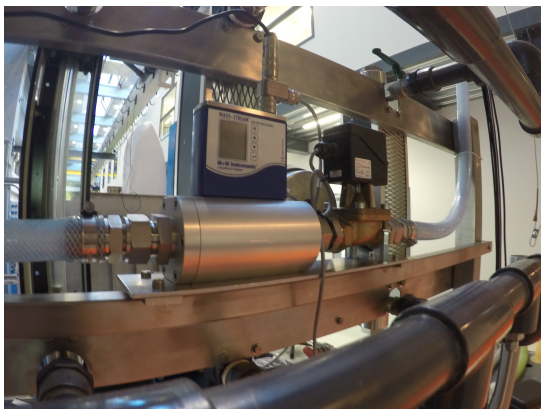

(a) Flowmeter

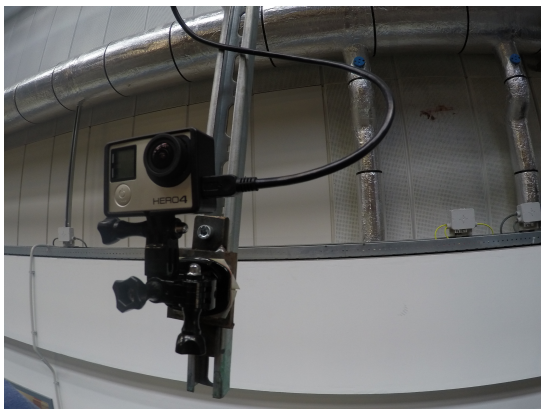


(b) GoPro camera

Figure B.4: Close-ups of measurement devices

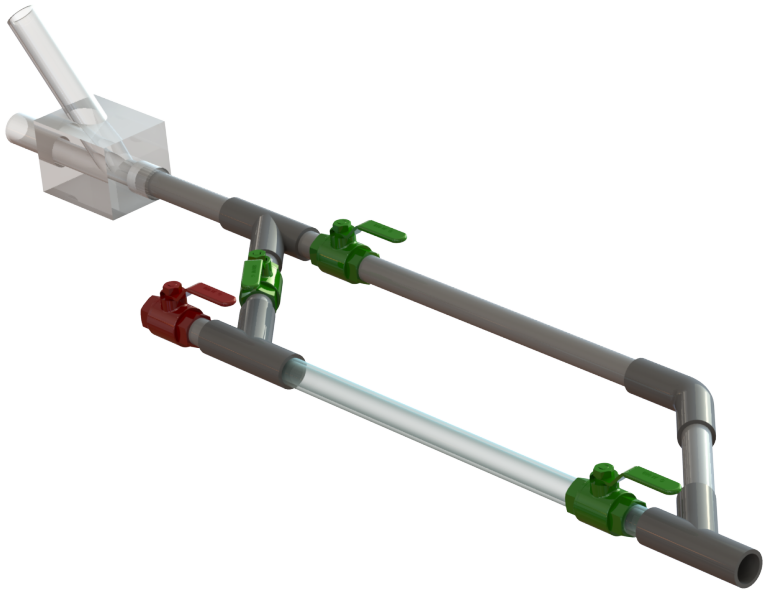

Figure B.5: Pig launcher

## B.2. Measurement apparatus

### B.2.1. Gas flowmeter

The setpoint of the flowmeter should be inserted as a certain percentage of the maximum flow flux. This percentage is denoted as $\Phi$. The expected velocity is converted from the flux in liters per minute to the velocity as follows:

$$\bar{v} = \Phi \frac{900}{100} \frac{1}{60 \cdot 1000} \frac{1}{\frac{1}{4}\pi \frac{1}{10^6} 52^2} \tag{B.1}$$

$$= \Phi \frac{150}{\frac{1}{4}\pi 52^2} \tag{B.2}$$

$$= 0.0706 \cdot \Phi \tag{B.3}$$

Due to an inaccuracy of the flowmeter and a tolerance of the inner pipe diameter, the actual velocity might differ. The range within is computed as follows.

$$v = \Phi \cdot \frac{900}{100} \frac{1}{60 \cdot 1000} \frac{1}{\frac{1}{4}\pi \frac{1}{10^6} (52 \pm tol)^2} \pm 4 \cdot \frac{900}{100} \frac{1}{60 \cdot 1000} \frac{1}{\frac{1}{4}\pi \frac{1}{10^6} (52 \pm tol)^2} \tag{B.4}$$

$$= \Phi \cdot \frac{150}{\frac{1}{4}\pi (52 \pm tol)^2} \pm \frac{3600}{\frac{1}{4}\pi (52 \pm tol)^2} \tag{B.5}$$

$$= \Phi \cdot \frac{150}{\frac{1}{4}\pi \cdot 52^2} \left( \frac{52}{52 \pm tol} \right)^2 \pm \frac{36}{\frac{1}{4}\pi \cdot 52^2} \left( \frac{52}{52 \pm tol} \right)^2 \tag{B.6}$$

$$= \Phi \cdot 0.0706 \left( \frac{52}{52 \pm tol} \right)^2 \pm 0.2825 \left( \frac{52}{52 \pm tol} \right)^2 \tag{B.7}$$

$$= \bar{v} \left( \frac{52}{52 \pm tol} \right)^2 \pm 0.2825 \left( \frac{52}{52 \pm tol} \right)^2 \tag{B.8}$$

Substituting a tolerance of 0.7 $mm$ yields:

$$v = \bar{v} \left( \frac{52}{52 \pm 0.7} \right)^2 \pm 0.2825 \left( \frac{52^2}{(52 \pm 0.7)^2} \right) \tag{B.9}$$

The above equations define a maximum and minimum velocity when setting a certain $\Phi$ (or $\bar{v}$):

$$v_{min} = \bar{v}\left(\frac{52}{52+0.7}\right)^2 - 0.2825\left(\frac{52^2}{(52+0.7)^2}\right) \tag{B.10}$$

$$= \bar{v}\,(1-0.0264) - 0.2825\,(1-0.0264) \tag{B.11}$$

$$= 0.9736\,\bar{v} - 0.275 \tag{B.12}$$

$$v_{max} = \bar{v}\left(\frac{52}{52-0.7}\right)^2 + 0.2825\left(\frac{52^2}{(52-0.7)^2}\right) \tag{B.13}$$

$$= \bar{v}\,(1+0.0275) + 0.2825\,(1+0.0275) \tag{B.14}$$

$$= 1.0275\,\bar{v} + 0.290 \tag{B.15}$$

where: $\Phi$ = Prescribed percentage of maximum flow flux (=900 liter/min)

$\bar{v}$ = Expected (prescribed) cross-sectional averaged velocity

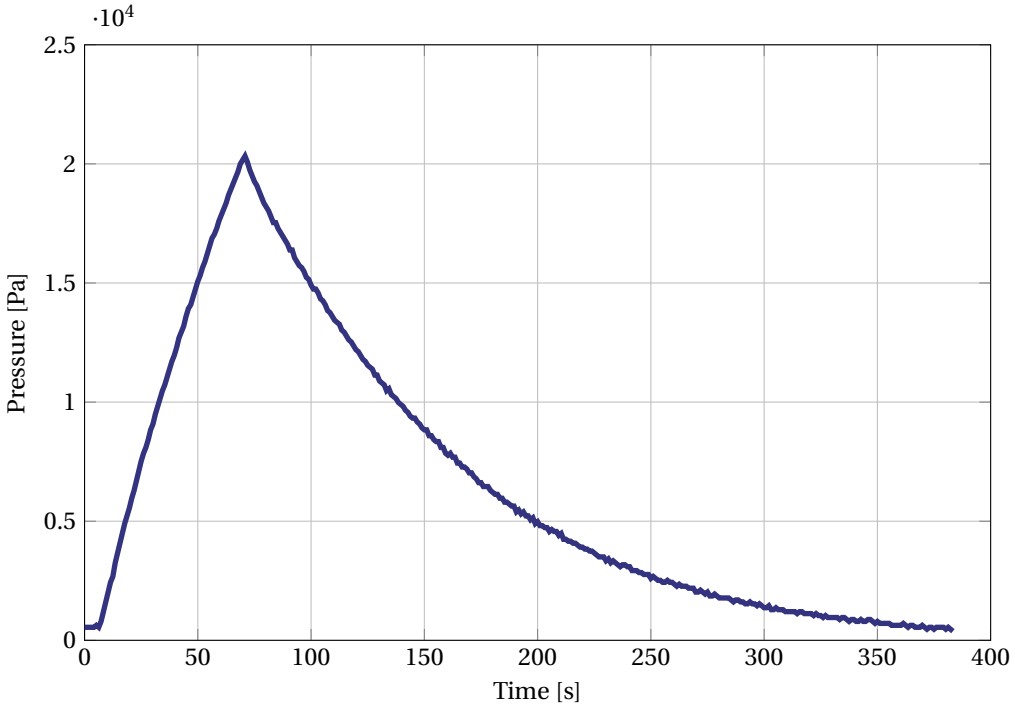


Figure B.6: Measured pressure when flowloop was closed at inlet and outlet

### B.2.2. Pressure sensors

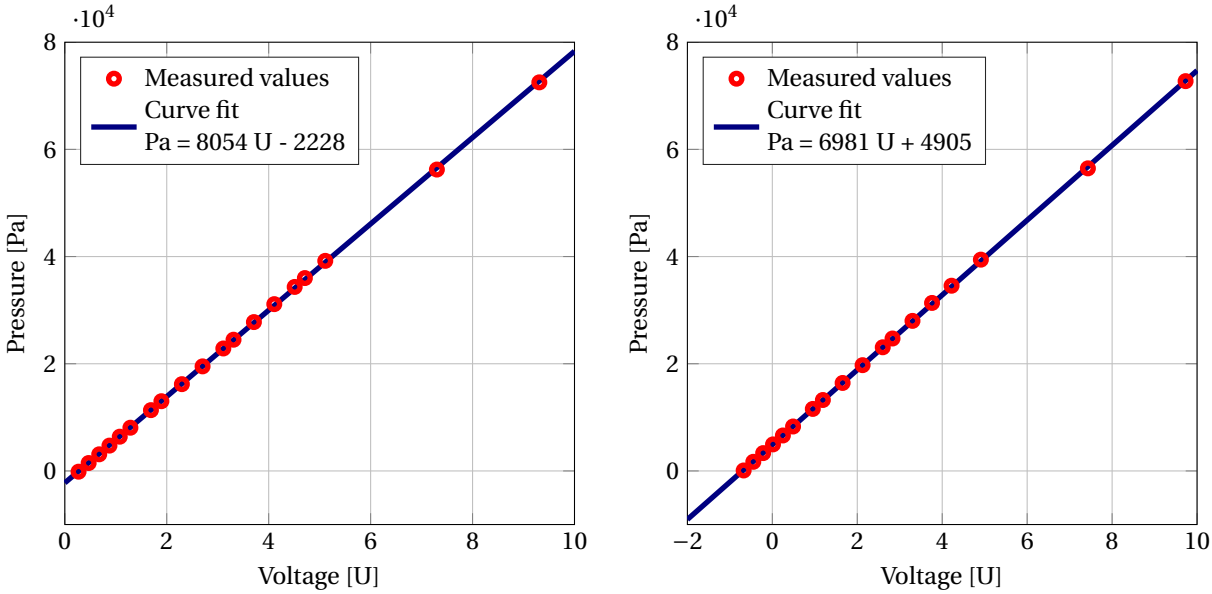


(a) Upstream pressure sensor

(b) Pressure sensor at measurement section

Figure B.7: Calibration curves

$$P_1 = 6981 \cdot U + 4905 \qquad \begin{cases} \text{lower confidence bound:} & 6957 \cdot U + 4817 \\ \text{upper confidence bound:} & 7005 \cdot U + 4994 \end{cases} \tag{B.16}$$

$$P_2 = 8054 \cdot U - 2228 \qquad \begin{cases} \text{lower confidence bound:} & 8018 \cdot U - 2367 \\ \text{upper confidence bound:} & 8090 \cdot U - 2089 \end{cases} \tag{B.17}$$

### B.2.3. Data acquisition

## B.3. Pig characteristics

### B.3.1. Dimensions

Table B.1: Properties of pig configurations

| Property | Configuration 1 | Configuration 1 | Unit |
|---|---|---|---|
| Material core | PVC | PVC | - |
| Length | 86 | 86 | $mm$ |
| Diameter core | 40 | 40 | $mm$ |
| Pipe-hole area ratio | 0 | 0 | - |
| | 0.01 | 0.01 | - |
| | 0.02 | 0.02 | - |
| | 0.04 | 0.04 | - |
| | 0.08 | 0.08 | - |
| Diameter nuts | 40 | 40 | $mm$ |
| Shrew-thread | 3/4 | 3/4 | $"BSP$ |
| Material sealing disk 1 | EPDM | Para rubber | - |
| Hardness sealing disk 1 | 35 * | 45 | $ShoreA$ |
| Outer diameter sealing disk 1 | 57 | 57 | $mm$ |
| Thickness sealing disk 1 | 4 | 2 | $mm$ |
| Material sealing disk 2 | EPDM | EPDM | - |
| Hardness sealing disk 2 | 35 | 35 | $Shore$ |
| Outer diameter sealing disk 2 | 55 | 48 | $mm$ |
| Thickness sealing disk 2 | 4 | 4 | $mm$ |
| Material clamping disks | perspex | perspex | - |
| Outer diameter clamping disk 1 | 47 | 48 | $mm$ |
| Thickness clamping disk 1 | 5 | 5 | $mm$ |
| Outer diameter clamping disk 2 | 47 | 41 ** | $mm$ |
| Thickness clamping disk 1 | 5 | 2 | $mm$ |
| Outer diameter clamping disk 3 | - | 41 | $mm$ |
| Thickness clamping disk 3 | - | 2 | $mm$ |
| Material rings | perspex | perspex | - |

* The hardness is measured according Shore 00 standards. A comparable Shore A value is given here to compare with the other material

** The edges are rounded to space for the sealing disks to bend backwards

### B.3.2. Sealing disk properties

## Celrubberplaat EPDM zwart 3x1000mm

**Technische specificaties en applicaties**

| | |
|---|---|
| Kwaliteit | EPDM |
| Celstructuur | Gesloten |
| Kleur | Zwart |
| Uitvoering | Zonder lijmlaag |
| Dikte | 3 mm |
| Maximale rollengte | 20 meter |
| Temperatuurbereik | -40 °C / +95 °C |
| Piektemperatuur | +130 °C |
| Dichtheid | 120 Kg/m3 (+/- 20) |
| Hardheid Shore 00 (*) | 40 (+/-5) |
| Hardheid Shore A (**) | ca. 10 - 15 |
| Verlenging | Min. 150% |
| Brandwerend | O.K. (FMVSS 302 - FIAT 50433) |
| Water absorptie (3 min.) | 2% |
| Eigenschappen | - Veroudering- en vochtbestendig<br>- Weerbestendig<br>- Afdichtend en isolerend<br>- Slijtvast<br>- Flexibel<br>- Veerkrachtig |
| Chemische resistentie | - Verdunde chemicaliën<br>- Zouten<br>- Glycol (antivries)<br>- Ozon<br>- Warm en koud water<br>- Stoom<br>- Ultraviolet licht |
| Beperkte toepasbaarheid | - Minerale oliën<br>- Vetten<br>- Brandstoffen |
| Toepassingen | - Bouw<br>- Automotive sector<br>- Vliegtuigindustrie |

** De hardheid voor celrubber materialen wordt gemeten volgens de Shore 00 standaard.*

*** De vermelde waarde voor de Shore A standaard is uitsluitend vermeld als indicatie.*

Figure B.8: Material properties of EPDM [1]

[1] Obtained from: `http://www.rubbermagazijn.nl/collectie/celrubber/celrubberplaat/2627_zwart_celrubberplaat-3-mm-1-mtr-breed.html`

# Plaatrubber para grijs 2 mm

## Afname per meter / maximale rollengte = 10 meter

### Afdichtingsrubber van hoge kwaliteit

*Para plaatrubber* staat bekend als universele rubberplaat en wordt gebruikt voor diverse toepassingen in de bouw, scheepvaart, industrie en wagenbouw. Deze para rubberplaat kan ook gebruikt worden voor diverse andere toepassingen door het te snijden in stroken, pakkingen of ringen. Daarnaast is para rubberplaat ook geschikt voor isolatie-, demping- en schokabsorptie doeleinden en is het bestand tegen temperaturen tussen -50° C tot +90° C. Deze rubberplaat heeft uitstekende mechanische eigenschappen, lage permanente indrukking en hoge veerkracht. Deze **rubberplaat** beschikt over uitstekende dynamische en herstellende eigenschappen. De hardheid van deze **rubberplaat** is +/ - 45 graden shore en hebben een dichtheid van 1.05 g/cm3. Para rubberplaten zijn goed bestand tegen zuren en zouten maar worden niet aanbevolen om het in contact te brengen met oliën en koolwaterstoffen. Dit product is aan beide zijden glad.

Treksterkte: 16 N/mm2
Soortelijk gewicht: 1,05 g/cm3
Uitvoering: beide zijden glad

| Toepassing afdichtingsrubber | |
|---|---|
| Benzine | Slecht |
| Smeeroliën | Slecht |
| Zuren | Matig |
| Alkali | Matig |
| Hydraulische fosfaten | Slecht |
| Vloeibare silicaten | Slecht |
| Slijtvastheid | Goed |
| Scheursterkte | Goed |
| Schokbestendigheid | Uitstekend |
| Veerkracht | Uitstekend |
| Ondoordringbaar voor gassen | Matig |
| Compressieverhouding | Goed |

Figure B.9: Material properties of para rubber [2]

[2] Obtained from: `http://www.rubbermagazijn.nl/collectie/pakkingmateriaal/plaatrubber-para-grijs/2413_grijs_para-plaatrubber-grijs-2-mm.html`

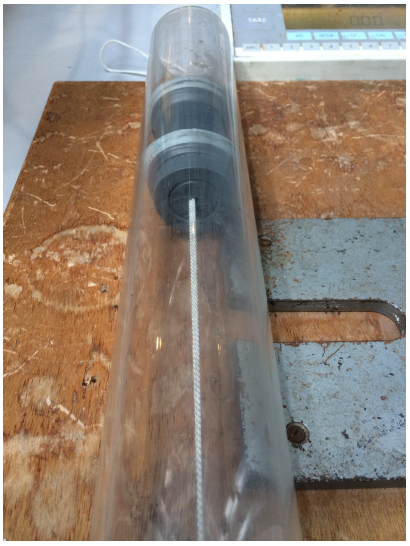

(a) Pull test to measure the static friction

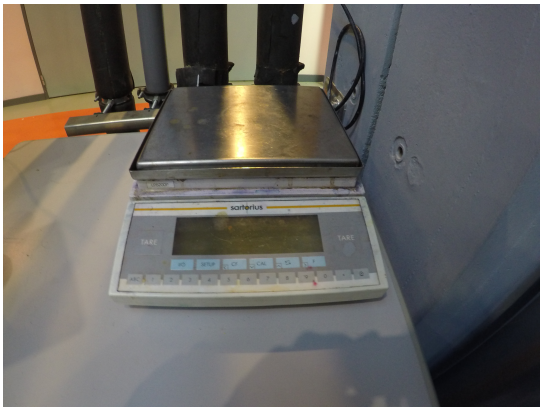


(b) Weighting scale

Figure B.10: Static pressure measurement

# C

# Results

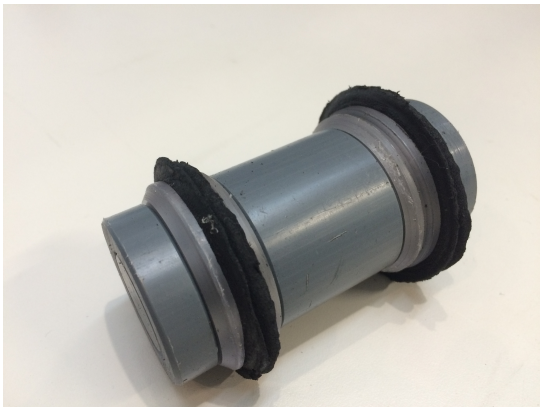

(a) Configuration 1

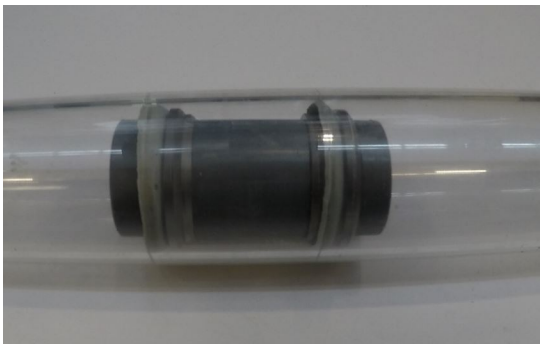

(b) Configuration 2

Figure C.1: Sealing disks of after a run